2009

Glia Are Required For Sensory Neuron Morphology And Function In Caenorhabditis elegans

Taulant Bacaj

GLIA ARE REQUIRED FOR SENSORY NEURON MORPHOLOGY AND FUNCTION IN *CAENORHABDITIS ELEGANS*

A Thesis Present to the Faculty of

The Rockefeller University

in Partial Fulfillment of the Requirements for

the degree of Doctor of Philosophy

by

Taulant Bacaj

June 2009

GLIA ARE REQUIRED FOR SENSORY NEURON MORPHOLOGY AND FUNCTION IN *CAENORHABDITIS ELEGANS*

Taulant Bacaj, Ph.D.

The Rockefeller University 2009

The nervous system emerges from the coordinated development of neurons and glia. To better understand the processes that enable nervous system development and function we have studied the sensory organs of *Caenorhabditis elegans* because their anatomy and function are well-characterized. Specifically, we have focused on two aspects of sensory organs: how do glia interact with neurons to enable proper development and function and how are sensory cilia generated.

To uncover any glial roles, we ablated the major glial cell of the amphid sensilla. Embryonic glial ablation did not affect neuronal survival and resulted in sensory neuron dendrites that were far too short, revealing a glial role in anchoring sensory neuron dendrites.

To examine post-developmental glial roles, we ablated glia after the amphid sensory organ was fully formed. These glia-ablated animals exhibited profound sensory deficits as determined by behavioral assays, failed to maintain the proper morphology of some modified sensory cilia, and had defects in neuronal uptake of lipophilic dyes. Further, animals lacking glia showed no Ca^{2+} responses in the ASH sensory neuron after stimulation with a high osmolarity solution. To understand the molecular bases of these glial activities, we characterized a sheath glia expressed gene, *fig-1*, that encodes a

protein with thrombospondin type I domains. FIG-1 likely functions extracellularly, is essential for neuronal dye uptake, and also affects behavior.

To characterize the molecular basis of cilia morphogenesis and function, we cloned the *che-12* and *dyf-11* mutants which have chemotaxis and dye uptake defects. CHE-12 and DYF-11 are conserved ciliary proteins required for maintenance of cilium morphology and function. Furthermore, DYF-11 undergoes intraflagellar transport (IFT) and may function at an early stage of IFT-B particle assembly.

Our results suggest that glia are required for multiple aspects of sensory organ function. Moreover, as thrombospondin 1 is a glial-secreted protein required for synapse formation in mice, these results suggest that some of the molecular components underlying glia-neuron interactions in *C. elegans* might be conserved.

Acknowledgments

My greatest thanks go to my mentor Shai for helping me learn from how to do injections to how to ask appropriate scientific questions. Just as importantly, he has fostered a great lab environment in which I had fun every day.

I want to thank Yun Lu who performed all the EM work for this thesis, and Maya Tevlin with whom I collaborated for some of the *fig-1* work and who shared the *F16F9.3* promoter which helped me tremendously.

I have enjoyed working in Shai's lab because of all the people that were my companions through the years. It is rare to get such a great collection of smart and fun people and it was my pleasure to work with them. I want to thank all lab members for putting up with me, especially two who had to deal with me the longest: my classmate, baymate, and [Aussie] mate Carl for all the discussions about everything, and Max who I unduly burdened with many questions scientific, cultural, and linguistic.

I feel privileged to have had as members of my thesis committee Cori Bargmann and Jim Hudspeth who provided many helpful and insightful suggestions. I am also thankful to Marc Freeman for travelling to serve as my outside committee member.

The Bargmann lab has been very helpful, particularly I thank Sreekanth Chalasani for teaching me G-CaMP imaging and Navin Pokala for sharing his ChR2 strains.

Life in NYC has been fun because of my closest classmates and friends. The Dean's Office has been very supportive, including writing all sorts of letters for visa applications.

I am grateful to Mary for everything.

Përfundimisht dua të falenderoj familjen: prindërit e mi për të gjitha sakrificat e tyre dhe motrën time Gerta për zemërgjerësinë e saj. Ia përkushtoj këtë vepër gjyshit tim, Serjan Bacaj, që u nda nga ne këtë javë.

* Many, many worms were harmed in the making of this thesis. *

Table of Contents

List of Figures

List of Tables

Chapter 1

General overview and background

The ultimate brain teaser

The human mind and the machine that gives rise to it, the brain, have fascinated people for centuries. The daunting complexity of unraveling the workings of the brain, however, requires that one ask and study much humbler questions regarding specific issues of nervous system development and function. In humans as in other animals, the main function of the nervous system is to monitor changes in the environment and generate appropriate responses. To achieve this, the nervous system takes advantage of its two main cell types: neurons and glia. Neurons detect, transmit, and integrate stimuli, and have, therefore, been the focus of extensive study over the last century. The ability to eavesdrop on neurons and manipulate them using electrodes has enabled and fueled the growth of their study. Glia, on the other hand, have received considerably less attention, since their functions are not readily apparent. To better understand the nervous system, we have sought to uncover potential glial roles that aid or enable proper neuronal function.

Categorization of glia

In mammals, where glia were first described, four major types of glia are recognized: astrocytes, oligodendrocytes, Schwann cells, and microglia. Astrocytes are stellate cells that project processes that ensheath synapses and contact capillaries (Grosche et al., 1999; Bushong et al., 2002). They are thought to insulate synapses, control the chemical composition of the perisynaptic space, and induce the formation of the blood brain barrier (Banerjee and Bhat, 2007; Barres, 2008). Oligodendrocytes and

Schwann cells are primarily myelin-producing cells found in the central and peripheral nervous system, respectively. These cells wrap around axons to allow for efficient conduction (Geren and Raskind, 1953; Jessen and Mirsky, 2005; Nave and Trapp, 2008). Microglia are thought to function as the resident immune cells of the central nervous system (Vilhardt, 2005).

The apparent simplicity in defining glia is misleading, however, as numerous other cell types exist that have been described as glia, including Bergmann glia, Müller cells, olfactory ensheathing cells, etc. While no all-encompassing definition of glia exists, it is accepted that these non-neuronal cells must be closely associated with neurons. Furthermore, astrocytes, oligodendrocytes, Schwann cells, and nearly all other glia derive from the neuroectoderm (Le Douarin et al., 1991; Marshall et al., 2003), making this another criterion that is useful in distinguishing glia. Microglia, the exception, derive from the hematopoietic lineage (Streit, 2001), consistent with their immune roles.

Glia-neuron interactions

With the spotlight on neurons, the roles that glia might play in nervous system function and dysfunction remain relatively underexplored. Recent advances, however, indicate that these cells might be an integral part of the nervous system, playing many important roles (Barres, 2008). Below, I highlight some of these findings and their significance.

Trophic interdependence

Neurons require glia for their survival. For example, hippocampal neurons (Banker, 1980) or retinal ganglion cells (Meyer-Franke et al., 1995) die when cultured separately from glia. Similarly, the death of cortical astrocytes in mice lacking the epidermal growth factor receptor (EGFR) is accompanied by neuronal cell death (Wagner et al., 2006). In *Drosophila*, neuronal degeneration is seen after toxin-induced ablation of glial cells (Booth et al., 2000) as well as in mutants that fail to completely specify glial fates (Hosoya et al., 1995; Jones et al., 1995; Xiong and Montell, 1995). Reciprocally, glia depend on neurons for their survival. For example, the axons of dorsal root ganglia neurons express neuregulin-1, an EGFR ligand (Holmes et al., 1992), while Schwann cells express its receptors, ErbB2/3. In transgenic mice lacking neuregulin-1 or its receptors, Schwann cells die (Meyer et al., 1997; Riethmacher et al., 1997; Woldeyesus et al., 1999), suggesting a role for this neuronal protein in glial survival. Vein, the *Drosophila* neuregulin-1 homologue, also promotes survival of longitudinal glia (Hidalgo et al., 2001). Another neuron-glia matching mechanism is observed in the *Drosophila* midline where ten glia are born in each segment. These cells compete for Spitz, a TGFα-like ligand, secreted by neurons. Spitz acts through the MAP kinase pathway to repress Hid, a proapoptotic factor (Bergmann et al., 2002), thus promoting cell survival. Due to limiting amounts of neuronal Spitz, only three midline glia survive.

Why might neurons and glia depend on each other for survival? One possibility is that co-dependent survival provides a matching mechanism that ensures that the appropriate number of each cell type is present in the adult nervous system.

Migration

To reach their final destinations, most neurons and glia must migrate through a complex environment. As these two cell types are closely associated in adult structures, it has been suggested that they might instruct each other's migration. Indeed, several studies support the idea that glia guide neuronal migration and neurite pathfinding. For example, neuronal migration along Bergmann glia in the cerebellum (Rakic, 1971) and along radial glia in the cortex (Rakic, 1972) was postulated based on electron microscopy time series. Consistent with this hypothesis, migration of granule neurons along cerebellum-derived glia has been observed in culture, where it was imaged directly (Edmondson and Hatten, 1987). In *Drosophila*, glial ablation can result in axonal pathfinding defects (Hidalgo and Booth, 2000), suggesting that glia provide cues that guide axonal growth cones. Indeed, midline glia express guidance molecules such as Slit (Rothberg et al., 1990) that act as repellents to prevent ipsilateral axons from crossing the midline and commissural axons from recrossing (Battye et al., 1999; Kidd et al., 1999).

In some instances neurons seem to guide glial cell migration. In zebrafish, lateral line glia follow the axons of neurons in the lateral line mechanosensory organs (Gilmour et al., 2002). In mutants with misdirected axons, glia follow the roundabout route of axons. Furthermore, laser ablation of the extending lateral line axons stops glial migration (Gilmour et al., 2002). Similarly, in the *Drosophila* visual system, glial migration depends on photoreceptor axons as it does not occur if retina innervations are eliminated (Dearborn and Kunes, 2004). And in *dachsous* mutants, which have aberrant axonal projections from the retina, glia follow the abnormal axonal tracks (Dearborn and Kunes, 2004), supporting the notion that glia use these axons as a migration scaffold.

Modulation of synaptic activity

Although masters of electrical transmission, most neurons talk to their partners by releasing neurotransmitter molecules in the specialized structures where two neurons meet, synapses. Synaptic transmission and its plasticity are thought to underlie many nervous system properties, including learning and memory. In the last decade it has become evident that glia listen in on this communication and, in some cases, may be able to modulate it.

Synaptic roles for glia at the neuromuscular junction (NMJ) were demonstrated by studying *Xenopus* perisynaptic Schwann cells (PSC) that ensheath this synapse. High frequency stimulation of motor neurons results in decreased muscle activity as well as increased PSC Ca^{2+} levels (Jahromi et al., 1992; Reist and Smith, 1992). These observations suggested a model in which PSCs might detect acetylcholine released by the motoneuron, leading to elevated Ca^{2+} in these glia. Ca^{2+} elevation might, then, promote long-term depression in the muscle. To test this hypothesis, advantage was taken of the observation that PSCs express the metabotropic G protein-coupled acetylcholine receptor. Glial G proteins were blocked by injecting GTP-βS into the PSC. Remarkably, this was sufficient to block the depression of muscle activity (Robitaille, 1998). Moreover, activation of PSC G proteins by GTP-γS injection induced depression of muscle activity even under low frequency stimulation (Robitaille, 1998). This elegant study showed that glia play important roles in synaptic transmission and might affect processes such as long-term depression that are thought to be important in memory formation.

Many CNS synapses are ensheathed by astrocytes (Spacek, 1985; Grosche et al., 1999; Ventura and Harris, 1999), which secrete a number of molecules that might affect synaptic transmission. Among these, D-serine, a co-agonist of the NMDA receptor (Danysz and Parsons, 1998), has been implicated in long-term potentiation (LTP) and depression (LTD). The astrocytes that ensheath synapses of thalamic supraoptic nucleus (SON) neurons normally release D-serine, an endogenous NMDAR co-ligand in this brain region (Panatier et al., 2006). Astrocytes retract their processes from SON synapses in lactating female rats (Theodosis and Poulain, 1993), leading to a decrease in D-serine concentration in these synapses (Panatier et al., 2006). Interestingly, while normal LTP and LTD could be induced in the SON in virgin female rats, LTP and LTD could not be induced in lactating females, which have less perisynaptic D-serine, without addition of exogenous D-serine (Panatier et al., 2006). Consistent with roles for glial D-serine in synaptic activity, hippocampal neurons undergo LTP when cultured in the presence of astrocytes (Yang et al., 2003). When D-serine produced by cultured astrocytes was enzymatically degraded, LTP was blocked (Yang et al., 2003), suggesting that D-serine released by glia might also be important in the hippocampus.

The NMJ and D-serine studies are convincing findings of glial roles in modulation of synaptic transmission and emerging evidence suggests that this glial function might be quite widespread. For example, paralleling the NMJ findings, neurotransmitter release at synapses may result in increased astrocytic Ca^{2+} levels in many brain regions through what are thought to be GPCR-dependent mechanisms (Agulhon et al., 2008). Specifically, in cerebellar slices, neuronal activity elicits Ca^{2+} increases in Bergmann glial cells (Grosche et al., 1999; Kulik et al., 1999; Matyash et al.,

2001; Beierlein and Regehr, 2006; Piet and Jahr, 2007). Neuronal stimulation results in Ca^{2+} level increases in neighboring astrocytes in hippocampal slices (Pasti et al., 1997; Porter and McCarthy, 1997; Kang et al., 1998; Araque et al., 2002; Perea and Araque, 2007). In isolated retinas, flickering light induces transient increases in Müller glial Ca^{2+} levels, a process mediated by neuronal ATP release (Newman, 2005). Astrocytic Ca^{2+} responses can be triggered by a number of different neurotransmitters that activate glial mGluRs (Porter and McCarthy, 1996; Pasti et al., 1997; Fellin et al., 2004), γ-amino-butyric-acid B ($GABA_B$) receptors (Kang et al., 1998), muscarinic acetylcholine receptors (Araque et al., 2002; Perea and Araque, 2005), and endocannabinoid receptors (Navarrete and Araque, 2008).

More recently, dynamic regulation of Ca^{2+} concentrations has also been observed *in vivo* in response to physiological stimuli. *In vivo* two-photon Ca^{2+} imaging of ferret visual cortex showed that astrocytes respond to visual stimuli and that the astrocytic response exhibits the same tuning to stimulus orientation as nearby neurons (Schummers et al., 2008). This suggests that astrocytic Ca^{2+} is a reflection of underlying neuronal activity (Schummers et al., 2008). In a striking finding, the authors found that astrocytic tuning was maintained even in orientation pinwheels, suggesting that in the visual cortex there is tight spatial regulation of astrocytic processes, which might enable them to associate with particular neurons or synapses, and that astrocytes might possess microdomains that can independently undergo Ca^{2+} elevations in response to neuronal activation.

Other studies also support the hypothesis that astrocytes can respond to neuronal activation. Astrocytic Ca^{2+} imaging in the barrel cortex of anesthetized mice revealed

that glia respond to whisker stimulation (Wang et al., 2006). This response was delayed by 3 s from whisker stimulation and was likely mediated by synaptic glutamate spillover as it was reduced by inhibition of metabotropic glutamate receptors and did not require postsynaptic activity. In addition, astrocytic Ca^{2+} transients in sensory cortex could be detected in mobile mice. These Ca^{2+} transients trailed neuronal activation by approximately 2 s and were correlated with running behavior (Dombeck et al., 2007).

Thus, evidence from *in situ* and *in vivo* studies suggests that increased neuronal activity results in Ca^{2+} transients within astrocytes. What might be the role of this astrocytic Ca^{2+}? Could it be involved in regulating secretion from glia? An important study of neuron-glia co-cultures showed that increasing astrocytic Ca^{2+} levels using bradykinin led to NMDA receptor-dependent Ca^{2+} increases in neighboring neurons (Parpura et al., 1994). Several subsequent reports suggest that astrocytic Ca^{2+} elevations under certain conditions *in situ* can result in release of glutamate, which may modulate synaptic transmission through pre- or postsynaptic mechanisms (Bezzi et al., 1998; Fiacco and McCarthy, 2004; Lee et al., 2007; Navarrete and Araque, 2008). However, the evidence for glutamate release is indirect as it depends on pharmacological manipulations that might affect both glia and neurons (Agulhon et al., 2008). Furthermore, it is unclear if glutamate release can occur *in vivo* or if it has any physiological role. For example, to selectively activate astrocytes, the MrgA1 GPCR-coupled metabotropic receptor from DRG neurons was expressed only in astrocytes. Although astrocytic Ca^{2+} levels increased as expected upon stimulation with RF amide MrgA1 ligands, synaptic transmission was not affected (Fiacco et al., 2007), suggesting that astrocytic Ca^{2+} transients are not sufficient for glutamate secretion. This study does

not prove, however, that glutamate release cannot occur *in vivo* in response to neuronal activity as in this work astrocytes were activated in a non-physiological manner using a non-native receptor.

Stronger evidence suggests that astrocytes might affect synaptic transmission through ATP release. For example, Schaffer collateral (SC) stimulation evokes Ca^{2+} increases in astrocytes that associate with SC-CA1 synapses (Porter and McCarthy, 1996). This glial activation is thought to induce release of ATP that then suppresses presynaptic glutamate release (Pascual et al., 2005; Serrano et al., 2006). This mechanism presumably enables astrocytes to tonically suppress synaptic transmission, therefore enhancing the dynamic range of LTP. In agreement with this model, blocking astrocytic ATP release, by expressing a dominant-negative synaptobrevin 2 mutant, prevented induction of LTP or heterosynaptic depression *in situ* (Pascual et al., 2005). In support of these findings, GABA released from interneurons led to increased Ca^{2+} levels in astrocytes associated with SC-CA1 synapses and chelating Ca^{2+} within astrocytes or inhibiting ectonucleotidase activity, which is thought to convert the secreted ATP into adenosine, prevented heterosynaptic depression (Serrano et al., 2006).

Together, these results suggest that increased synaptic activity promotes glial Ca^{2+} accumulation that might, in turn, modulate synaptic transmission through secretion of neuromodulators. These findings hint at a more integral glial role in synaptic function beyond the usually ascribed glial roles in synaptic cleft homeostasis.

Synaptogenesis and circuit remodeling

A critical part of neurodevelopment is the formation of proper neuronal circuitry. Circuits arise by long-range guidance cues that guide axonal migration (Yu and Bargmann, 2001) as well as from local interactions that enable connections of the proper neurons through synapses (Colón-Ramos et al., 2007). As already mentioned, many synapses in the CNS are ensheathed by astrocytes (Spacek, 1985; Ventura and Harris, 1999) raising the possibility that glia might play a role in synapse formation and elimination.

Several studies suggest that astrocytes play important roles in synapse formation. A particularly useful approach has been to study the synaptogenic potential of highly purified retinal ganglion cells (RGCs) (Meyer-Franke et al., 1995) when cultured in the absence or presence of glia. These co-culture experiments have shown that addition of astrocytes or astrocyte-conditioned medium to a culture of RGCs leads to a ten-fold increase in synapse number as well as a dramatic increase in synaptic efficacy (Pfrieger and Barres, 1997; Ullian et al., 2001). Fractionation studies revealed that one glial component responsible for these effects is astrocyte-derived cholesterol, which enhances presynaptic function (Mauch et al., 2001). However, it is unclear whether cholesterol acts as a constituent of the plasma membrane or whether it can initiate signaling events.

The increase in synapse number induced by glia in RGC co-cultures is largely mediated by astrocyte-derived thrombospondins (TSPs), large extracellular matrix proteins. TSPs are sufficient to induce the formation of anatomically normal but silent synapses that are unresponsive to glutamate (Christopherson et al., 2005). TSPs consist

of a family of five homologous proteins (Adams and Tucker, 2000; Adams, 2001), all of which are synaptogenic (Barres, 2008). At least four TSPs are expressed in the developing mammalian brain, and mice lacking both TSP1 and TSP2 have fewer synapses (Christopherson et al., 2005), suggesting that TSPs promote synaptogenesis *in vivo*. The EGF-like type II domain of TSP1/2 binds to the α2δ subunit of the neuronal voltage-dependent Ca^{2+} channel and this interaction is required for synapse formation (C. Eroglu and B. Barres, personal communication). Additionally, mice treated with pregabalin or gabapentin, two α2δ antagonists, have defects in synapse formation (C. Eroglu and B. Barres, personal communication). The adult brain expresses TSP4 (Arber and Caroni, 1995), suggesting possible postdevelopmental roles for TSPs in circuit plasticity.

Like astrocytes, Schwann cells help to promote the formation of the *Xenopus* neuromuscular junction (Peng et al., 2003) through a TGF-β1 pathway (Feng and Ko, 2008). Furthermore, Schwann cells promote synapse formation between cultured spinal motor neurons (Ullian et al., 2004). Together, these findings suggest that promoting synaptogenesis or stabilizing immature synapses might be key glial activities.

In addition to stabilizing synapses, glia might also play a role in synapse elimination. For example, transplantation of immature astrocytes into the adult primary visual cortex of cats restored ocular dominance plasticity (Muller and Best, 1989), supporting the notion that glia are important for synaptic alterations. In *Drosophila*, glia engulf and consume degenerating axons in the mushroom body (Watts et al., 2003; Watts et al., 2004). Glia are also required for larval neuronal reorganization, as inhibiting endocytosis specifically within glia inhibits axon pruning (Awasaki and Ito, 2004).

Draper/CED-1, a protein involved in phagocytic clearance of apoptotic cells (Freeman et al., 2003), acts within glia to promote axonal pruning during development (Awasaki et al., 2006) as well as during injury (MacDonald et al., 2006). Interestingly, Draper binds to Shark, a protein similar to the immune system non-receptor tyrosine kinase Syk, through an immunoreceptor tyrosine-based activation motif (Ziegenfuss et al., 2008). Thus, glia may use pathways resembling those of the immune system to eliminate axons. This mechanism might be conserved in mammals as transcripts of phagocytic genes, including CED-1/Draper, are highly enriched in astrocytes (Cahoy et al., 2008).

When cultured in the presence of astrocytes, RGCs upregulate expression of C1q (Stevens et al., 2007), a protein that initiates the classical complement cascade. C1q binds to pathogens or dead cells and triggers a protease cascade that eliminates pathogens by phagocytosis (Gasque, 2004). In the developing brain, C1q localizes to synapses, presumably tagging them for elimination; consistent with this hypothesis, C1q null mice have too many synapses (Stevens et al., 2007).

In sum, ample evidence suggests the glia play important roles in synapse formation and elimination.

Glial ablation experiments

The utility of glia-free neuronal cultures in the elucidation of glial roles in synaptogenesis suggests that removal of glia *in vivo* might be a powerful strategy for uncovering glial roles in the nervous system. *In vivo* glial removal has been attempted

using several approaches. In many instances, these experiments have failed to yield clear results, mainly due to the neuronal loss that followed glial ablation. A brief overview of glial removal experiments in different settings follows.

CNS glial ablations

To ablate glia in mice, the glial fibrillary acidic protein (GFAP) promoter, which is expressed in some glia as well as in other cell types, has been used to drive expression of the herpes simplex virus-thymidine kinase (HSV-TK) toxin gene (Brenner et al., 1994). Mice carrying the GFAP pro::HSV-TK transgene display granule cell loss as well as Purkinje cell dendritic defects (Delaney et al., 1996; Bush et al., 1998; Sofroniew et al., 1999). The granule cell loss was attributable to excitotoxicity as it could be prevented by treatment with NMDAR antagonists (Delaney et al., 1996). The Purkinje cell dendritic defects were most likely secondary to the granule cell loss as these dendrites are shaped by the granule cell input (Delaney et al., 1996). Ablation of Bergmann glia in the cerebellum yielded largely the same results (Cui et al., 2001).

The myelin basic protein (MBP) promoter drives gene expression in oligodendrocytes (Takahashi et al., 1985). MBP pro::HSV-TK transgenic mice show a loss of oligodendrocytes in the cerebellum. These animals show decreased myelination as well as tremors, seizures, and premature death, but have not been studied beyond myelination (Mathis et al., 2000). Importantly, a significant portion of oligodendrocytes remains after ablation and their continued proliferation might mask defects that would be observed after removal of all oligodendrocytes.

Schwann cell ablations

Elimination of the neuregulin receptors ErbB2/3 results in mutant mice that lack most Schwann cell precursors. Even the few Schwann cells that are born fail to migrate to the periphery, thus neuromuscular junctions (NMJs) are devoid of glia. Although motor neurons do migrate in this setting, defects in their fasciculation are observed. However, detailed analysis of these bare NMJs is impossible since the vast majority of motor and sensory neurons in the DRG undergo cell death shortly after axonal migration (Riethmacher et al., 1997; Woldeyesus et al., 1999; Lin et al., 2000).

Taking advantage of a monoclonal antibody specific for perisynaptic Schwann cells, these cells have been ablated from NMJs in adult frogs by complement-induced lysis (Reddy et al., 2003). In ablated NMJs, axonal retraction was seen during the course of a week. No significant short-term defects in synaptic function were observed after ablation but before retraction (Reddy et al., 2003), however, synaptic functions such as activity-induced depression, known to be regulated by the perisynaptic Schwann cell (Robitaille, 1998), were not tested. Two possible technical concerns limit any conclusions that can be drawn from this experiment. The neuronal degeneration that is observed, as indicated by the retracting axons, suggests that glia might play some trophic roles. Furthermore, axonal Schwann cells, which are not ablated by this treatment, might compensate for the loss of some perisynaptic Schwann cell roles. Schwann cell ablation studies have clearly shown that these cells provide trophic support to neurons and help induce the formation of the NMJ. However, these studies have been unable to assess the presence of more active Schwann cell roles that are suggested by experiments that modulate GTP levels in perisynaptic Schwann cells (Robitaille, 1998).

Drosophila glial ablations

Glia in *Drosophila* have been ablated in two ways. First, in *glial cells missing* (*gcm*) mutant animals the cells destined to become glia instead express neuronal fates (Hosoya et al., 1995; Jones et al., 1995). Since these mutants lack some glial functions, they have proven useful in analyzing glial roles in neuronal function. In addition, glial *gcm*-expressing cells have been ablated by expression of ricin A, a protein translation inhibitor (Hidalgo et al., 1995; Booth et al., 2000; Hidalgo and Booth, 2000). Characterization of *gcm* mutants and animals lacking *gcm*-expressing cells revealed that glia provide neurons with trophic support, guide axonal migration, provide cues for nerve fasciculation, and help form the blood-brain barrier (Hidalgo et al., 1995; Hosoya et al., 1995; Jones et al., 1995; Booth et al., 2000; Hidalgo and Booth, 2000; Stork et al., 2008).

Although the analysis of *gcm* mutants has been fruitful, the transformation of glia into neurons is not complete in this background. For example, it appears that the converted cells retain some glial characteristics since they divide and migrate in the pattern of glia (Hosoya et al., 1995; Jones et al., 1995; Vincent et al., 1996); and some glial cells, such as perineurial glia, are specified normally in *gcm* mutants (Awasaki et al., 2008). Significantly, while *gcm* mutants have revealed glial roles in nervous system development, detailed analysis of glial roles in neuronal function is hindered by the neuronal death that occurs in these mutants (Hosoya et al., 1995; Jones et al., 1995). Neuronal cell death is also observed when ablating *gcm*-expressing glia (Hidalgo et al., 1995; Booth et al., 2000; Hidalgo and Booth, 2000).

Other nonspecific methods used for glial ablations in a number of species have included radiation (Kalderon et al., 1990; Pippenger et al., 1990), antimitotic agents (Smith et al., 1984; Politis and Houle, 1985), and toxic compounds that inhibit cellular metabolism (Khurgel et al., 1996; Largo et al., 1996), although complete and consistent glial removal could not be achieved in these settings.

In summary, glial ablation experiments have clearly shown two glial roles in the nervous system: trophic support of neurons and developmental requirements, in particular for axon guidance. These experiments have been less useful in characterizing postdevelopmental glial roles since often neurons degenerate in the absence of glia, precluding further characterization. Further, most experimental manipulations to remove glia have not been able to achieve complete glial removal. Thus, a novel experimental setting is needed in which removal of glia can be performed efficiently and does not affect neuronal survival.

Sensory organs as simplified models of the nervous system

As just described, analysis of neurons in the absence of glia is often precluded by the trophic support glia provide neurons. Moreover, it is often difficult to remove all glia present in a particular region of the nervous system or to assess neuronal dysfunction at single cell resolution after removal of a limited number of glia. These problems might be limited, or even overcome, by focusing on sensory organs, since these self-contained structures typically contain sensory neurons of a specific class associated with only a few

glial cells. Sensory organs provide an attractive model of the nervous system in general since the sensory input (light, sound, temperature) can be experimentally controlled and perturbations of the organ might result in altered behavior. In addition, the small number of neurons and glia in these organs makes them experimentally accessible. Thus, one approach to understand glial functions *in vivo* is to study them in the context of sensory perception. A brief description of some sensory organs and glial roles within them follows.

Retina

Vision is mediated by rod and cone photoreceptor cells. Opposed to these photoreceptors is a monolayer of support cells, the retinal pigment epithelium (RPE), whose apical microvilli act as membrane sheaths that surround the terminal third of individual photoreceptor cilia (Steinberg et al., 1977). RPE cells play important roles in supporting photoreceptor function. Like astrocytes, RPE cells associate closely with blood vessels and mediate the transport of nutrients, particularly glucose, to the photoreceptor cells (Strauss, 2005). RPEs also maintain the pH and regulate the ionic composition of the subretinal space to enable photoreceptor excitability (Strauss, 2005). In photoreceptors, 11-*cis*-retinal is converted to all-*trans*-retinal after photon detection, and RPE cells reisomerize all-*trans*-retinal and make it available to the photoreceptors for their continued function (Baehr et al., 2003). The photoreceptor outer segments are continually shed, presumably due to the high oxidative stress within the cilium, and RPE cells are responsible for phagocytosing and recycling of these components (Gal et al.,

2000; Finnemann, 2003). Thus, although RPEs might not be usually defined as glia, they perform several functions generally attributed to glia.

Taste buds

Taste buds are onion-like structures composed of 50-100 cells whose apical surfaces barely protrude from the taste pore in the tongue epithelium (Roper, 1989) (Roper, 1992). At least three cell types are present in the taste bud based on electron microscopical criteria. Type II and III cells are elongated and end with microvilli thought to have sensory roles, and type III cells synapse onto presumably afferent fibers (Royer and Kinnamon, 1991). Type I cells are thought to be support cells since they have several glia-like properties. They express the glial glutamate/aspartate transporter (GLAST) (Lawton et al., 2000), might regulate K^+ levels within the taste bud (Bigiani, 2001), and maintain low extracellular ATP levels by expressing an ecto-ATPase (Bartel et al., 2006). This last function is similar to neurotransmitter clearance at synapses by astrocytes as type II cells, which do not have synapses, are thought to release ATP upon gustatory stimulation (Finger et al., 2005). Morphologically, type I support cells are distinguished by membrane-bound granules in the apical cytoplasm, which presumably are secreted and contribute to the amorphous substance present in the taste pore (Whitear, 1976). Furthermore, these glia-like cells are the most abundant cell type in the taste bud and might ensheath and insulate the taste receptors within each taste bud (Pumplin et al., 1997).

Olfactory epithelium

The detection of volatile compounds is mediated by about 1,000 olfactory receptors (Buck and Axel, 1991) that reside in the cilia of olfactory sensory neurons. These neurons, residing in the olfactory epithelium that lines the dorsal cavity of the nose, project a single dendrite that extends through the olfactory epithelium and ends in cilia that have access to the nasal cavity (Morrison and Costanzo, 1990, 1992). Surrounding the sensory neurons are glia-like cells, named sustentacular cells, which produce part of the mucus in which the sensory cilia reside (Okano and Takagi, 1974). These support cells perform a number of functions: they physically and chemically insulate olfactory sensory neurons (Breipohl et al., 1974; Nomura et al., 2004), actively phagocytose dead cells (Suzuki et al., 1996; Makino et al., 2009), and regulate the extracellular ionic environment (Getchell, 1986). Further, these cells are electrically coupled to each other (Vogalis et al., 2005) and, like astrocytes, exhibit complex Ca^{2+} dynamics when stimulated with extracellular ATP, although the physiological importance of these dynamics is not known (Hegg et al., 2009). Olfactory neurons are continually replaced, and sustentacular cells seem to promote the generation of new neurons in adult animals by producing neuropeptide Y, a mitogenic factor for olfactory neuron precursor cells (Hansel et al., 2001).

The Grueneberg ganglia

The Grueneberg ganglion is a structure composed of about 500 cells found at the tip of the nose in mammals (Fuss et al., 2005; Brechbuhl et al., 2008). The sensory

neurons of this ganglion are easily identified by expression of olfactory marker protein (OMP) and by their fasciculated axons that project to the olfactory bulb (Fuss et al., 2005; Koos and Fraser, 2005; Roppolo et al., 2006; Storan and Key, 2006). Although they do not possess distinguishable dendrites, these neurons project 30-40 cilia each. The cilia and at least part of the cell body are ensheathed by glial cells that stain with the astrocytic markers glial acidic fibrillary protein (GFAP) and S100β (Brechbuhl et al., 2008). Interestingly, the cilia are embedded in the glial cell and have no access to the nasal cavity (Brechbuhl et al., 2008). Grueneberg ganglia may detect volatile compounds, perhaps alarm pheromones (Brechbuhl et al., 2008), suggesting that pheromones must pass through the ensheathing glial cell before they can interact with the cilia-localized receptors. Because this sensory ganglion has been recognized only recently, not much is known about any roles that glia play in its function.

Insect sensory organs

Insects possess several types of sensory organs that are similar to each other and are conserved among species (Hallberg and Hansson, 1999; Mitchell et al., 1999). The mechanosensory and chemosensory sense organs, so called type I organs, are the main insect external sensilla. The former are composed of single bipolar neurons (Hartenstein and Posakony, 1989) while the later contain five neurons (Pollack and Balakrishnan, 1997). The neuronal cell bodies are located near the epidermis and project ciliated dendrites that approach the cuticle. The dendrites are surrounded by three concentric sheaths of support cells. The inner sheath is made by the thecogen (sheath) cell which is

penetrated by the growing dendrite during development (Hartenstein and Posakony, 1989). The very tip of the dendrite is not ensheathed by the thecogen but instead is embedded in an electron-dense extracellular cap secreted by the thecogen (Pollack and Balakrishnan, 1997). The two outer sheaths are formed by the wrapping of the trichogen (bristle) and tormogen (socket) cells around the dendrite (Hartenstein and Posakony, 1989). A fourth support cell is present in some sensory organs where it ensheathes part of the neuronal cell body and the initial part of the axon (Felt and Vande Berg, 1976).

The morphogenesis of these sensilla has been studied extensively (Hartenstein and Posakony, 1989) as this organ derives from a single lineage, thus providing a nice model for studying the segregation of asymmetric cell fates. However, less is known about the functions of the support cells in sensory organ function. The major proposed role of these support cells is to pump K^+ into the receptor lymph cavity (Hartenstein, 1997; Pollack and Balakrishnan, 1997). Another proposed role for these cells is secretion of odor-binding proteins, which might facilitate odor recognition by neuronal receptors (Vogt and Riddiford, 1981; Vogt et al., 1991). This latter function is probably limited to support cells of taste organs (Shanbhag et al., 2001) and olfactory sensilla (McKenna et al., 1994; Pikielny et al., 1994).

Sensory organs and glia in *C. elegans*

Like other animals, the nematode *Caenorhabditis elegans* monitors its environment with sensory neurons. Most of these neurons are organized in sensory organs that are similar in morphology to those found in insects. *C. elegans* sensilla are

composed of one or more sensory neurons associated with two support cells: a sheath cell that ensheathes the ending of the sensory dendrites and a socket cell that wraps around the cilia present at the tip of these dendrites (Ward et al., 1975). Sheath and socket cells are closely associated with neurons (Ward et al., 1975) and derive from ectodermal lineages, their sister cells being either neurons, other glia, or epithelial-like cells (Sulston et al., 1983). Four sheath glia – the cephalic sheath cells – extend processes that ensheath the nerve ring, the main neuropil of the animal, where association of these glia with specific synapses has been observed (White et al., 1986; Colón-Ramos et al., 2007).

Sensory neurons and cilia function

The neurons of most sensory organs, including those of *C. elegans*, possess dendrites that project one or more non-motile cilia (Wheatley et al., 1996). These sensory cilia are positioned at the interface between an animal and its environment and are believed to be the sites of sensory transduction. The ability of cilia to act as sensors is due in part to their specialized morphologies which allow for compartmentalization of signaling components such as cell-surface receptors, signal transduction molecules, and specialized ion channels (Pazour and Witman, 2003; Efimenko et al., 2006; Singla and Reiter, 2006). Sensory cilia, like motile cilia, nucleate from a centriolar-like structure termed the basal body, or the transition zone in *C. elegans* (Perkins et al., 1986). Most sensory cilia are composed of an inner doublet microtubule structure which transforms into an outer segment composed of single microtubules (Rosenbaum and Witman, 2002).

Cilia architecture arises through a transport mechanism that moves ciliary proteins from the basal body to the tip of the cilium. Because it was first observed in the flagella of *Chlamydomonas reinhardtii* (Kozminski et al., 1993; Kozminski et al., 1995), this process is named intraflagellar transport (IFT). Anterograde transport within the cilium is powered by two kinesin-2 molecular motors that move IFT particles and cargo to the distal part of the cilium (Orozco et al., 1999; Snow et al., 2004). Interestingly, only one of the kinesin-2 motors, OSM-3, is capable of transport along the distal singlet microtubules (Snow et al., 2004). The IFT particle, along with the anterograde motors, is then transported back to the base of the cilium by a dynein motor (Orozco et al., 1999; Signor et al., 1999; Snow et al., 2004).

Observation of the movements of the IFT particle by light microscopy suggested that this macromolecular complex must be rather large. Taking advantage of this, Rosenbaum and colleagues isolated IFT particles from *Chlamydomonas* in sucrose gradients and determined that the IFT particle is composed of two biochemically-defined complexes, A and B (Cole et al., 1998; Cole, 2003). This also led to the identification of proteins that compose the IFT particles. Since then, a large number of ciliary proteins that associate with the IFT particle have been described both in *Chlamydomonas* as well as *C. elegans*. The current understanding suggests that IFT-A binds to the Kinesin-II motor while IFT-B binds OSM-3 (Snow et al., 2004; Ou et al., 2005), however, because the A and B complexes are bound together by the BBS-7/8 proteins, the IFT particle moves as a whole (Blacque et al., 2004). Additional complexity is suggested by the observation that OSM-3 is required for the formation of singlet distal segments in some neurons but not others (Mukhopadhyay et al., 2007).

To obtain a complete list of genes required for cilia biogenesis and function, proteomic and comparative genomic studies have been performed that have identified sets of proteins conserved in all cilia (Avidor-Reiss et al., 2004; Emoto et al., 2004; Blacque et al., 2005; Efimenko et al., 2005). In *C. elegans*, the ability to purify single cell types has allowed the comparison of the transcriptome of neurons with different types of modified sensory cilia with the goal of identifying factors required for cilia diversification (Colosimo et al., 2004).

While the cataloguing and characterization of ciliary genes is leading to a fuller understanding of ciliary transport, less is known about the cargo the IFT particle carries. Although many signaling molecules localize to cilia (Efimenko et al., 2006; Singla and Reiter, 2006), how they get there remains poorly understood. While it is reasonable to expect that signaling molecules move into the cilium by IFT, few such proteins have been observed undergoing movements along cilia. The transient receptor potential channels OSM-9 and OCR-2 (Colbert et al., 1997; Tobin et al., 2002), for example, have been observed undergoing IFT (Qin et al., 2005). Other signaling proteins that have been shown to undergo IFT are IFTA-2, a Rab-like factor with some cilia defect phenotypes (Schafer et al., 2006) and TUB-1, a gene with roles in cilia function and lipid homeostasis (Mukhopadhyay et al., 2005). In general, membrane proteins are thought to get access to the cilium in a Rab8-mediated process that might link vesicles transported along the dendrite with the IFT particle so that transmembrane proteins can subsequently enter the cilium (Nachury et al., 2007).

Mutations in many *C. elegans* genes encoding IFT complex subunits lead to animals that have sensory defects in chemotaxis, odortaxis, and avoidance of areas of

high osmolarity (Scholey, 2003; Inglis et al., 2006). They also have defects in a practical assay, the ability of some sensory neurons to uptake lipophilic fluorescent dyes (Herman, 1984; Hedgecock et al., 1985). Although the mechanisms of dye uptake are unclear, only some of the amphid neurons that presumably have access to the dye through the amphid channel are able to take it up (Perkins et al., 1986). In wild-type animals, 6 amphid neurons (ADL, ASH, ASI, ASJ, ASK, and AWB) and both phasmid neurons (PHA and PHB) uptake DiI (Herman, 1984). Uptake of FITC is largely similar except that instead of AWB, ADF takes up dye (Hedgecock et al., 1985). Most mutants that affect cilia morphology and function exhibit abnormal dye filling (Dyf phenotype) (Perkins et al., 1986), and screens to identify Dyf animals have yielded many mutants with abnormal ciliary function (Starich et al., 1995).

The amphid sensory organs

The main sensilla of *C. elegans* are the bilaterally symmetric amphids (Figure 1.1). The amphid neurons mediate many behaviors including chemotaxis (Ward, 1973), thermotaxis (Hedgecock and Russell, 1975), high osmolarity avoidance (Culotti and Russell, 1978), dauer pheromone detection (Riddle et al., 1981), odortaxis (Bargmann, 1993), and nose touch (Kaplan and Horvitz, 1993). Mutants for each of these behaviors have been isolated (Dusenbery et al., 1975; Hedgecock and Russell, 1975; Culotti and Russell, 1978; Albert et al., 1981; Swanson and Riddle, 1981; Bargmann et al., 1993; Kaplan and Horvitz, 1993).

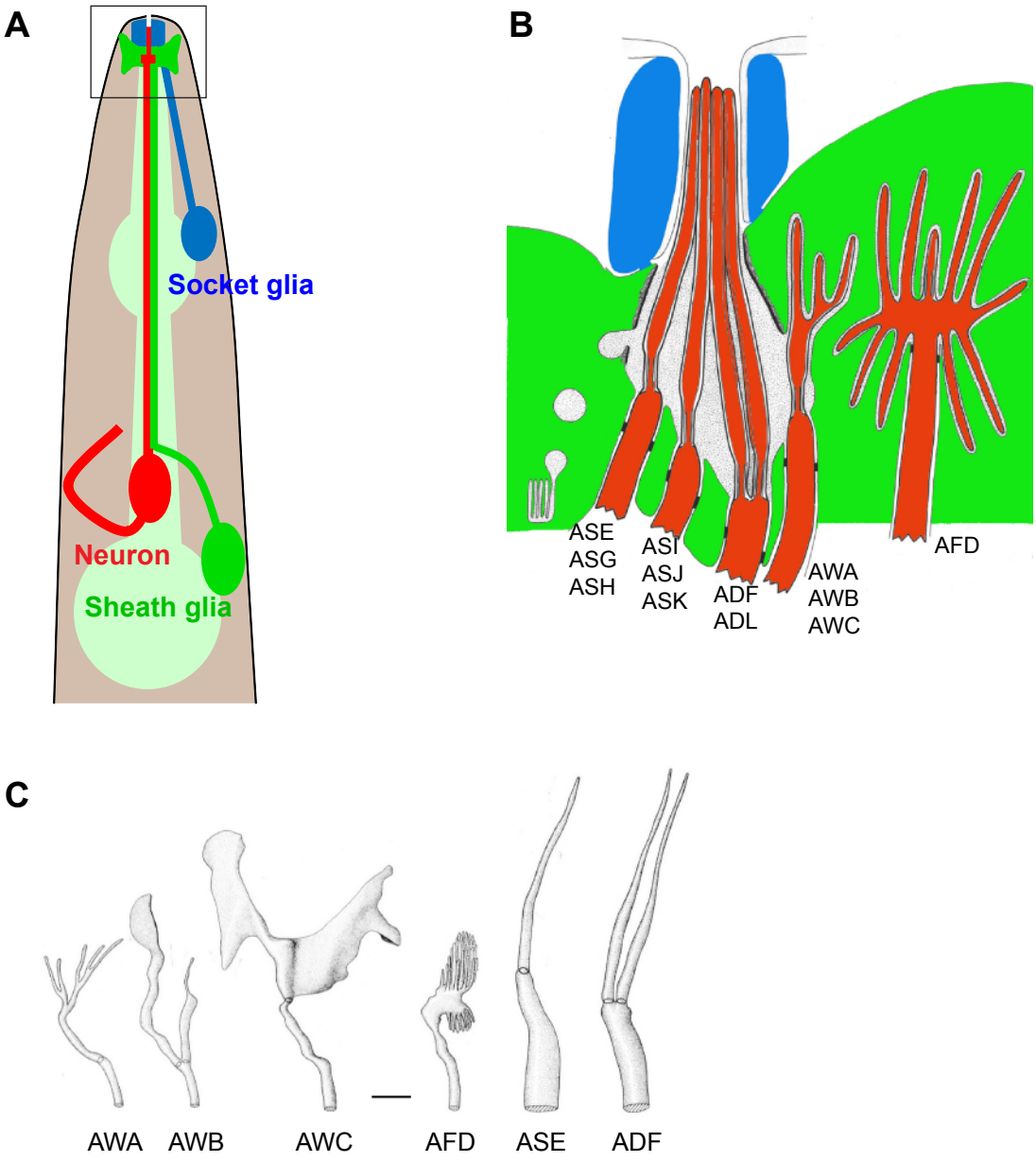

Figure 1.1: The amphid sensory organ

(**A**) Cartoon representation of the amphid sensory organ. Twelve sensory dendrites, only one of which is depicted, bundle together and project to the anterior tip of the animal. (**B**) Higher magnification of the square in **A** showing the sensory cilia. Eight cilia (only 3 shown in red) enter the socket channel (blue); three cilia enter the sheath channel briefly (one shown) but reside in the sheath glia (green); the AFD cilia are completely embedded in the glia. The location of each neuron is indicated. (**C**) The five types of amphid cilia morphology. Six simple cilia are present, only ASE is shown. Two doubly ciliated neurons are found in the amphid, ADF and ADL. Scale bar, 1 μm. Image in **B** adapted from (Perkins *et al*, 1986). Image in **C** adapted from (Ward *et al*, 1975).

The amphids are composed of 12 sensory neurons, a sheath cell, and a socket cell. In adult animals, each neuron projects a single, 100 μm long, unbranched dendrite to the tip of the nose where the dendrites end in modified cilia (Ward et al., 1975; Ware et al., 1975; Perkins et al., 1986), Figure 1.1B. The sheath cell also projects a single process that ensheathes the last portion of the 12 fasciculated dendrites. The socket glial cell makes an opening in the cuticle through which some of the ciliated dendrites can access the environment (Figure 1.1B). To make this opening, the socket cell wraps around and forms belt junctions onto itself in a manner analogous to insect tormogen cells.

Based on their ciliary morphology, the amphid neurons can be assigned to four classes (Figure 1.1C): wing-like, comprised of the AWA, AWB, and AWC neurons, whose modified dendritic cilia spread within the sheath glial cell; finger-like, comprised of the AFD neuron, whose dendritic ending contains several microvilli-like structures that are also embedded entirely within the sheath; singly ciliated, comprised of the ASE, ASG, ASH, ASI, ASJ, ASK neurons which possess an unmodified cilium; and doubly ciliated, consisting of the ADF and ADL neurons (Ward et al., 1975; Perkins et al., 1986). The singly and doubly ciliated neurons penetrate through the sheath and access the outside environment through the socket channel.

The sheath cell channel in which the cilia reside is filled with an electron-dense matrix which appears to be secreted by the sheath cell (Wright, 1980). The matrix is transported in membrane-bound vesicles that can be seen fusing with the channel lumen (Ward et al., 1975; Wright, 1980; Perkins et al., 1986). Although the chemical composition of this matrix remains largely unknown, the sheath glia produce a number of factors predicted to be secreted including collagens, metalloproteases, immune-like short

peptides, etc (work of Maya Tevlin (Bacaj et al., 2008)). Resembling the amphids, the phasmids are sensilla located in the tail. Each phasmid is composed of two neurons, a sheath, and a socket cell. They are thought to act as a second chemodetector in the tail and might enable the animal to perform nose-to-tail gradient measurements (Hilliard et al., 2002).

The amphid as a model for glia-neuron interactions

The amphid is an excellent setting for studying sensory cilia development. We reasoned that the amphid might also be an appropriate model in which to study glia-neuron interactions since it would be possible to remove the sheath glia, which contacts the sensory neurons, and observe neuronal function in its absence. Because amphid neurons have been well characterized, the function of many of them can be monitored by behavioral assays, and any defects observed can be ascribed to dysfunction of a particular sensory neuron. The anatomy of the amphid suggests that the sheath cell might be required for the development and function of amphid neurons. Indeed, anecdotal reports have indicated that this might be the case. Embryonic sheath and socket ablations resulted in neurons that inappropriately associate with sockets of other sensilla found in the head (Sulston et al., 1983). The sheath glia is required for dauer entry (Vowels and Thomas, 1994), and limited sheath ablations yielded animals with defects in chemotaxis and osmolarity sensation (Bargmann et al., 1990). Furthermore, in mutants with abnormal cilia morphology, matrix-filled vesicles accumulate within the sheath glia (Lewis and Hodgkin, 1977; Perkins et al., 1986), suggesting that dendrites might control

the rate of glial secretion. Together, these results suggest that the sheath glia might influence neuronal function, warranting further examination.

In this thesis, I attempt to extend our knowledge of sensory organ development and function by investigating sensory cilia development as well as the roles that glia play within these organs.

Chapter 2

Developmental requirements for glia in sensory organs

Summary

The nervous system emerges from the coordinated development of neurons and glia. To uncover the roles glia play in neuronal development, one would like to examine the effects of removing glia. This approach proves difficult in most species as glia are required for neuronal survival. To overcome this limitation, we have focused on the sensory organs of *C. elegans*, where we find that neurons survive even after ablation of sensory organ glia. Further, in the absence of glia, the dendrites of sensory neurons fail to extend normally, revealing a potential role for glia in dendrite formation.

Uncovering glial roles

The nervous system is composed primarily of two cells types: neurons and glia. The birth and morphogenesis of these cells must be precisely coordinated to create the proper cellular architecture. For example, to generate the correct ratio of neurons to glia, each cell type secretes mitogenic and survival factors that control the abundance of the other (Banker, 1980; Riethmacher et al., 1997; Hidalgo et al., 2001). Likewise, since many neurons are born away from their final position within the nervous system, they must migrate to reach their proper location and these movements can be orchestrated by glia, which secrete cues to guide neuronal migration (Battye et al., 1999; Kidd et al., 1999). Glia can also act as the substrate upon which neurons migrate (Rakic, 1971; Edmondson and Hatten, 1987).

A straightforward and unbiased approach to identify glial roles in nervous system assembly is to remove glia and monitor neuronal development. To observe neuronal development in the absence of their associated glia, we have focused on the nematode *C. elegans*. The nervous system of the *C. elegans* hermaphrodite is composed of 302 neurons whose morphology and connectivity has been described (Ward et al., 1975; White et al., 1986). Moreover, the morphology and location of each of the 50 glial cells of the animal is also known. These glia are all associated with sense organs, with each sensory neuron contacting only a few glial cells in a stereotyped manner.

Within *C. elegans*, we have studied the amphid sensory organs. Each amphid is composed of twelve ciliated sensory neurons which project their dendrites to the tip of the animal; a sheath glial cell which ensheathes the terminal part of the dendrites; and a

socket glial cell (Ward et al., 1975). Thus, the amphid sensilla provide a suitable model for investigating glia-neuron interactions *in vivo* as there is a single major glial cell, the neurons possess elaborate morphologies, and neuronal function can be assessed by behavioral assays.

Results

Glia are not required for neuronal survival in *C. elegans*

To ask whether the amphid sheath glia is required for amphid neuron survival, we performed laser ablation (Bargmann and Avery, 1995) of the amphid sheath glial precursor cell. Embryonic ablations in *C. elegans* are facilitated by the almost invariant cell lineage, which has been determined (Sulston and Horvitz, 1977; Sulston et al., 1983). Success in ablating the cell was judged by lack of *vap-1* pro::GFP expression, an amphid sheath cell marker, as well as by visual inspection for the absence of the sheath glial cell body under Nomarski optics. The strain also carried an *odr-1* pro::RFP transgene to visualize the AWC neuron. In 3/3 animals, ablation of the sheath glial precursor cell did not affect neuronal survival (Figure 2.1B).

We also observed no amphid neuron cell death when genetically ablating most glia in the animal (Figure 2.1, C-D). To perform these ablations, a 400 bp *lin-26* promoter region, which drives expression in some hypodermal and most glial cells, including the amphid sheath glia, but not in neurons (Landmann et al., 2004), was used to express the apoptosis-inducing protein EGL-1 in amphid sheath glia in early embryos.

However, we noted that genetically ablated animals were rather unhealthy, probably because the *lin-26* promoter expresses in many cells including hypodermal cells. In fact, reconstruction by electron microscopy of one such animal revealed large, extracellular, vacuole-like spaces filled with a light-staining matrix. Presumably, these correspond to the empty space left after ablation of a large number of cells.

To ablate glia after the amphid sensilla have formed, a 2 kb promoter region of the *F16F9.3* gene was used to drive expression of an attenuated diphtheria toxin (DT-A^{G53E}), a protein synthesis inhibitor that catalyzes the ADP-ribosylation of eukaryotic aminoacyl-transferase II (EF-2) (DeLange et al., 1979; Fares and Greenwald, 2001). The *F16F9.3* promoter drives expression in amphid and phasmid sheath cells (work of Maya Tevlin in our laboratory), the phasmid being a sensory organ in the tail similar to the amphid. Expression in the amphid initiates at the three-fold stage of embryogenesis, after amphid morphogenesis is complete. We found that neuronal survival was also unaffected by these post-embryonic ablations. In more than 100 laser-ablated animals and more than 500 genetically ablated animals scored, no amphid neuronal death was observed as judged by marker expression (see Chapter 3). Further, in all sheath-ablated animals, amphid neurons expressed appropriate markers [e.g. *odr-3* and *odr-10* (AWA), *str-1* (AWB), *odr-1* (AWC), *gcy-8* (AFD), *gcy-5* (ASER), T08G3.3 (ADF)] indicating normal gross differentiation. Thus, in the *C. elegans* amphid, sheath glia are dispensable for neuronal survival and maintenance of cell fate.

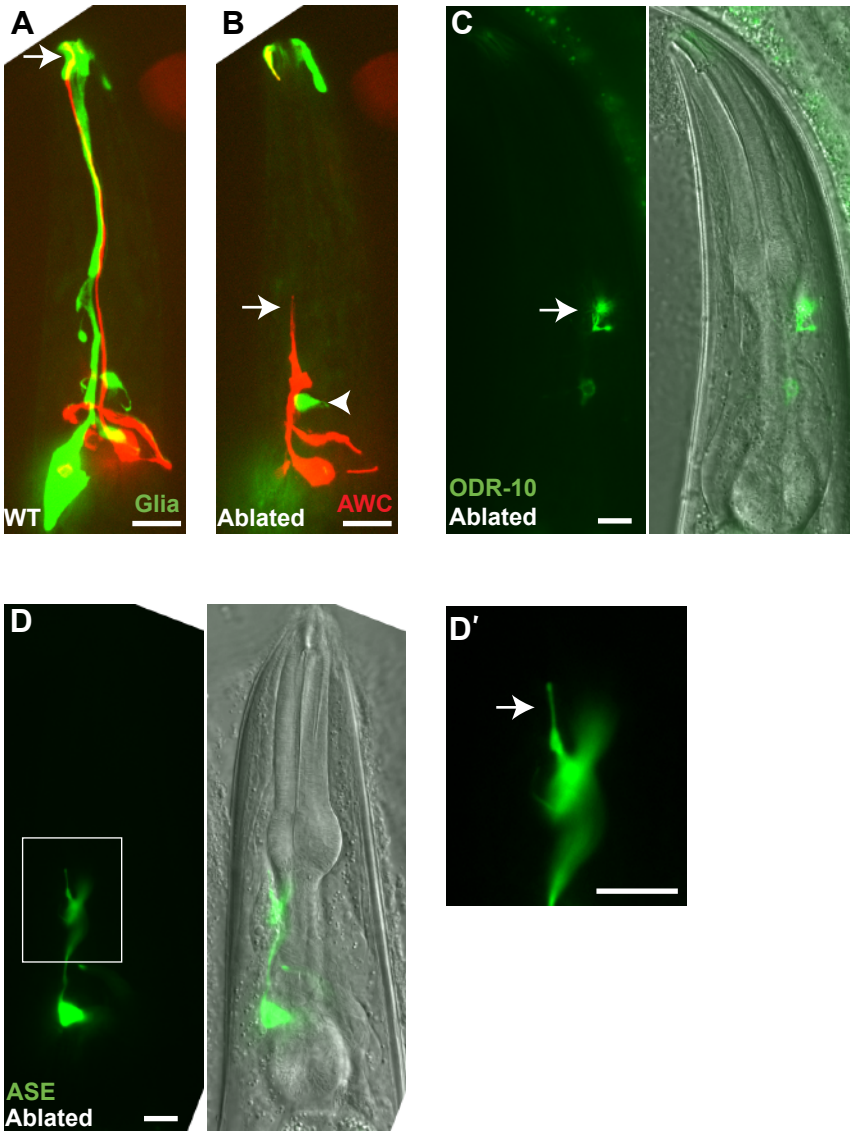

Figure 2.1: Embryonic glia ablation results in short sensory dendrites

(**A, B**) Animals bearing *odr-1* pro::RFP (AWC, red) and *vap-1* pro::GFP (sheath glia, green) were subjected to embryonic laser ablation of the sheath glia precursor cell in the left or right amphid. **A**, a wild-type amphid; **B**, contralateral amphid of the same animal in which the sheath precursor cell was ablated (the GFP at the anterior tip is from z-stacks of the contralateral amphid). The glia promoter used also expresses faintly in the AFD neuron (green, arrowhead). (**C**, **D**) Expression of the death-promoting factor EGL-1 in most glia of the animals, including the amphid sheath glia, results in short dendrites. Cilia appear to form normally in these neurons as the odorant receptor ODR-10 localizes normally to the cilia of the AWB neuron (**C**) and cilia morphology appears normal (**D**). (**D′**) Higher magnification of the rectangle in D. Anterior is up. Scale bar, 10 μm.

A developmental role for sheath glia in determining dendrite length

To determine if the sheath glia plays any role in neuronal morphogenesis, we examined neurons within amphids in which the sheath glial precursor cell had been ablated. In 3/3 sheath-ablated amphids, the AWC dendrite failed to project to the tip of the animal, instead displaying 20-50% of the wild-type length (Figure 2.1B). The contralateral mock-ablated amphids of these same animals were normal (Figure 2.1A).

Laser ablation of the sheath glial precursor cell also removes the URB neuron, its sister cell. To rule out the unlikely scenario that the observed morphological defects are due to URB ablation, sheath glia were also genetically ablated during early development by expression of the apoptosis-inducing gene *egl-1*. Transgenic animals displayed the same dendrite length defects observed in laser-ablated animals (Figure 2.1, C-D). Abnormal dendrite length was observed for all amphid neurons tested. In ablated amphids, the twelve dendrites appeared bundled and had the same length based on observation of animals expressing markers in two or more amphid neurons. Examination of short dendrites in the same animal in different larval stages revealed that the dendrites increased in size as the animal grew in length during larval development. Thus, glia are required specifically for embryonic dendrite growth.

The short dendrites of glia-ablated animals contain sensory cilia

To determine the extent of dendritic defects in the absence of glia, we examined the cilia of the short dendrites that result after glial removal. Imaging of the ASER

neuron cilium in *lin-26* pro::*egl-1*animals using fluorescence microscopy revealed that abnormally short dendrites contained a grossly normal cilium (Figure 2.1D). Thus, cilia length was normal, approximately 7 μm, and cilia shape appeared wild-type at the resolution afforded by light microscopy. To assay cilia integrity, at least partially, we asked whether these cilia can accumulate proteins that normally reside within them, such as sensory transduction molecules. Specifically, we checked the localization of ODR-10, a G protein-coupled receptor normally found in the AWA neuron cilia. Proper ciliary localization of an ODR-10::GFP fusion protein was observed in the short dendrites of the AWB amphid neuron indicating that proper intraflagellar transport occurs normally in glia-ablated animals (Figure 2.1C). Thus, glia are required for establishing dendrite length and are not required for generating sensory cilia.

Glial removal does not affect axon development

Examination of glia-ablated animals showed that axon morphology appeared grossly normal. Further, in glia-ablated animals *str-2* pro::GFP expression was always limited to a single AWC neuron. Asymmetric *str-2* expression requires axon-axon contact between the two AWC neurons (Troemel et al., 1999), suggesting that the two axons form properly in absence of glia. Therefore, the morphological defects observed are limited to dendrites and are not likely to result from gross defects in amphid sensory organ development as the axons develop properly in glia-ablated amphids.

Discussion

Glia are not required for neuronal survival in *C. elegans*

Here we demonstrate that *C. elegans* provides a good model for glial studies as specific removal of glia associated with a set of neurons allows examination of the resulting neuronal phenotypes *in vivo*. In most organisms, glial removal leads to neuronal death. Previously, a limited number of ablations performed during embryogenesis had not been conclusive as to whether glia are required for neuronal survival, since neurons could not always be located in EM reconstructions of glia-ablated animals (Sulston et al., 1983). Our results explain this anomaly: nerurons survive, but due to ther shorter dendrites, they would not be seen in the anterior portion that was reconstructed in these animals from previous work. Here, we further show that the neuron defect is specific to dendrite length as neurons appear grossly normal, display at least partly normal cilia, and express cell-specific markers. Later work in our laboratory has extended these observations to other sensory organs of *C. elegans*, specifically the cephalic sensilla, which also do not require their associated glia for survival (Yoshimura et al., 2008).

Glia-dendrite interactions in sensory organs

Removal of the sheath glial cell prior to amphid development leads to sensory dendrites that are far too short. By imaging sensory neurons in the earliest stages of wild-type amphid development, Maxwell Heiman has shown that the neurons are born in the

anterior part of the embryo and form local attachments there. Afterwards, the neuronal cell body migrates posteriorly leaving behind a trailing edge which becomes the dendrite (Heiman and Shaham, 2009). In mutants in which neurons fail to maintain the initial local connection, the dendrite is dragged posteriorly by the cell body, resulting in shortened dendrites similar to those seen after glial ablation. In light of this mechanism of dendrite growth, sheath glia might either provide the initial anchoring or stabilize the neuronal attachment after it has formed. Interestingly, mutants that affect dendrite length affect the whole dendritic bundle as well as the sheath glia (Heiman and Shaham, 2009), suggesting that the length is set at the organ level. As there is a single sheath glia versus twelve neurons, it is possible that the length of the organ is set by the glial cell.

There are several other sensory organs in *C. elegans* and their length might be set in a similar manner to the amphid. For example, removal of the cephalic sheath glia results in cephalic neurons with shorter dendrites (Yoshimura et al., 2008), although in this case the dendrite is typically at least 80% of the wild-type length.

The no-mechanoreceptor-potential A (*nompA*) mutants of *Drosophila* also have short (about 70-80% of normal length) sensory dendrites in their mechanosensory organs. In these mutants the dendrites are initially formed normally but fail to grow appropriately (Chung et al., 2001). nompA encodes a transmembrane protein with a zona pellucida (ZP) domain and five plasminogen N-terminal (PAN) modules, is expressed only in the thecogen support cell that ensheathes the mechanosensory dendrite, and localizes to the dendritic cap (Chung et al., 2001). The dendritic cap comprises the thecogen-secreted matrix in which the cilia are embedded. Interestingly, one of the mutants with shortened amphids also encodes a ZP domain protein (Heiman and Shaham, 2009) suggesting that

the function of this domain in controlling sensory organ structure is conserved. Further, several PAN module (Zhou et al., 1998; Tordai et al., 1999) proteins are expressed by the amphid sheath glia (work of M. Tevlin). These proteins could be responsible for mediating dendrite-glia interactions in setting organ length in the amphid.

Coordinated morphogenesis of glia and neurons is observed in other settings, such as in the developing cortex (Rakic, 1972) and cerebellum (Rakic, 1971) where neurons migrate along the processes of radial glia and Bergman glia, respectively. Although these migration processes are different from the potential adhesive roles the amphid sheath glia might play, better characterization of neuron-glia interactions during *C. elegans* development might uncover common pathways that enable the generation of complex neuronal architecture.

Chapter 3

Glia are required for sensory neuron morphology and function

Summary

Sensory organs are composed of neurons, which convert environmental stimuli to electrical signals, and glial cells, whose functions are not well-understood. To decipher glial roles in sensory organs, we ablated the sheath glial cell of the major sensory organ of *C. elegans*. We found that glia-ablated animals exhibit profound sensory deficits as determined by behavioral assays. Further, glia were required for the maintenance of the proper morphology of some of the modified sensory cilia, and neuronal uptake of lipophilic dyes was abolished in the absence of glia. Glial removal eliminated the normal ASH neuron Ca^{2+} responses elicited by presentation of a high osmolarity solution. Providing exogenous Ca^{2+} through channelrhodopsin stimulation restored normal ASH behaviors, suggesting that the glia are only required for one of the early steps of sensory transduction prior to Ca^{2+} elevation. Our results suggest that glia are required for multiple aspects of sensory organ function.

Glial contributions to neuronal development and function

Glia, the largest cell population in the vertebrate nervous system, have been implicated in numerous processes that govern nervous system development and function (Haydon, 2001). However, to a large extent, the functions of these cells remain poorly characterized and roles for only a few glial proteins have been described. In vertebrates, the most extensively studied central nervous system glia are oligodendrocytes and astrocytes. Astrocytes are often positioned near synapses, and can respond to and participate in synaptic activity (Perea and Araque, 2005; Panatier et al., 2006; Perea and Araque, 2007). Likewise, perisynaptic Schwann cells, which ensheath neuromuscular junctions, can also influence the response of postsynaptic cells to presynaptic stimulation (Robitaille, 1998).

Sensory neurons convert environmental stimuli into neuronal activity, and their sensory receptive endings are often associated with glia. Thus, it is possible that glia associated with sensory neurons impact neuronal activity in ways analogous to synaptic astrocytes or perisynaptic Schwann cells; however, sensory organ glial functions have not been extensively explored. We have studied the major glial cell of the amphid sensory organs. The twelve amphid neurons can be classified based on their association with the single amphid sheath glial cell: the dendritic receptive endings of four neurons (AWA, AWB, AWC, and AFD) are entirely surrounded by the sheath glial cell in a hand-in-glove configuration, while the remaining neurons are encased by a tubular channel formed by the same glial cell and are exposed to the outside environment through a cuticle-lined pore (Ward et al., 1975; Perkins et al., 1986; Perens and Shaham, 2005).

To reveal glia-neuron interactions within the amphid, we ablated sheath glia in first-stage (L1) larvae, after the organ has formed, either using a laser microbeam (Bargmann and Avery, 1995), or by expressing the diphtheria toxin A gene from a sheath glia-specific promoter. We examined three neuronal properties in adults following ablation: neuronal function, as determined by animal behavior assays; sensory receptive ending morphology; and uptake of lipophilic dyes, a property of some, but not all, amphid neurons that correlates with the integrity of their receptive endings (Hedgecock et al., 1985; Perkins et al., 1986). An advantage offered by *C. elegans* as a model system is the extensive functional characterization of most neurons by laser ablations which means that behavioral defects can be correlated to dysfunction of specific sensory neurons.

Results

Post-developmental sheath glial ablation results in dysfunction of 'wing' neurons

To test for post-developmental functions of sheath glia, we ablated these cells once the amphid organ was fully formed by expressing an attenuated form of the diphtheria toxin A subunit (DT-A^{G53E}). Genomic integration of the *F16F9.3* pro::DT-A^{G53E} transgene afforded two independent lines, *nsIs109* and *nsIs113* (referred to as "no glia 1" and "no glia 2" hereafter), in which the DT-A toxin is expressed in two- to three-fold embryos and the sheath glia cannot be observed in L1 larvae.

To determine if sheath glia are required for the function of amphid 'wing' neurons (AWA, AWB, and AWC), we tested both glial ablation lines in odortaxis assays (Bargmann et al., 1993). Briefly, assays are performed on 10 cm plates on which an

attractant and diluent (acting as negative control) are spotted on opposite sides. Sodium azide is added to these spots to anesthetize the animals that reach these areas. About 200 animals are placed at the lower part of the plate and allowed to roam for one hour at which point the assay is stopped. The chemotaxis index is calculated by counting the animals at the attractant minus those at the control spot divided by the total number of animals.

Wild-type animals odortaxed robustly to benzaldehyde while both ablation lines showed severe defects ($p<0.001$, Student's t-test in all cases), Figure 3.1A. Further, both lines did not behave significantly different from *che-2(e1033)* control animals (Figure 3.1A), a mutant in which sensory cilia do not form properly and hence displays abnormal behavior for many amphid senses, including detection of volatile and soluble compounds (Fujiwara et al., 1999). Similar defects were observed for odortaxis toward isoamyl alcohol in both ablation lines (Figure 3.1A). Benzaldehyde and isoamyl alcohol are AWC-sensed odorants (Bargmann et al., 1993), suggesting that amphid sheath glia are required for proper AWC neuron function.

Ablated lines also had impaired AWA function (Bargmann et al., 1993) as determined by odortaxis defects towards methyl pyrazine ($p<0.001$) and diacetyl ($p<0.001$), Figure 3.1C. In contrast, AWB function (Troemel et al., 1997) was not affected by sheath glial ablation as both lines avoided 2-nonanone as well as did wild-type animals, Figure 3.1E. Preservation of normal AWB function in sheath glia-ablated amphids suggests that the observed defects in AWA and AWC do not result from non-specific damage due to sheath glial removal.

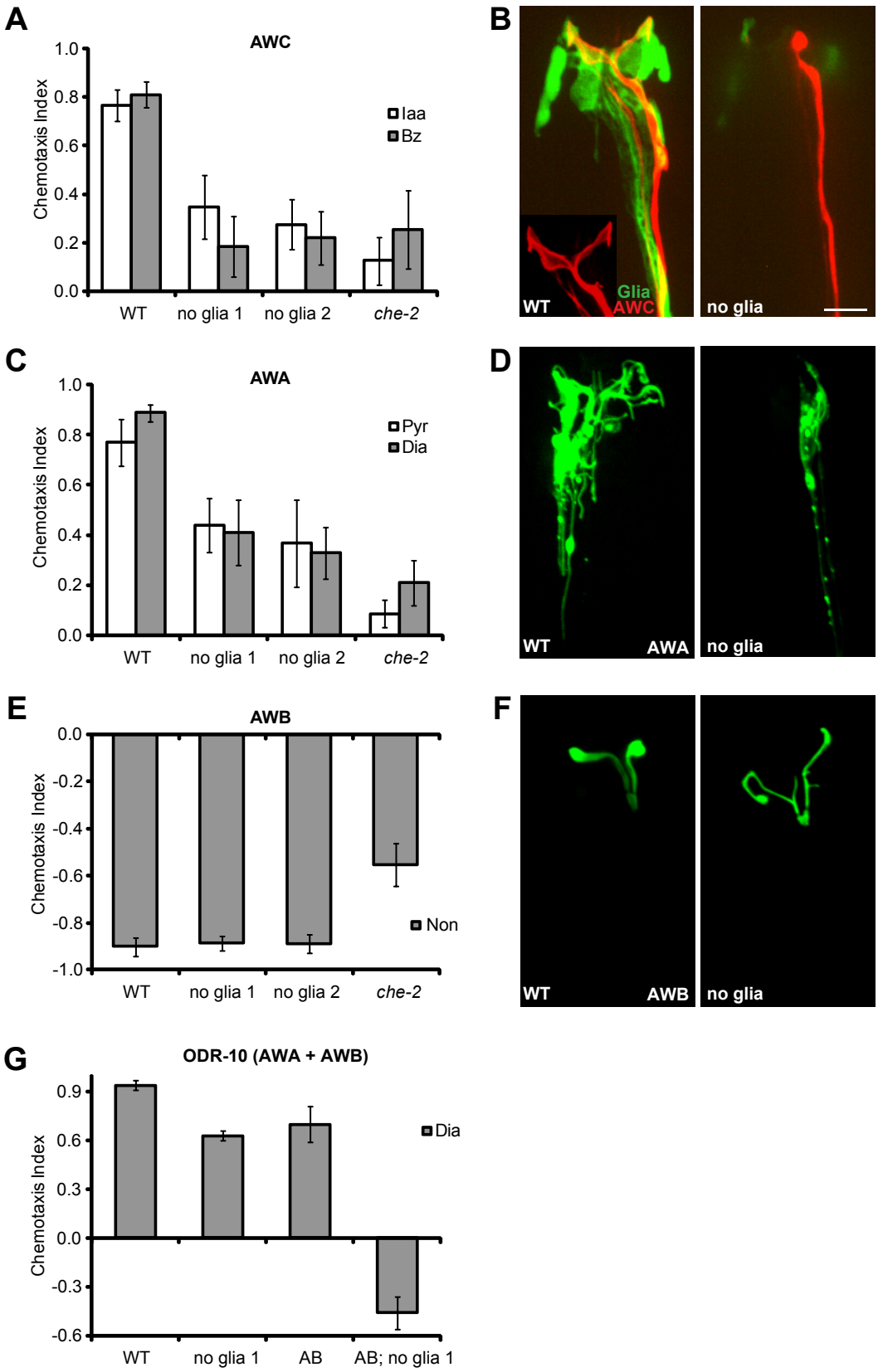

Figure 3.1: Sheath glia are required for sensory neuron function and cilia morphology

Figure 3.1: Sheath glia are required for sensory neuron function and cilia morphology

(**A**) Glia-ablated animals have defective AWC neuron function as determined by chemotaxis toward 1% isoamyl alcohol (Iaa) and 0.5% benzahldehyde (Bz), $p<0.001$ (Student's t-test). (**B**) A wild-type AWC cilium (red, *odr-1* pro::RFP) ensheathed by the amphid sheath glia (green, *vap-1* pro::GFP). Glial ablation in the contralateral amphid results in an amorphous cilium. (**C**) Glia-ablated animals have defective AWA neuron function as determined by chemotaxis toward 1% methyl pyrazine (Pyr) and 0.1% diacetyl (Dia), $p<0.001$. (**D**) Glial removal decreases the degree of branching of the AWA cilium (*odr-3* pro::*odr-3*p::GFP). (**E**) Glia are not required for AWB neuron function as determined by 10% 2-nonanone avoidance. (**F**) AWB cilium morphology appears grossly normal in many glia-ablated animals although additional branching and failure of the two cilia to spread is often observed (*str-1* pro::*odr-10*::GFP). (**G**) Differential glial requirements in the amphid. Animals that express the diacetyl receptor ODR-10 in both the attractive AWA neuron and repellent AWB neuron (AB) are less attracted to diacetyl and so are glia-ablated animals, $p<0.001$. These assays were performed on square plates so both attraction and repulsion can be measured, hence the difference with the diacetyl attraction level of 'no glia 1' in **C**. Dual-sensing animals that lack glia are repelled by diacetyl. WT, wild type; no glia, transgenic lines in which amphid sheath glia are killed by expression of diphtheria toxin; *che-2, che-2(e1033)* chemosensory mutants; error bars, standard deviation of 12 or more assays. Anterior, up. Scale bar, 5 μm.

To confirm these neuron-selective effects of glia on the response of *C. elegans* to odorants, we expressed the ODR-10 diacetyl receptor, normally found only in the attractant AWA neurons (Sengupta et al., 1996), also in the AWB neurons which mediate avoidance. As previously described (Troemel et al., 1997), animals expressing ODR-10 in both neurons are less attracted to diacetyl than wild-type animals, reflecting the opposing behavioral outputs of these neurons (Figure 3.1G). Sheath glia-ablated animals expressing ODR-10 in both AWA and AWB were repelled by diacetyl (Figure 3.1G). This result is consistent with our assessment that AWA, but not AWB, requires sheath glia for function. In addition, because the extracellular environment of AWA and AWB sensory neurons is similar in glia-ablated animals, this result shows that odorant molecules can access and interact with neuronal odorant receptors in the absence of glia.

C. elegans can discriminate between odorants. Thus, animals can migrate properly toward a source of methyl pyrazine in a saturating concentration of diacetyl (Bargmann et al., 1993). Both glia-ablated lines could discriminate odors normally (Appendix Figure 1A). We also tested diacetyl adaptation in both lines and observed at least the presence of some adaptation in absence of sheath glia, although the data is difficult to interpret due to the defects in diacetyl odortaxis the lines display (Appendix Figure 1B).

Glial ablation results in abnormal modified cilia morphology of 'wing' neurons

Reasoning that the observed deficits in neuronal function might result from underlying morphological defects, we examined the shape of the three winged neurons in

ablated animals. The AWC dendrite ends in a modified cilium that resembles spread wings, Figure 3.1B inset. This wing-like structure is completely ensheathed by the sheath glia. In the same animal, laser ablation of the contralateral sheath glia in L1 larvae – a time at which the wing cilia are fully developed – resulted in a complete loss of the wing structure, Figure 3.1B. This phenotype was fully penetrant; in 63/63 laser-ablated animals and in more than 100 genetically ablated animals we failed to observe the AWC wings spreading properly. To further examine the AWC morphological defects, electron microscopy (EM) of ablated animals was performed. In control amphids, the AWC cilia spread about 140^{o} within the sheath. Ablated amphids instead displayed an enlarged AWC cilium that failed to elaborate wings but did contain normal microtubules (Figure 3.2C).

The AWC cilium increases dramatically in size, as does the amphid sheath glia, in dauer larvae (Albert and Riddle, 1983), an alternative larval stage *C. elegans* enters under harsh conditions (Cassada and Russell, 1975). In dauer animals lacking sheath glia, the AWC cilium failed to grow (Figure 3.2B) suggesting that the natural remodeling that takes place during dauer requires the amphid sheath glia.

The AWA cilium consists of a network of highly branched cilia (Figure 3.1D). Post-developmental genetic ablation of the sheath glia greatly reduced both the extent of branching and the size of this modified cilium (Figure 3.1D). Although the phenotype was severe, the AWA cilia did exhibit at least some degree of branching in most animals examined. The remnant branches observed could be the initial branches that developed before sheath glial ablation in L1 larvae or, alternatively, they could be new branches that have failed to form a proper AWA cilium.

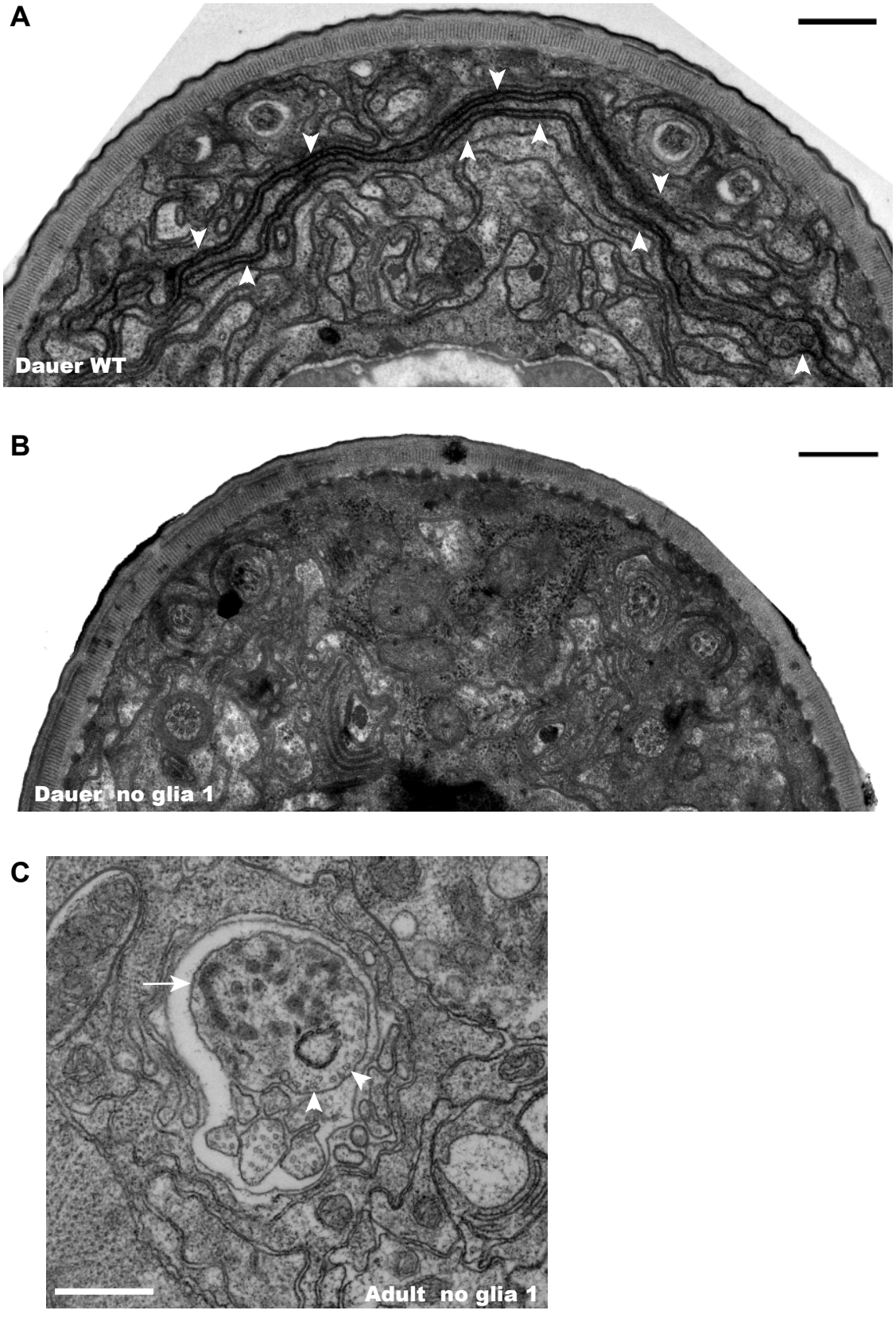

Figure 3.2: AWC fails to extend wing-like cilia during dauer in absence of glia

Figure 3.2: AWC fails to extend wing-like cilia during dauer in absence of glia

(**A**) EM image of a wild-type dauer animal, only the dorsal third of a cross section is shown. Two overlapping AWC wings can be seen, arrowheads. (**B**) A glia-ablated animal ("no glia 1") at the same cross section level has no AWC cilia extensions. (**C**) The abnormal, bulbous AWC cilium (arrow) of an adult animal is shown. Glial removal was performed by laser ablation in L1 larvae; similar results are seen in genetically ablated animals. Microtubules, the 8-like structures (arrowhead), appear to be normal inside the AWC cilium. Dorsal is up. Scale bar, 500 nm.

While some AWB cilia morphology abnormalities could be observed in about 60% of glia-ablated animals, in many cases the AWB cilia appeared essentially normal (Figure 3.1F), indicating that AWB cilia can maintain their shape in the absence of glia.

In summary, amphid sheath glial ablation results in abnormal AWA and AWC cilia morphology as well as function, while the AWB neurons appear normal in both aspects in absence of glia.

Glial ablation impairs the morphology and function of the AFD thermosensor

In a temperature gradient, *C. elegans* will migrate to the cultivation temperature if this is associated with food (Hedgecock and Russell, 1975; Mori and Ohshima, 1995). The circuitry underlying this behavior has been characterized. The main thermosensory neuron in *C. elegans* is the AFD neuron (Mori and Ohshima, 1995) whose microvilli-like dendritic ending is completely encased by the sheath glia (Ward et al., 1975). To test if glia-ablated animals can properly sense temperature, we tested them in thermotaxis assays. Assays were performed on a linear temperature gradient with extremities set at 18^{o}C and 26^{o}C. Wild-type animals accumulated at their cultivation temperature (Figure 3.3A). For example, when grown at 20^{o}C most animals migrate to the center of the gradient, approximately 20^{o}C (Figure 3.3A). Both glia-ablated lines failed to migrate appropriately and displayed features of thermophilic behavior (Figure 3.3, B-C). This is clearest for animals grown at 20^{o}C which accumulate evenly at all temperatures greater than 20^{o}C (Figure 3.3, B-C). Note that little difference from control animals is expected when ablated animals are cultivated at 25^{o}C if they display thermophilic behavior.

ttx-1 mutants display cryophilic behavior and also have defects in AFD development (Hedgecock and Russell, 1975; Mori and Ohshima, 1995; Satterlee et al., 2001). We found that *ttx-1(p767)* animals in which amphid sheath glia had been genetically ablated were also cryophilic (Figure 3.3D). This finding suggests that glial removal specifically affects only some aspects of AFD functions but does not abolish thermosensation. Importantly, it also implies that the AFD defects observed do not result from general degeneration of the neuron upon sheath ablation as they can be suppressed in *ttx-1* mutants.

To determine whether the observed defects in AFD function could be due to underlying morphological defects, we examined the AFD neuron by fluorescent microscopy and EM. In glia-ablated animals, the AFD neuron lacked the microvilli-like protrusions that are seen in wild-type animals (Figure 3.3, E-F). EM analysis supported these observations. In animals in which a single amphid sheath glia was laser ablated, the mock-ablated amphid contained about 25 microvilli, visible as double-membrane rings indicated by arrowheads in Figure 3.3G. In contrast, no microvilli were detected in the glia-ablated amphid (Figure 3.3H).

In *ttx-1(p767)* mutants the AFD microvilli are not present and the neuron ends in a single, long cilium (Perkins et al., 1986). As development of a single long cilium is probably the default fate of ciliated neurons in *C. elegans*, the *ttx-1* phenotype has been interpreted as indicating incomplete differentiation of the AFD neuron (Satterlee et al., 2001). Since a long cilium is not observed in glia-ablated animals, AFD differentiation is likely to be normal and the glia might be specifically required for microvilli elaboration.

The current model proposes that the AFD neuron mediates thermophilic responses in *C. elegans* and that perhaps another neuron is required for cryophilic responses. This other hypothetical neuron might be AWC (Kuhara et al., 2008). As amphid sheath glial removal is likely to affect other amphid neurons including AWC, the thermophilic behavior of sheath-ablated animals might be explained by defects in this other hypothetical cryophilic neuron with AFD function being intact. However, as the data in support of a second temperature sensing neuron is weak and because AFD morphology is abnormal in ablated animals, it is likely that proper AFD function requires the presence of sheath glia. However, laser-ablation of AFD neurons results in athermotactic animals (Mori and Ohshima, 1995) suggesting that glial removal does not abolish AFD function.

Channel neuron behavioral deficits in sheath glia-ablated animals

Eight amphid neurons end in unmodified cilia that have direct access to the environment through a channel provided by the sheath and socket glial cells. One of these channel neurons, ASE, mediates chemotaxis toward NaCl (Bargmann and Horvitz, 1991a). To examine ASE function, we tested whether glia-ablated animals could properly migrate in a NaCl gradient. As shown in Figure 3.4A, wild-type animals preferentially migrate towards the NaCl peak concentration. Sheath glia-ablated animals failed to accumulate at the peak of the NaCl gradient. Thus, both glia-ablated lines migrate randomly in the gradient ($p<0.001$) and perform as poorly as do *che-2(e1033)* control animals, Figure 3.4A.

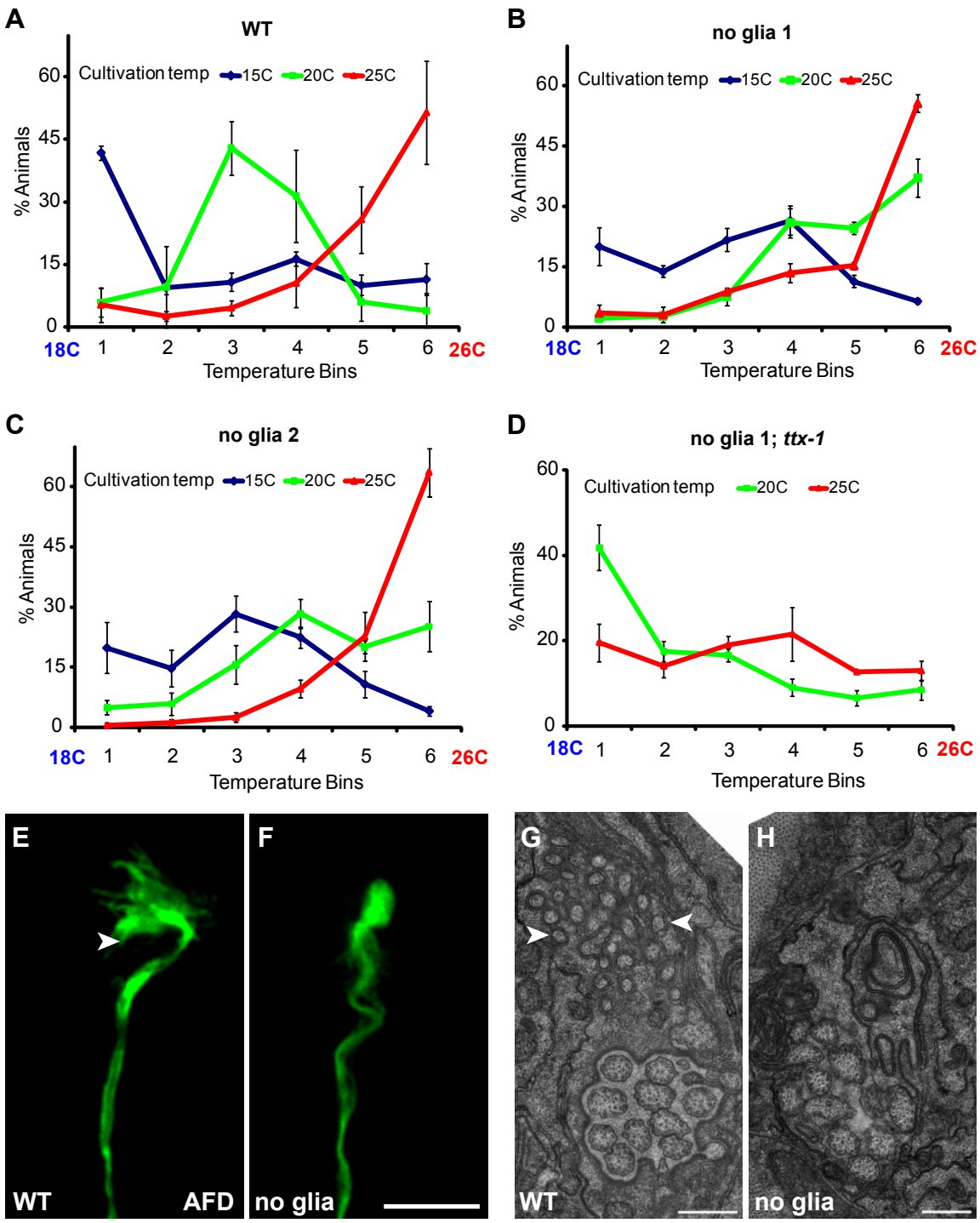

Figure 3.3: AFD functional and morphological defects in glia-ablated animals

(**A**) Thermotaxis profile of wild-type animals cultivated at three different temperatures. (**B** and **C**) Glia-ablated animals show thermophilic behavior. (**D**) Glia-ablated *ttx-1(p767)* animals are cryophilic, the reported behavior of *ttx-1(p767)* mutants. (**E** and **F**) Glia-ablated animals lack the AFD villi seen in wild-type animals (arrowhead). Scale bar, 5 µm. (**G** and **H**) EM showing lack of AFD villi in absence of glia. Scale bar, 0.5 µm.

C. elegans avoids certain noxious stimuli such as high osmolarity (Culotti and Russell, 1978). This behavior is mediated by the ASH amphid neuron, which acts as a polymodal nociceptor (Bargmann et al., 1990). Osmolarity avoidance was tested by placing a single animal inside a 4M fructose ring, serving as an osmotic barrier, and determining how many times the animal avoided the barrier, indicated by a sharp turn upon reaching the barrier. Most (90%) wild-type animals responded properly, i.e. they never crossed the barrier during the ten minutes of observation or did so after being repelled by it more than eight times (Figure 3.4B). Most sheath-ablated animals crossed the barrier on their first or second attempt with only 20% ($p<0.001$) responding to the barrier (Figure 3.4B). Both lines lacking glia tested were as defective as *osm-6(p811),* a mutant with severe osmosensation defects (Collet et al., 1998), Figure 3.4B.

C. elegans detects volatile repellents with at least three neurons: AWB, ASH, and ADL. To assess the function of ADL, we assayed animals for avoidance of 1-octanol. In long-range assays, 1-octanol avoidance is mediated mostly by the ADL neurons with ASH also mediating part of the response (Troemel et al., 1995; Troemel et al., 1997; Chao et al., 2004). Glia-ablated animals were completely defective in long-range avoidance of 1-octanol (Figure 3.4C). Given the severity of the defect, it is likely that both ADL and ASH neurons cannot sense 1-octanol properly in absence of sheath glia.

Sheath glia are required for sensory neuron lipophilic dye uptake

When *C. elegans* are soaked in a solution of lipophilic dye, such as DiI, some amphid channel neurons, as well as the AWB sheath glia-embedded neuron, take up and

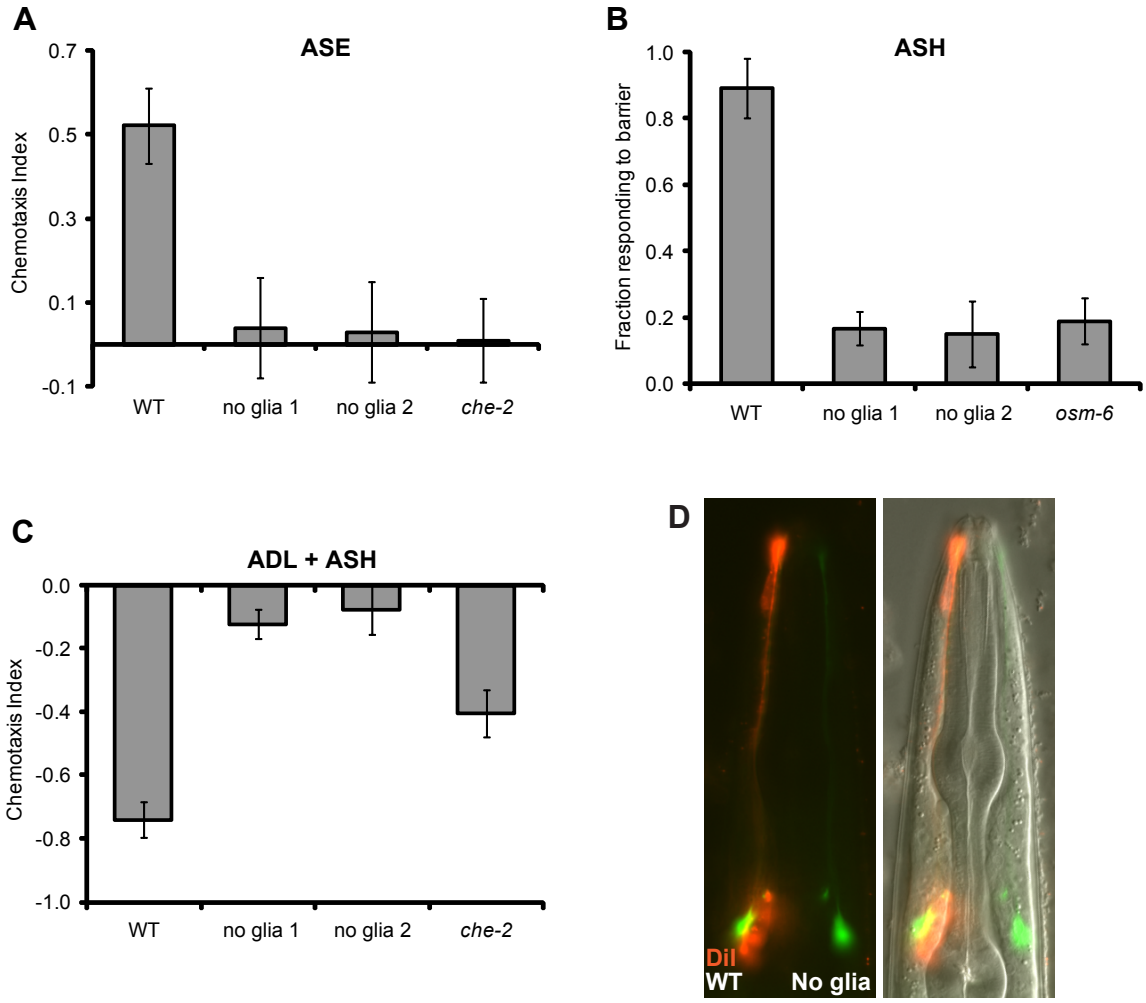

Figure 3.4: Glia removal affects channel neuron function

(**A**) Glia-ablated animals fail to detect the source of a 0.2 M NaCl gradient ($p<0.001$), an ASE-mediated behavior. (**B**) Glia-ablated animals fail to avoid a 4M fructose osmotic barrier ($p<0.001$), an ASH-mediated behavior. *osm-6, osm-6(p811)* chemosensory mutants. (**C**) Glia-ablated animals fail to avoid 1-octanol in a long-range assay ($p<0.001$), a behavior mediated by the ADL and ASH neurons. (**D**) Glia are required for neuronal uptake of DiI (red). Only the right amphid sheath glia is ablated. The AWC neuron (green, *odr-1* pro::YFP) is shown to indicate the location of the dendrite bundle. Error bars, standard deviation of 12 or more assays.

concentrate the dye. Mutants with structurally defective cilia fail to uptake dye (Perkins et al., 1986; Starich et al., 1995), indicating that a normal sensory cilium is required for this activity. We found that uptake of DiI was completely blocked in all amphid neurons in glia-ablated animals (Figure 3.4D). In the animal in Figure 3.4D, only the right sheath glia is ablated, thus dye filling is abolished only in the right amphid. Further, we never observed dye uptake in more than 1000 genetically ablated animals.

The mechanisms of dye filling remain unclear. Based on the chemical structure of the dyes, they should label any cell membrane they come in contact with as the processes should be passive. However, while all channel cilia should have equal access to the external environment, and presumably dyes, only a subset of the cilia are able to concentrate the dye, suggesting that some specialized membrane composition facilitates dye uptake in these neurons. In addition, while most neurons can take up different dyes, AWB uptakes DiI but not FITC while ADF concentrates FITC but not DiI (Herman, 1984; Hedgecock et al., 1985). Regardless of the underlying mechanisms, dye filling might serve as a proxy for neuronal function as it correlates with the presence of abnormal cilia and behavioral defects (Perkins et al., 1986; Starich et al., 1995).

Sheath glial ablation does not affect channel neuron cilia morphology

Because previously we found morphological abnormalities in neurons displaying behavioral deficits, we examined the morphology of two neurons, the right ASE neuron (ASER) and ADF. Surprisingly, the morphology of both neurons appeared normal in glia-ablated animals as visualized by confocal microscopy (Figure 3.5, A-D).

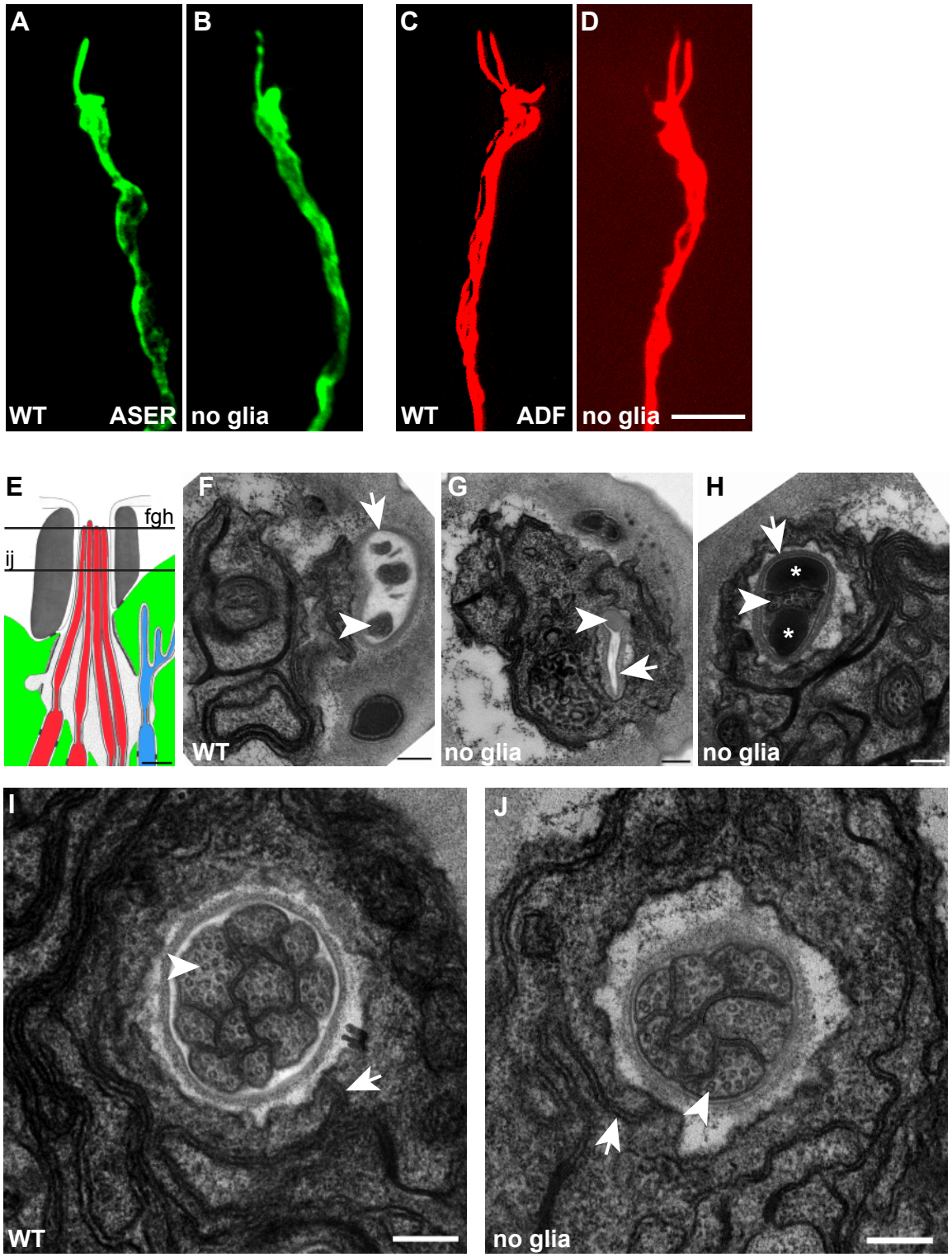

Figure 3.5: Channel neuron cilia are not affected by glia removal

Figure 3.5: Channel neuron cilia are not affected by glial removal

(**A** through **D**) The morphology of amphid channel neurons is not affected by glial removal. ASER, *gcy-5* pro::GFP; ADF, T08G3.3 pro::RFP. Scale bar, 5 μm. (**E**) A schematic depiction of the amphid opening indicating the level of the cross sections in **F** to **J**. Adapted from (Perkins et al., 1986). Sheath glia, green; socket glia forming the pore, dark grey; channel neurons, red; sheath embedded neurons, blue. In cartoons, anterior is up, scale bar 1 μm. (**F**) A wild-type amphid near the beginning of the cilia (arrowhead). The cuticle lining the pore is indicated by the arrow. (**G**) A glia-ablated animal in which the amphid channel appears open. Arrowhead, beginning of a cilium. (**H**) Another glia-ablated animal in which the beginning of a cilium is seen (arrowhead). An abnormal EM-dense matrix (asterisks) is seen within the channel. (**I**) Wild-type channel cilia (arrowhead) displaying the proper microtubule arrangement. The autocellular junction of the socket glia is indicated by the arrow. (**J**) Glia-ablated animals also have normal channel cilia (arrowhead). In EM images, dorsal is up, scale bar 200 nm.

EM analysis confirmed that channel neuron cilia morphology remained unaltered in glia-ablated animals. All eight channel neurons possessed cilia that were of wild-type length and displayed proper anatomy as judged by microtubule organization (Figure 3.5, I-J). However, EM examination revealed that in about half the animals (4/9) an uncharacterized EM-dense matrix accumulated within the socket channel at the very tip of the cilia. Whereas in wild-type amphids the socket channel opening is empty and clearly visible (Figure 3.5F), in the glia-ablated amphid of the same animal an EM-dense matrix appears to plug the socket channel (Figure 3.5H, asterisks; note the first cilium appearing, arrowhead). In other analyzed animals (5/9), no matrix was seen plugging the socket channel, but the channel appeared partially collapsed (Figure 3.5G). It is unlikely that this matrix completely blocks the cilia from accessing the environment or that molecules such as fructose and DiI cannot diffuse through the matrix. In animals in which no matrix is observed but the socket channel appears collapsed, small molecules should be able to reach the cilia given the size of the channel opening that is observed, about 70 nm (Figure 3.5G). If socket channel collapse was the cause of the Dyf defects observed, one might expect a range of severity in the phenotype mirroring the extent of channel collapse in different animals. As genetically ablated animals are 100% Dyf, it is unlikely that this phenotype is caused by a defect in physical access to the cilia.

Cilia resident proteins localize normally in absence of glia

As channel cilia have abnormal function yet wild-type morphology, we asked if proteins that localize within these cilia fail to do so after glial removal. Cilia morphology

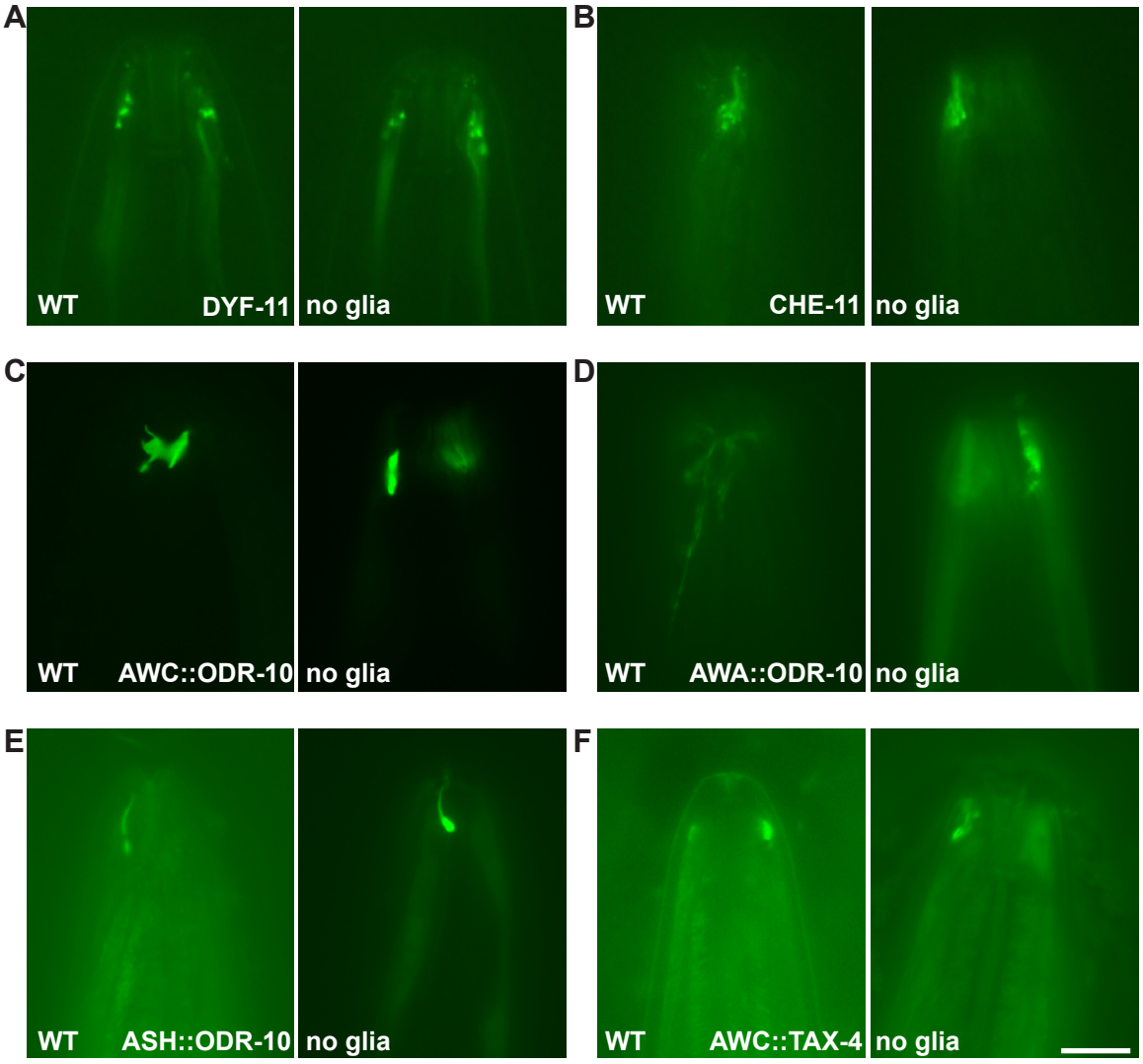

Figure 3.6: Cilia components localize properly in absence of glia

(**A**) DYF-11, an IFT-B particle component and (**B**) CHE-11, an IFT-A particle component (Qin et al., 2001), localize normally in amphid cilia of glia-ablated animals. ODR-10, an odorant receptor (Sengupta et al., 1996), localizes normally when expressed in the AWC (**C**), AWA (**D**), or ASH (**E**) cilia of glia-ablated animals. (**F**) TAX-4, a cyclic nucleotide gated channel subunit (Komatsu et al., 1996), localizes normally in glia-ablated animals. Anterior is up, scale bar 10 μm.

and function depends on intraflagellar transport (IFT). Two IFT component proteins, CHE-11 (IFT-A) and DYF-11 (IFT-B), localized normally in animals lacking glia (Figure 3.6, A-B).

Furthermore, despite the morphological defects observed in some neurons, normal localization to the remaining ciliary rudiments was observed for many olfactory signaling proteins: the odorant receptor ODR-10 localized properly in AWB (Figure 3.1F), AWA, AWC, and ASH (Figure 3.6, C-E); the G-alpha protein ODR-3 in AWA (Figure 3.1D); and the cyclic nucleotide gated channel subunit TAX-4 in AWC (Figure 3.6F). Together, these findings suggest that some cilia functions, minimally IFT, remain normal in glia-ablated animals.

Glia are required for Ca^{2+} dynamics in the ASH neurons

The AWA, AWC, and AFD behavioral defects in glia-ablated animals might be explained by the abnormal cilia morphology of these neurons. However, channel neuron cilia appear normal in absence of glia, so at least for these neurons, glia are required for sensory neuron function. To examine where in the signal transduction pathway this defect might arise, we imaged Ca^{2+} levels in sensory neurons. We chose to image Ca^{2+} as it is thought that the main output of sensory transduction in *C. elegans* cilia is an elevation of somatic Ca^{2+} levels since *C. elegans* lacks action potentials typical of most other organism's neurons (Bargmann, 1998). We used the genetically encoded Ca^{2+} sensor G-CaMP (Nakai et al., 2001) to test whether the ASH neuron, which cannot mediate proper osmosensation in absence of glia, undergoes normal Ca^{2+} level changes in

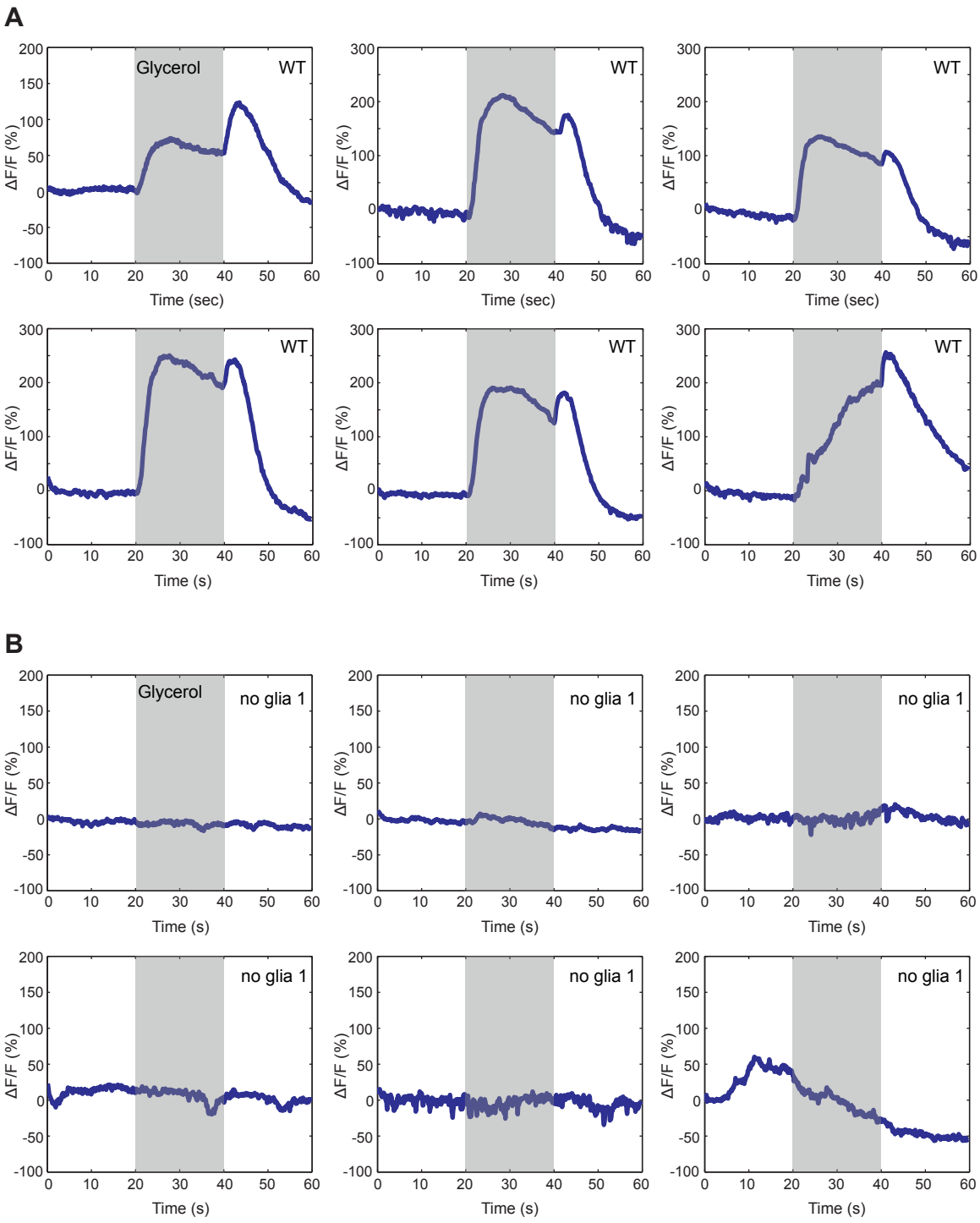

Figure 3.7: Glia are required for Ca responses in sensory neurons

(**A**) As determined by G-CaMP fluorescence, ASH responds to both the application and removal of 1M glycerol. Shaded region corresponds to stimulus duration, 20 seconds. (**B**) In glia-ablated animals, ASH fails to respond to glycerol.

response to high osmolarity. As previously described (Hilliard et al., 2005), wild-type animals display increases in intracellular Ca^{2+} following exposure to and removal of an osmotic stimulus of 1M glycerol (Figure 3.7A). ASH neurons in sheath glia-ablated animals fail to respond to both the onset and removal of the glycerol (Figure 3.7B). This total absence of any Ca^{2+} dynamics indicates that glia are required for the early steps of sensory transduction.

To determine whether neuronal signaling activity downstream of Ca^{2+} elevation was disrupted, we expressed the light-activated cation channel channelrhodopsin-2 (ChR2) (Nagel et al., 2003) within ASH in sheath glia-ablated animals. ASH is a general nociceptor neuron (Bargmann et al., 1990; Kaplan and Horvitz, 1993; Hilliard et al., 2005), hence its exogenous activation with light should result in a backing motion as the animal tries to avoid the phantom noxious stimulus. In the absence of retinal, a compound not synthesized by *C. elegans* and an obligate cofactor of ChR2, animals fail to exhibit backward locomotion in response to a 1 s light pulse (Figure 3.8). However, in the presence of retinal, both wild-type and glia-ablated animals initiate backward locomotion (Figure 3.8). These results suggest that signaling in ASH downstream of Ca^{2+} elevation is intact, and provide evidence that glia are not required for ASH health or viability. Moreover, they suggest that glia can affect Ca^{2+} increases within sensory neurons in response to environmental stimuli.

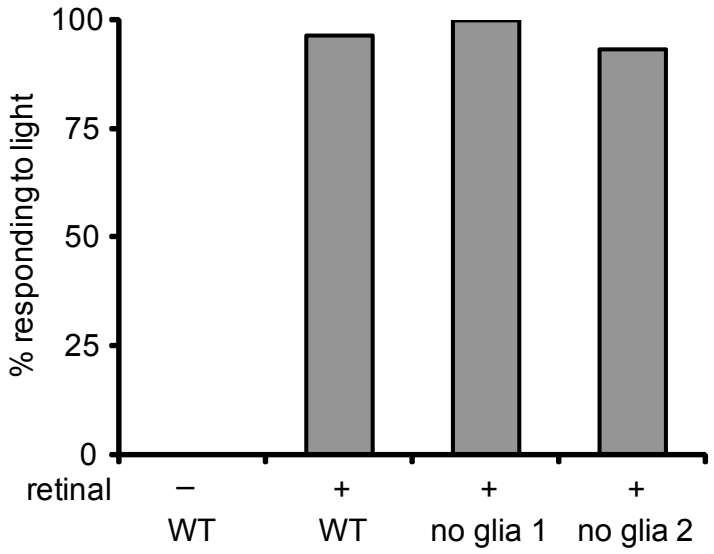

Figure 3.8: Glia are not required for neuronal function downstream of Ca entry
Activation of ASH-expressed channelrhodopsin2 by light, in the presence of retinal, causes animals to move backwards. n=30 for each condition.

Discussion

Here we demonstrate that *C. elegans* provides a good model for dissecting glial roles in sensory neuron function. The simple approach of removing glia and then assaying sensory neurons for function and morphology proved fruitful for the amphid and can be extended to other *C. elegans* sensilla.

Taken together, our observations suggest that glia regulate at least three different properties of sensory neurons: 1) cilia morphology, which is defective mainly in AWA, AWC, and AFD after glial ablation; 2) neuronal function as assayed by behavior generation, which is defective in some channel neurons despite the fact that they appear morphologically normal; and 3) neuronal dye uptake, which is defective even in the AWB neurons which retain their shape and function after glial removal. Thus, each of these properties in at least some of the amphid sensory neurons requires the presence of the sheath glia.

Glia are required for cilium morphology

The amphid sensillum is composed of twelve sensory neurons whose dendritic cilia display stereotyped morphology. How might glia affect cilia shape? Two broad models can be defined: glia affect intraflagellar transport which is required for cilium formation or glia act through signaling events that result in microtubule reorganization. It is unlikely that glia affect IFT *per se* as channel cilia have no morphological defects in glia-ablated animals, but glia might be required for the transport of specific proteins

within cilia. Although we have been unable to find cilia-resident proteins mislocalized in absence of glia, there is some evidence that supports this hypothesis.

Previous EM analysis has shown that mutants with defective IFT possess abnormal cilia (Lewis and Hodgkin, 1977; Perkins et al., 1986). These ciliary defects could be grouped in two classes. The first class, composed of the amphid channel neurons which possess simple singly or doubly ciliated dendrites, displays short cilia in IFT mutants. These defects result from abnormalities in the cilium itself which lacks parts of its axonemal proteins and is therefore not properly assembled (Scholey, 2003). The AWC cilium, defining the second class, fails to properly spread within the sheath glia in IFT mutants (Perkins et al., 1986). The AWA cilia can likely be grouped with AWC but their EM reconstruction is difficult so it has not been characterized to the same extent. The AWC cilium defects observed in IFT mutants are unlikely to result directly from the shorter cilium but rather from lack of intraflagellar transport of particular proteins within the cilium. For example, mutants with defective dendritic transport, such as *unc-101*, a μ-1 subunit of the AP-1 clathrin adaptor complex, possess normal cilia in terms of microtubule organization but have defective AWC cilia wings (Dwyer et al., 2001). Together, these observations suggest that dendritic and IFT transport is required for specific molecules to reach the AWC cilium in order to control its morphology. What these molecules might be remains unknown and our efforts to identify them have been unsuccessful (see below).

While IFT is required for the proper formation of almost all amphid cilia, the AFD neuron microvilli-like structures do not depend on this process (Perkins et al., 1986), although a recent report has claimed abnormal thermotaxis in IFT mutants (Tan et

al., 2007). However, glia are required for the proper formation of AFD protrusions. Thus, glial removal does not affect channel cilia but does abolish AFD villi, the opposite phenotype of IFT mutants, further evidence that glia do not disrupt general IFT. It is interesting to note that although no finger-like projections remain in the absence of glia, the animals can still sense temperature as they display thermophilic behavior, indicating that these structures are not absolutely required for temperature sensation. This conclusion is supported by *ttx-1* mutants, which have no villi but retain some level of thermosensation (Satterlee et al., 2001).

AWC dysfunction in absence of glia

In the simplest explanation, the AWC odortaxis defects of glia-ablated animals arise from the underlying morphological defects. Although it is unclear why AWC cilia adopt the wing-like shape, one hypothesis is that this increases the total surface area resulting in better odorant detection. Thus, glial removal decreases the total area of the cilium and, therefore, its sensitivity.

However, the opposite could be true, namely that abnormally functioning cilia cannot maintain their proper morphology. In support of this view, abnormal sensory transduction within the AWC cilia results in abnormal cilia morphology. For example, removal of the G-alpha protein *odr-3*, an olfactory transduction component, or overexpression of a constitutively active form of this protein results in abnormal AWC wing formation (Roayaie et al., 1998). Decreasing AWB neuron activity results in expansion of the AWB cilia membrane, a defect that is suppressed by increased levels of

ciliary cGMP or Ca^{2+} and that requires IFT (Mukhopadhyay et al., 2008). This suggests that, at least for these two sheath-embedded neurons, activity levels might affect cilia morphology.

Of course, a third possibility is that glia are required independently for cilia shape as well as function.

Sensory transduction in channel neurons requires glia

Amphid channel neurons display no morphological defects after glial removal yet fail to function properly. A confounding factor in the analysis of channel neurons is the channel opening defects of glia-ablated animals, as behavioral defects might arise due to lack of access of the cilia to the environment. This is unlikely to be the case for several reasons. While both NaCl chemotaxis and osmosensation require an open amphid channel, 1-octanol avoidance, a behavior defective in glia-ablated animals, does not. For example, in *daf-6* animals in which the sheath channel fails to form and all cilia are embedded in the sheath cytoplasm (Perens and Shaham, 2005), the ability to detect odorants is preserved. We found that *daf-6* animals can respond to 1-octanol as well as AWC- and AWA-sensed odors (data not shown). Thus, at least the ADL and ASH neurons, which mediate 1-octanol avoidance, require glia to function properly. Further, the EM-dense matrix is observed in only half of the animals, while dye uptake is defective in 100% of the animals. And as shown in the next chapter, the channel opening is completely normal in *fig-1(tm2079)* mutants but they fail to dye fill. *fig-1* is only expressed in the sheath glia, suggesting a role for these cells in dye uptake.

The Ca^{2+} imaging experiments suggest that glia are required for the early steps of sensory transduction that lead to somatic Ca^{2+} elevation. It is difficult to pinpoint the defect since we cannot read out activity along each step of the transduction pathway. To rule out the simplest explanations, we verified that several signal transduction proteins such as receptors, G-alpha proteins, and the cyclic nucleotide-gated channel localize properly in absence of glia. Furthermore, as the ODR-10 receptor can function normally in AWB but not in AWA cilia of glia-ablated animals, it is unlikely that glia are required for transportation or presentation of odors to neuronal receptors. An appealing hypothesis to explain glial roles is regulation of the extracellular ionic environment, as this can explain the extensive behavioral defects observed. However, at least AWB can function normally in absence of glia, suggesting either that this is not the case or that there are differential neuronal requirements for a defined extracellular environment.

Lastly, the observed defects are limited to the initial Ca^{2+} generating steps as elevating Ca^{2+} levels in ASH with channelrhodopsin induces the correct ASH behavior. This also indicates that the neurons do not generally degenerate in the absence of glia. Somatic Ca^{2+} elevation is thought to occur in a number of steps. Activation of cyclic nucleotide-gated channels allows direct inflow of Ca^{2+} but cytoplasmic Ca^{2+} might be further increased by either activation of voltage-gated Ca^{2+} channels or Ca^{2+} release from intracellular stores (Hilliard et al., 2005). It would be interesting to spatially restrict channelrhodopsin activation to cilia and assay whether this initial stimulation can cause the secondary Ca^{2+} level increases.

Identifying molecular components of glia-neuron communications

The goal of this project was to catalogue any glial roles in sensory neuron morphology and function in order to design genetic screens that could identify the molecular pathways that enable glia-neuron communication. The phenotypes discovered (defects in behavior, AWC morphology, and dye uptake) are the same as those observed in IFT mutants. Therefore, a screen for any of these phenotypes would yield not only mutants that affect sensory neuron development in general but also IFT components, two classes of mutants we attempt to avoid. The IFT proteins are particularly troublesome as there are approximately 250 of these proteins, which should cause a large background rate. Reasoning that the presence of all three phenotypes would likely be indicative of IFT mutants, we sought to find mutants that affect only one of these phenotypes in hopes of isolating mutations affecting sheath glia. We performed a visual screen for abnormal AWC morphology using a fluorescent compound microscope. Inspection of more than 12,000 animals yielded 35 mutants with abnormal AWC cilia morphology. Unfortunately, a secondary screen for dye uptake yielded no mutants that dye filled normally, suggesting that these mutants belong to the IFT class. In fact, inspection of the channel cilia revealed that in many of these mutants cilia were too short, an indication of IFT defects. Perhaps a more fruitful approach would be to screen for AFD shape abnormality as the microvilli-like extensions form in the absence of IFT. This is rather difficult due to resolution limitations, but might be facilitated by using membrane-tethered forms of GFP.

In conclusion, we have demonstrated that the *C. elegans* sensory organs are a good model system for analyzing glia-neuron interactions and that amphid sheath glia

provide their associated sensory neurons with at least three separate activities. In the next chapter, we describe a glial protein that is required for sensory neuron function and dye filling thus beginning the molecular characterization of the phenotypes uncovered here.

Chapter 4

fig-1: A glial gene required for sensory neuron function

Summary

Removal of the major glial cell in the amphid sensory organ of *C. elegans* results in sensory neuron deficits. Specifically, glial ablation affects neuronal morphology, behavior generation, and neuronal uptake of lipophilic dyes. To understand the molecular bases of these glial activities, we characterized a gene, *fig-1*, that encodes a labile protein with conserved thrombospondin type I (TSP1) domains. FIG-1 likely functions extracellularly, is essential for neuronal dye uptake, and also affects behavior. As thrombospondin 1 is a glial-secreted protein required for synapse formation in mice, these results suggest that some of the molecular components underlying glia-neuron interactions might be conserved.

Molecular pathways of glia-neuron interactions

Although several glial roles in nervous system function have recently been described, to a large extent, the molecular pathways underlying these functions remain poorly characterized (Barres, 2008). As described in the previous chapter, glial removal in the amphid sensory organ of *C. elegans* results in abnormal sensory neuron function, altered cilia morphology in some neurons, and inability of neurons to uptake lipophilic dyes. To understand how sheath glia contribute to these neuronal properties, we sought to uncover the relevant glial molecular players. Many *C. elegans* mutants that disrupt neuronal development and intraflagellar transport are defective in amphid sensory neuron behavior generation, morphology, and dye filling (Perkins et al., 1986; Starich et al., 1995). Therefore, forward genetic screens to identify glia-specific genes required for these processes would be encumbered by a large background rate of mutations affecting neuronal genes. To circumvent these difficulties, we took a candidate approach.

Choosing candidate genes was enabled by the work of Maya Tevlin, a post-doctoral fellow in the laboratory, who had compiled a list of amphid sheath glia-expressed genes. To identify genes enriched in these glia, she dissociated developing embryos expressing the amphid sheath glial reporter *vap-1* pro::GFP, cultured these dissociated cells, and sorted them into GFP-expressing and non-expressing groups using fluorescence-activated cell sorting (FACS). Comparison of the mRNA levels from each cell population identified 298 genes exhibiting greater than four-fold enrichment in amphid sheath glia. Of these genes, 159 are predicted to encode transmembrane or

secreted proteins that could potentially mediate glia-neuron interactions in the amphid sensory organs.

Three glia-enriched proteins were particularly interesting as they contained thrombospondin type I (TSP1) domains (Adams and Tucker, 2000; Adams, 2001). As well as having other roles, thrombospondins are a class of extracellular proteins that are secreted by astrocytes and are required for proper synapse formation (Christopherson et al., 2005). To test if TSP1 domain proteins might play a role in the amphid, Maya obtained deletions in 2 of these genes and found that a deletion in one of them, F53B7.5, prevented neuronal dye uptake.

Gene-specific knockouts are difficult to obtain in *C. elegans* and, often, the random mutagenesis performed to induce them results in complex rearrangements that complicate phenotype analysis. To screen through these 298 glial genes systematically, we performed RNA interference (RNAi) against most of these genes and tested neuronal morphology and dye uptake.

Results

An RNAi screen for glial factors with neuronal phenotypes

Glial ablations revealed two robust phenotypes that can also be scored in large numbers of animals: abnormal AWC morphology and dye filling (Dyf) defects. We sought to phenocopy these defects by performing RNAi against the set of glia-enriched genes. Although postembryonic glial removal is sufficient to induce these phenotypes,

we performed RNAi by plating L4 hermaphrodites and scoring the progeny to ensure maximal knock-down of the protein levels. To optimize knock-down efficiency, experiments were performed in *lin-35* mutants, a genetic background that is more sensitive to RNAi (Lehner et al., 2006). The *odr-1* pro::RFP transgene was used to image AWC morphology. Screening of progeny in L4 and young adult stages, when AWC morphology is easiest to score, yielded no hits for genes that might alter AWC cilium shape.

A second morphological defect resulting from glial removal is the lack of AFD villi-like projections. A similar RNAi screen was also unsuccessful in identifying glial genes that might underlie this phenotype. However, the difficulty of imaging this structure under conventional compound microscopy might result in a high false negative rate making it impossible to conclude that none of these genes affect AFD morphology.

Lastly, we screened the 298 sheath glia-enriched genes by RNAi for defects in neuronal dye filling in both *lin-35* and wild-type animals. Both screens yielded a single gene, F53B7.5, confirming that this gene is required for dye filling. Based on its phenotype and its glial expression (M. Tevlin), we renamed this gene *fig-1* (Dyf, expressed in glia).

fig-1 is continuously required for neuronal dye uptake

RNAi against *fig-1* resulted in dye filling defects in both the amphid and phasmid sensory organs (Figure 4.1B). Consistent with these defects, *fig-1* is expressed

exclusively in the amphid and phasmid sheath glia (data of Maya Tevlin). A 1,117 bp deletion in *fig-1*, allele *tm2079*, also perturbed amphid and phasmid dye filling (Figure 4.1B). This defect could be rescued by introduction of a cosmid spanning the *fig-1* locus into *fig-1*(*tm2079*) mutants, confirming that the *fig-1* lesion indeed disrupts amphid and phasmid neuron dye filling. *fig-1(tm2079*) mutants exhibit normal neuronal and amphid sheath glial structure as assessed using fluorescence reporter transgenes and EM reconstructions (Figure 4.1, C-D), suggesting that *fig-1* functions in a non-structural capacity to regulate amphid neuron dye filling.

Interestingly, *fig-1*(RNAi) defects can be induced at all developmental stages and can be observed within 24 hours of exposure of animals to bacteria expressing *fig-1* dsRNA (Table 4.1), suggesting that FIG-1 does not play a developmental role and is required continuously. This is consistent with the results of the ablation studies which revealed a post-developmental requirement for glia in dye uptake.

Table 4.1: *fig-1* activity is required continuously for dye filling

	Normal dye filling (%)	
Larval stage[a]	**Amphid**	**Phasmid**
L1 (empty vector)	100	100
L1	80	35
L2	85	43
L4	100	72

[a] Animals were grown on RNAi plates starting at different larval stages and were assayed for dye filling as adults. For L4 animals, this was 24 h of exposure. n=50 for each.

A

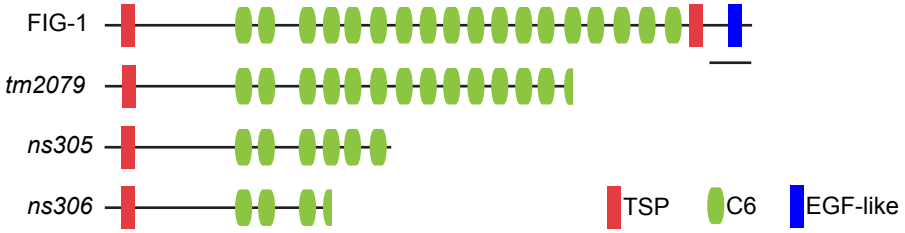

B

Genotype	Normal Dye Filling (%) Amphid	Phasmid
WT	100	100
fig-1 (RNAi)	60	30
fig-1(tm2079)	18	0
fig-1(tm2079); C38G2	90	100
fig-1(tm2079); P_{fig-1} *fig-1* (long)	50	44
fig-1(tm2079); P_{fig-1} *fig-1*	46	42
fig-1(tm2079); P_{glia} *fig-1*	60	15
fig-1(tm2079); P_{neuron} *fig-1*	80	0

C

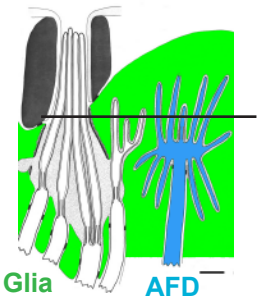

D

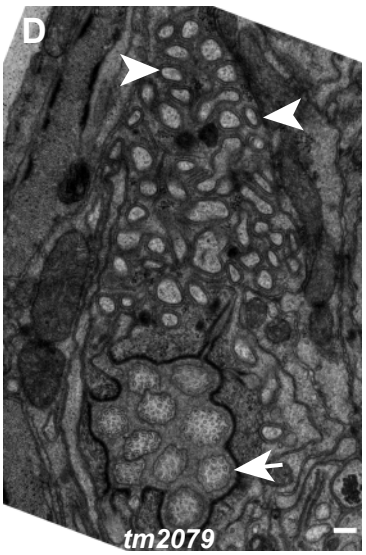

Figure 4.1: The glial gene *fig-1* is required for dye filling and neuronal function

(**A**) FIG-1 domain structure. Red, thrombospondin type 1 domain; green, C6 repeats; blue, EGF-like type II domain; bar, 200 amino acids. The predicted protein produced in different *fig-1* alleles. (**B**) *fig-1* is required for DiI accumulation. One representative line shown for each condition: C38G2, cosmid containing *fig-1*; glial promoter, T02B11.3; neuronal promoter, *sra-6*; n>40 for each. *fig-1* short isoform unless indicated. (**C**) Amphid cartoon with the AFD neuron shown in blue, note the villi-like projections at the level of the cross section. (**D**) In *fig-1(tm2079)* animals, the AFD villi appear normal (arrowhead) as do the channel cilia (arrow). Dorsal is up, scale bar 200 nm.

To determine whether FIG-1 protein can act cell non-autonomously, we expressed a *fig-1* cDNA transgene under either sheath glia (T02B11.3) or sensory neuron (*sra-6*, expressed in ASH, and weakly in ASI, PHA, and PHB) promoters. We found that both transgenes can rescue *fig-1*(*tm2079*) mutants (Figure 4.1B), as would be expected if FIG-1 acted extracellularly.

FIG-1 domain structure

The *fig-1* locus is predicted to generate two alternatively spliced mRNAs encoding proteins of 2892 (short) and 3095 (long) amino acids. Both predicted proteins contain an N-terminal signal sequence, followed by a type 1 thrombospondin domain (TSP1), 18 C6 domains, and a second TSP1 domain (Figure 4.1A). The larger protein is also predicted to contain an additional single EGF-like type II motif at its C-terminus. Although FIG-1 has no mammalian or *Drosophila* homologues, both the TSP1 and EGF-like motifs are characteristic domains found in astrocyte-secreted thrombospondin proteins implicated in synapse development (Christopherson et al., 2005). The C6 domain, so called because it contains six conserved cysteine residues, appears to be present only in nematodes and has no known functions.

To confirm the domain structure of FIG-1, we isolated the *fig-1* cDNA. We verified the presence of the short transcript, but were not able to isolate the predicted longer isoform. PCR-amplification from several cDNA libraries resulted in isolation of clones that contained the last 4 exons spliced to each other, but these were not properly spliced to the rest of the gene and should not result in successful translation.

Conservation of these last 4 exons in other species leads us to believe that they are likely to be part of the gene locus. It is possible that the long form is only spliced under certain conditions that were not represented in the animals used to make the cDNA libraries. However, we cannot be certain when or if the longer isoform containing the EGF-like motif is produced *in vivo*. In *tm2079* mutants, FIG-1 should be truncated at the 14th C6 repeat thus deleting the last 4 C6 repeats, the second TSP1 domain, and the EGF-like domain (Figure 4.1A).

tm2079 mutants are sluggish and avoid bacterial lawns

Mutants that harbor a deletion in the *fig-1* locus have prominent defects in bacteria sensation. When placed on an agar plate that contains a lawn of *E. coli*, the animal's food in laboratory conditions, *tm2079* mutants accumulate just outside the edge of the lawn. In contrast, wild-type animals prefer to stay on the lawn and disperse evenly on it. This bacteria avoidance phenotype is different from that of *npr-1* mutants (de Bono and Bargmann, 1998) which accumulate on the thickest part of the lawn, just inside the edge, since that is where oxygen levels are lowest (Gray et al., 2004). Perhaps due to this self-induced starvation from avoiding bacteria, *tm2079* animals are shorter than wild-type animals and appear unhealthy. Further, *tm2079* animals are sluggish on plates and move slowly when prodded. To confirm this observation, we measured body thrashes in buffer, a measurement of the animal's locomotion. Instead of the smooth sinusoidal bends of wild-type animals, *tm2079* animals often kinked and their thrashing rate (109 thrashes/min) was 59% that of wild-type animals (182 thrashes/min).

In contrast to the Dyf phenotype, which was rescued by introduction of the *fig-1* cDNA or cosmid, the bacteria avoidance and locomotion defects of *tm2079* were not. While this could be because the short cDNA isoform is not sufficient for rescue or because the genomic region present in the fosmid does not contain all regulatory elements (especially those in the 3' region), it raised the question whether these phenotypes are in fact due to loss of *fig-1* activity or another closely linked gene.

A non-complementation screen for new *fig-1* alleles

One way to confirm that a gene is responsible for a phenotype is to find independent alleles of the same gene that have similar phenotypes. To obtain new alleles of *fig-1*, we performed a non-complementation screen for dye uptake. Briefly, *unc-6(e78)* hermaphrodites, a strain that is almost paralyzed because of an X-linked mutation, were mutagenized and crossed to *fig-1(tm2079)* males. F1 cross progeny were identified by their ability to move properly and these animals were screened for those that failed to dye fill. From these F1 animals, F2 progeny that did not carry the *tm2079* deletion were selected by PCR analysis and were further verified for failure to uptake dye. Their *fig-1* locus was then sequenced to identify any mutations present.

This screen identified two new alleles of *fig-1*, *ns305* and *ns306*. DNA sequencing revealed that *ns305* contains a G-to-A transition 4791bp downstream of the start site causing a mutation in the splice-donor site GT at the beginning of intron 10. Intron 10 is 44 bp long thus lack of splicing should result in a shift in the reading frame; this intron also contains two stop codons. The *ns306* allele contained a 16 bp insertion,

TCCTCATATTCCAAAT, in the eighth exon 3805 bp after the start site that causes a frameshift. These two mutants should produce proteins of 1376 and 1088 amino acids respectively, Figure 4.1A. These protein fragments resemble that produced in *tm2079* animals but contain fewer C6 domains.

Only 76% of *fig-1(ns305)* animals failed to uptake dye in the phasmid and approximately a third of the Dyf phasmids showed very faint fluorescence; these defects are less severe than that of *tm2079* animals which show no dye filling. Importantly, *ns305* animals did not border on bacterial lawns. This would seem to suggest that bordering cannot be attributed to lack of *fig-1* activity, however, as this allele does not affect dye filling as strongly as *tm2079*, it is possible that *ns305* retains enough *fig-1* activity to not result in bordering defects. *ns306* animals had a severe Dyf phenotype with 100% of the phasmids and 90% of amphids failing to uptake dye. Although we have not had the chance to characterize these animals carefully, they appeared to avoid bacterial lawns but did not border to the same extent as *tm2079* animals.

tm2079 locomotion and bacteria avoidance defects require serotonin

The bacteria avoidance phenotype of *tm2029* animals is rather peculiar as bacteria are not only a natural food source of *C. elegans* but also the sole food provided for them on Petri dishes. There are two characterized *C. elegans* food responses: basal and enhanced slowing (Sawin et al., 2000). In the basal slowing response, an animal that has been briefly removed from food will slow down when encountering a bacterial lawn, presumably because this increases the chance it will not leave this nutrient-rich area.

This response is abolished in animals that cannot produce dopamine (Sawin et al., 2000). The enhanced slowing response occurs when starved animals encounter a bacterial patch at which time they come to almost a complete stop; no enhanced slowing is observed in animals lacking serotonin and addition of exogenous serotonin causes fed animals to slow down (Sawin et al., 2000).

To test if the phenotypes of *tm2079* animals required dopamine, we examined *fig-1(tm2079)*; *cat-2(e1112)* double mutants, CAT-2 being a tyrosine hydroxylase required for dopamine synthesis (Lints and Emmons, 1999). While the locomotion of these animals improved somewhat, they still avoided bacteria indicating that dopamine is not required for this response. Serotonin synthesis in *C. elegans* requires TPH-1, a tryptophan hydroxylase that catalyzes the rate-limiting step in serotonin biosynthesis (Sze et al., 2000), therefore, we examined *fig-1(tm2079)*; *tph-1(mg280)* animals. These animals did not avoid food, moved normally, and appeared healthy. However, dye uptake was still abnormal in absence of serotonin.

fig-1(tm2079) animals have limited chemotaxis defects

Behavioral testing of *fig-1(tm2079)* animals is confounded by their mobility defects, so we analyzed *fig-1(tm2079)*; *tph-1(mg280)* double mutants which move normally. The double mutants performed as well as *tph-1(mg280)* control animals in odortaxis and chemotaxis assays mediated by the AWA, AWB, AWC, and ASE neurons (Figure 4.2, A-D), suggesting that FIG-1 is not required for these neuronal functions.

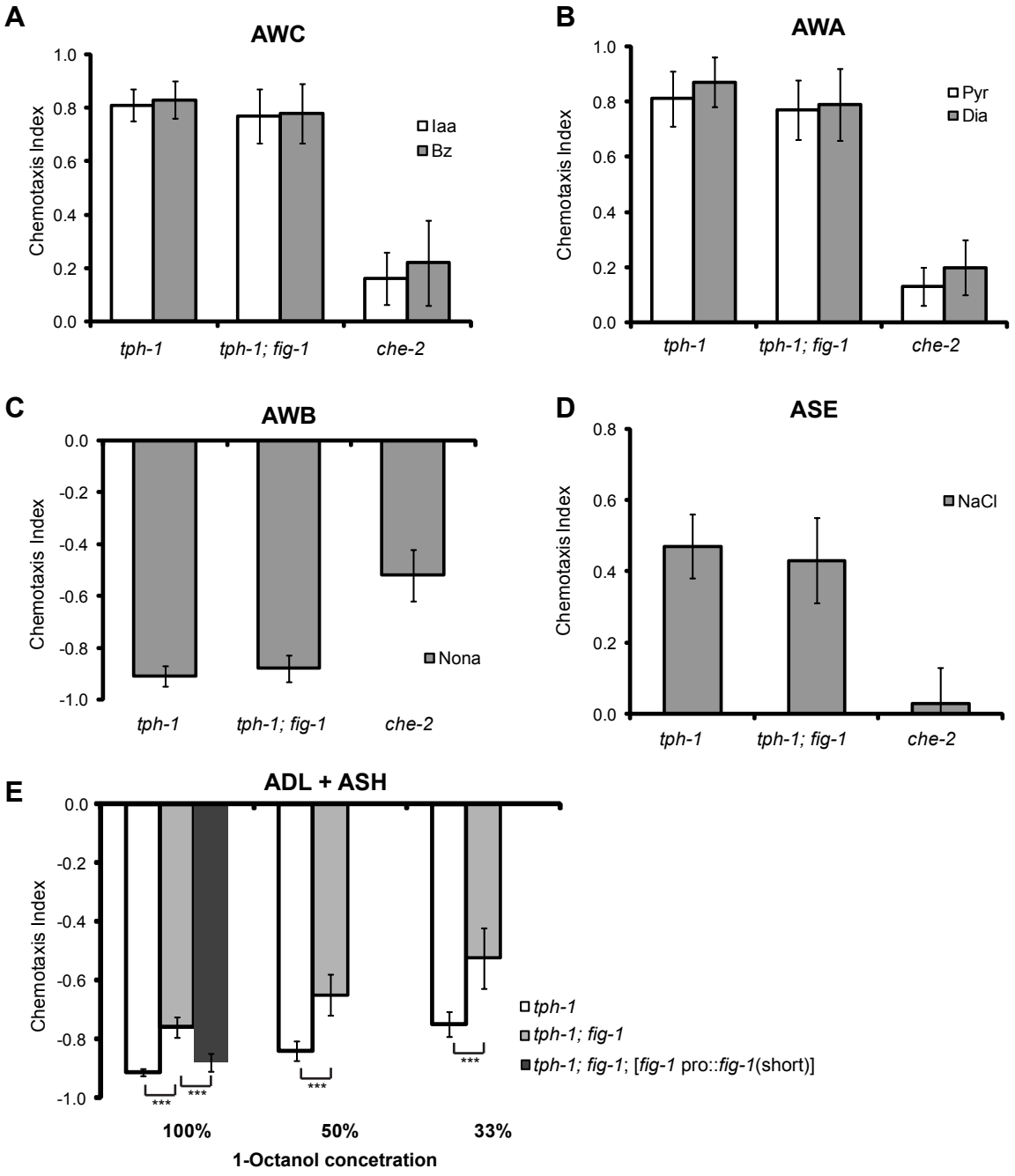

Figure 4.2: *fig-1* mutants have limited behavioral defects

AWC (**A**), AWA (**B**), AWB (**C**), and ASE (**D**) function is not affected in *fig-1(tm2079)* animals. *che-2, che-2(e1033)* chemosensory mutants; error bars, standard deviation of 8 or more assays. (**E**) *fig-1* is required for 1-octanol avoidance, an ADL and ASH mediated behavior. *fig-1(tm2079)* mutants perform worse at all three concentrations, and these defects can be rescued by *fig-1*(+). Asterisks, $p < 0.001$ (Student's t-test); error bars, confidence intervals at 95% from at least 24 assays. To suppress locomotory defects of *fig-1(tm2079)* animals, all assays were performed in the *tph-1(mg280)* background.

However, we did identify a modest but significant defect in long-range 1-octanol avoidance in these animals (Figure 4.2E). *fig-1(tm2079)*; *tph-1(mg280)* mutants performed significantly worse than *tph-1(mg280)* at all three 1-octanol concentrations tested. Importantly, this behavioral defect was rescued by introduction of the short FIG-1 isoform under its own promoter.

Avoidance of long-range 1-octanol is mediated by ADL and, to a lesser extent, ASH (Troemel et al., 1997) although ASH plays a more important role in short-range 1-octanol avoidance (Troemel et al., 1995; Chao et al., 2004). Thus, there are two possible explanations for the *fig-1* requirement in this behavior. FIG-1 could be required only for the proper function of ASH, which might explain the modest defect observed. Alternatively, FIG-1 could be required for ADL function, but acts redundantly with other factors hence only the minor defect. This might also explain why no defects are observed for the other neurons (Figure 4.2, A-D).

A potential role for FIG-1 in Ca^{2+} dynamics in ASH

The behavioral defects suggest that ASH or ADL require FIG-1 for proper function. Because we can monitor ASH status with G-CaMP, we measured its Ca^{2+} dynamics in response to stimulation with a high osmolarity solution in *tm2079* animals. In wild-type animals, exposure to 1M glycerol results in an increase in Ca^{2+} levels that is sustained for the duration of the stimulus, at least for 20 s, and a second Ca^{2+} increase upon removal of the stimulus, which decays in a few seconds (Figure 4.3A). Although the data is preliminary, *tm2079* animals respond to the onset and removal of the stimulus

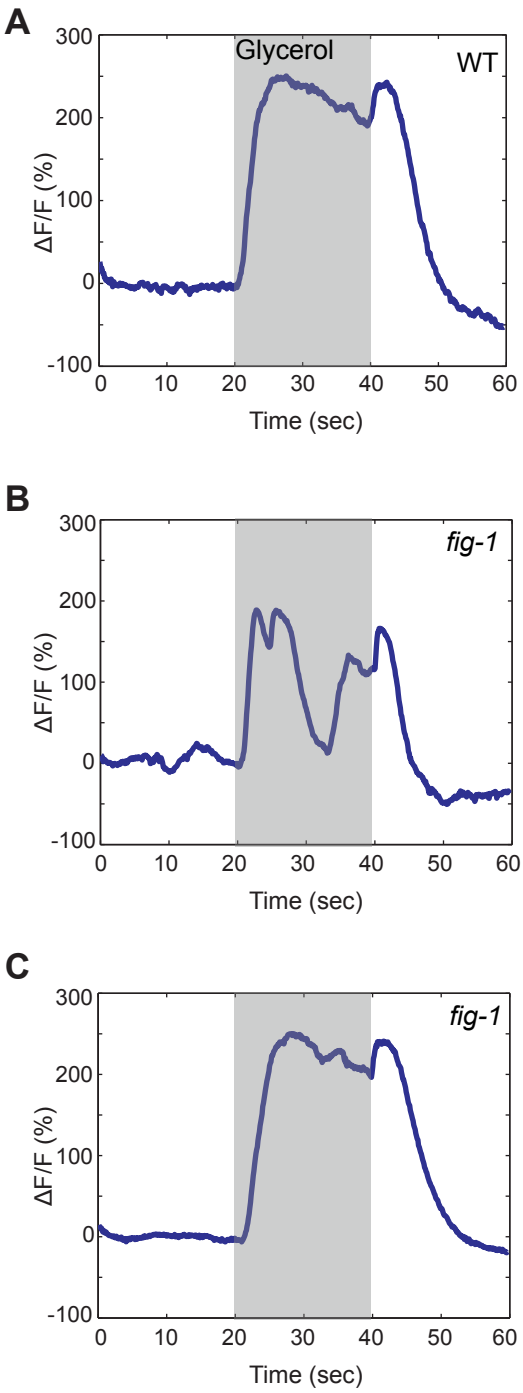

Figure 4.3: FIG-1 might play a role in ASH Ca responses

(**A**) ASH Ca levels remain elevated for the duration of the stimulus (1M glycerol, shaded region). (**B**) A trial in which a *fig-1(tm2079)* animal responds to stimulus onset and removal, but fails to sustain elevated Ca levels. (**C**) Another trial of the same animal as in B, this time showing a normal Ca response.

but, in half of the trials, they fail to sustain high Ca^{2+} levels for the duration of the stimulus (Figure 4.3B). Interestingly, the same animal can give both normal and abnormal responses in different trials (Figure 4.3, B-C). However, as only limited number of animals were tested (n=5, all recordings in one day), further characterization is required before any conclusion can be drawn. It would be interesting to increase the stimulus duration in order to observe if the Ca^{2+} oscillations become more evident.

Discussion

Sensory organs in many species are highly conserved in structure and organization. In addition, recent studies suggest that *C. elegans* glia share developmental similarities with vertebrate glia (Yoshimura et al., 2008). Thus it is possible that at least some of the functions and perhaps the molecular pathways of amphid sheath glia might be conserved in other sensory systems. Here we characterize a glial protein, FIG-1, that is important for sensory neuron function and dye filling. This protein contains two TSP1 domains, which is intriguing, as recent studies have found important postsynaptic roles for astrocyte-secreted thrombospondins in synapse assembly and function (Christopherson et al., 2005).

FIG-1 function in sensory organs

Analysis of the *tm2079* allele suggests that the TSP1 domains might be important for *fig-1* function in neuronal dye uptake and behavior. The *fig-1*(*tm2079*) lesion is a

deletion predicted to truncate the protein before the second TSP-1 domain, suggesting that this domain is required for dye filling and behavior generation which are defective in these mutants. Moreover, both these defects can be rescued by introduction of the short FIG-1 isoform (Figure 4.1), suggesting that the TSP1 but not the EGF-like type II domain is required for these FIG-1 activities.

How might FIG-1 act in sensory organs? The two prominent domains of the short FIG-1 isoform are TSP1 and C6 repeats. The function of the C6 repeats has not been characterized as they are a nematode-specific module but given the large number present in FIG-1 it is likely that they play a structural role or mediate interactions with the extracellular matrix. The latter function is consistent with the well-characterized matrix interactions of TSP1domains in many species (Adams and Tucker, 2000). We note that extracellular localization of FIG-1 could not be established in these studies as we were unable to detect GFP fluorescence of FIG-1::GFP chimera proteins. However, rescue of the dye filling defects of *fig-1(tm2079)* animals could be achieved by neuronal or glial expression suggesting that the protein is secreted. Consistent with this observation, FIG-1 contains a signal peptide as well as the two extracellular domains, TSP1 and C6 repeats. Still, it would be informative to image the extracellular localization of FIG-1 to see if it is released specifically within the amphid channel. Further, FIG-1 might be only secreted around the channel neurons but not the sheath-embedded neurons which would be consistent with the normal odortaxis in *tm2079* mutants.

The TSP1 domain can interact with many proteins including collagen, fibronectin, TGF-β, heparan sulfate, proteoglycans, and many glycoproteins (Adams and Tucker, 2000). A major function of thrombospondin is the modulation of extracellular matrix

proteases. Particularly in clotting, thrombospondin 1 downregulates the activity of thrombin through a mechanism in which the two proteins form a complex mediated by intermolecular disulfide bonds (Browne et al., 1988). The abundance of interactions of TSP1 domains with extracellular matrix components suggests that they might control multiple aspects of the environment in which the sensory cilia reside.

The extracellular matrix present in the amphid channel is most likely secreted by the amphid sheath glial cell, which has a prominent secretory organelle as determined by EM (Ward et al., 1975; Perkins et al., 1986). Indeed, the sheath glial cell transcriptome is enriched for secreted proteins (M. Tevlin). These glial secreted proteins probably act through a number of mechanisms to form an appropriate extracellular space in which the sensory cilia can function. One of these glial proteins required for neuronal dye uptake is FIG-1. Interestingly, RNAi against *fig-1* in adult animals is sufficient to induce dye filling defects, suggesting that FIG-1 must have a high turnover rate. The continuous turnover of the amphid channel matrix raises the possibility that the glia might be able to change the composition of this matrix depending on environmental conditions (e.g. starvation). This might in turn modulate the function of amphid neurons on the timescale of several hours. This hypothesis predicts that sheath glial gene expression may be modulated by environmental factors. While we have not observed differential expression of FIG-1, the expression of a glial receptor tyrosine kinase (*ver-1*) is upregulated at higher temperatures (unpublished data of Carl Procko in our laboratory).

fig-1 mutants have only limited behavioral defects. This could be because the deletion does not remove the whole protein or, FIG-1 might act redundantly with other proteins to promote neuronal function. The amphid sheath glia secretes at least two other

TSP1 domain-containing proteins, suggesting that they might function in the same manner as FIG-1, although FIG-1 might act in conjunction with other proteins. To identify these proteins, a candidate approach could be taken by making double mutants to enhance the behavioral defects of *fig-1(tm2079)* animals. To isolate the neuronal molecules that might interact with FIG-1, one could try to suppress the *fig-1* defects. This is easiest for the dye uptake defects since a very large number of animals can be screened allowing the isolation of even rare gain of function mutations. This screen is likely to yield neuronal genes that bypass the need for FIG-1 in dye uptake.

Might FIG-1 modulate neuronal voltage-gated Ca^{2+} channels?

Recent work has shown that the EGF-like type II motif might mediate a large part of thrombospondin glial functions. Specifically, the EGF-like domain binds to the α2δ subunit of the neuronal voltage-dependent Ca^{2+} channel and this interaction is required for thrombospondin-mediated synapse formation (C. Eroglu and B. Barres, personal communication). We have been unable to confirm that this domain is part of the FIG-1 protein *in vivo*, but it is possible that this domain is spliced only under specific conditions so we may speculate about its function. Interestingly, *fig-1* animals appear to have defects in their Ca^{2+} responses (Figure 4.3). Although the data is preliminary, FIG-1 might be required to maintain high neuronal Ca^{2+} levels during stimulation. The only *C. elegans* L-type voltage-gate calcium channel EGL-19 is required for proper ASH neuron intracellular Ca^{2+} dynamics, as in *egl-19* mutants only 50% of the normal Ca^{2+} increase is observed (Hilliard et al., 2005). The *C. elegans* genome encodes two α2δ subunits, *unc-*

36 and T24F1.6, and only *unc-36* is required alongside *egl-19* for achieving maximal Ca^{2+} responses in cultured mechanosensory neurons (Frokjaer-Jensen et al., 2006). Further, at least in the mechanosensory neurons, Ca^{2+} release from internal stores is not required as blocking internal release does not affect Ca^{2+} dynamics (Frokjaer-Jensen et al., 2006). Therefore, in light of the mammalian data, a likely mechanism by which FIG-1 affects ASH Ca^{2+} levels could be by interacting with UNC-36 to modulate the activity of the L-type calcium channel. If this is the case, rescue of the abnormal Ca^{2+} dynamics of *fig-1(tm2079)* mutants should require expression of the full-length protein, which is the only isoform that contains the EGF-like domain.

Does *fig-1* play a role in bacterial avoidance?

The most obvious defect of *tm2079* animals is their avoidance of bacterial lawns. However, we have been unable to rescue this defect by expressing the wild-type form of *fig-1*, raising doubts about the causation of this phenotype by the lesion in *fig-1*. To determine if this phenotype is due loss of *fig-1* activity, we isolated two new alleles that disrupt this gene. One of these alleles, *ns306*, results in bacteria avoidance as most animals are found outside of the bacterial lawn, but animals do not congregate at the edge as do *tm2079* mutants. Further characterization of these mutants after performing back crosses is required to determine if this is a *fig-1* phenotype. However, it is likely that FIG-1 plays some role in sensation of bacteria. Even if *ns306* animals do not border, analysis of *tm2079/ns306* animals might reveal if this phenotype is caused by loss of FIG-1.

What role might fig-1 play in bacterial avoidance? In *C. elegans*, exposure to pathogenic bacteria induces olfactory avoidance of that specific pathogenic strain (Zhang et al., 2005). The pathogenic infection results in increased serotonin levels in the ADF amphid neurons and *tph-1* animals, which cannot synthesize serotonin, cannot learn to avoid pathogenic bacteria (Zhang et al., 2005). Interestingly, the bacterial avoidance of *fig-1(tm2079)* animals is suppressed by *tph-1*. Thus, *fig-1(tm2079)* animals might recognize standard *E. coli* as pathogenic. One explanation for this phenotype is that *tm2079* animals have compromised innate immunity and are prone to infection. We did not observe bacterial infection when inspecting these animals under a compound microscope but more careful examination is required to rule out this possibility. Alternatively, ADF serotonin upregulation might occur constitutively in *fig-1* animals, causing them to wrongly classify any bacteria present as pathogenic. As ADF is part of the amphid, it is plausible that FIG-1 might modulate the activity of this neuron. However, further characterization of this phenotype is required before conclusions can be drawn. It is important to establish that *fig-1* lesions lead to bacterial avoidance and it must be shown that this phenotype depends on serotonin being present only within ADF and not the other serotonergic neurons of the animal.

In summary, we have identified a glial protein mediating some of the glial functions uncovered by the glial ablation experiments. FIG-1 is required for dye filling and has some effects on neuronal function. This suggests that other glial proteins might be required for enabling neuronal function.

Chapter 5

The conserved proteins CHE-12 and DYF-11 are required for sensory cilium function

Summary

Sensory neurons view the world through their cilia, evolutionarily conserved dendritic appendages that convert environmental stimuli into neuronal activity. Although several cilia components are known, the functions of many remain uncharacterized. Furthermore, the basis of morphological and functional differences between cilia remains largely unexplored. To understand the molecular basis of cilia morphogenesis and function, we studied the *C. elegans* mutants *che-12* and *dyf-11*. These mutants fail to concentrate lipophilic dyes from their surroundings in sensory neurons, and are chemotaxis defective. In *che-12* mutants, sensory neuron cilia lack distal segments, while in *dyf-11* animals, medial and distal segments are absent. CHE-12 and DYF-11 are conserved ciliary proteins that function cell-autonomously and are continuously required for maintenance of cilium morphology and function. CHE-12, composed primarily of HEAT-repeats, may not be part of the intraflagellar transport (IFT) complex, and is not required for the localization of some IFT components. DYF-11 undergoes IFT-like movement and may function at an early stage of IFT-B particle assembly. Intriguingly, while DYF-11 is expressed in all *C. elegans* ciliated neurons, CHE-12 expression is restricted to some amphid sensory neurons, suggesting a specific role in these neurons. Our results provide insight into general and neuron-specific aspects of cilium development and function.

Sensory cilia biogenesis and function

Sensory cells, such as vertebrate photoreceptors, mechanosensory hair cells in the ear, and olfactory neurons, project non-motile cilia (Wheatley et al., 1996). These sensory cilia are positioned at the interface between an animal and its environment, and transduce information through cell-surface receptors, signal transduction molecules, and specialized ion channels to the nervous system (Pazour and Witman, 2003; Efimenko et al., 2006; Singla and Reiter, 2006). The ability of cilia to act as sensory transduction sites is due, at least in part, to their specialized morphologies that allow for compartmentalization of sensory and signaling components. How this specialized ciliary architecture arises and how signaling molecules are organized within cilia remain poorly understood, although genomic and proteomic studies have identified sets of proteins conserved in all cilia (Avidor-Reiss et al., 2004; Emoto et al., 2004; Blacque et al., 2005; Efimenko et al., 2005).

The hermaphrodite nematode *C. elegans* contains 60 ciliated sensory neurons, 28 of which are assembled into the bilateral amphid and phasmid sensilla (Ward et al., 1975; White et al., 1986), located in the head and tail of the animal, respectively. *C. elegans* sensory cilia are comprised of a proximal basal body, a medial segment containing doublet microtubules, and a distal segment consisting of singlet microtubules (Ward et al., 1975; Perkins et al., 1986). Some *C. elegans* sensory neurons end in modified cilia that have a wing- or finger-like morphology (Ward et al., 1975). Defects in amphid cilia structure result in behavioral deficits, as manifested by abnormal chemotaxis to soluble attractants (Che phenotype) or to volatile attractants and repellants (Perkins et al., 1986;

Bargmann, 1993). Some amphid sensory neurons can take up and concentrate lipophilic dyes from their surroundings through a pore and channel generated by two associated glial cells (Hedgecock et al., 1985; Blacque et al., 2005). This dye uptake is generally disrupted in animals with abnormal cilia (Dyf phenotype) (Perkins et al., 1986), providing a convenient assay for identifying mutants with defects in sensory cilia biogenesis and function.

The assembly and maintenance of *C. elegans* cilia, like that of flagella, depends on intraflagellar transport (IFT), the process by which IFT particles are thought to transport cargo in and out of the cilium (Scholey, 2003). Studies of *Chlamydomonas reinhardtii* flagella suggest that each IFT particle is composed of two biochemically-defined complexes, A and B (Rosenbaum and Witman, 2002). The anterograde movement of the IFT particle is powered by kinesin-2 molecular motors (Orozco et al., 1999; Snow et al., 2004), while the retrograde movement depends on an IFT-specific dynein (Orozco et al., 1999). In *C. elegans*, several components of the IFT-A and IFT-B subparticles have been characterized and shown to move within cilia. Disruption of these components results in Che and Dyf defects (Collet et al., 1998; Scholey, 2003; Bell et al., 2006; Chen et al., 2006).

Mutants in the *C. elegans che-12* and *dyf-11* genes were isolated in genetic screens for animals displaying dye uptake defects (Perkins et al., 1986; Starich et al., 1995). The phenotype of these two mutants is consisted with sensory organ dysfunction, and they are likely to encode components of the ciliary proteome. To better understand sensory neuron morphogenesis and function, we cloned and characterized these two mutants.

Results

che-12 animals exhibit a restricted set of dye uptake and behavioral defects

Amphid sensory neurons of *C. elegans* mutants defective in cilium formation and function fail to concentrate lipophilic dyes, such as FITC and DiI, from their surroundings and fail to perform some sensory neuron-mediated behaviors, such as chemotaxis (Perkins et al., 1986). Three alleles of the *che-12* gene, *e1812*, *mn389*, and *mn399*, were previously isolated based on the inability of animals carrying these alleles to concentrate FITC (Perkins et al., 1986; Starich et al., 1995). To further characterize these alleles, we tested them in dye uptake and behavioral assays. 100% of *che-12*(*e1812*), *che-12*(*mn389*), and *che-12*(*mn399*) animals failed to take up FITC in amphid neurons (n=100 for each allele; Figure 5.1B). However, only 2% of *che-12*(*e1812*) and *che-12*(*mn389*) mutants, and 51% of *che-12*(*mn399*) mutants, failed to take up DiI (n=100 for each allele) (Figure 5.1E), a selectivity that has not been previously described.

Contrary to a previous report describing normal chemotaxis of *che-12(e1812)* mutants towards NaCl (Perkins et al., 1986), we observed defects in this ASE amphid neuron-mediated behavior (Bargmann and Horvitz, 1991b) for all three *che-12* alleles (Figure 5.1G). Furthermore, all *che-12* mutants were defective in avoidance of a high osmolarity 4 M fructose barrier, a behavior mediated by the ASH amphid neurons (Kaplan and Horvitz, 1993) (Figure 5.1G). However, *che-12* mutants were normally attracted to the volatile odorants isoamyl alcohol (1%) and methyl pyrazine (1%) (Figure 5.1G), behaviors mediated by the AWC and AWA amphid neurons (Bargmann, 1993), respectively. Thus, *che-12* is required for some, but not all, amphid cilia functions.

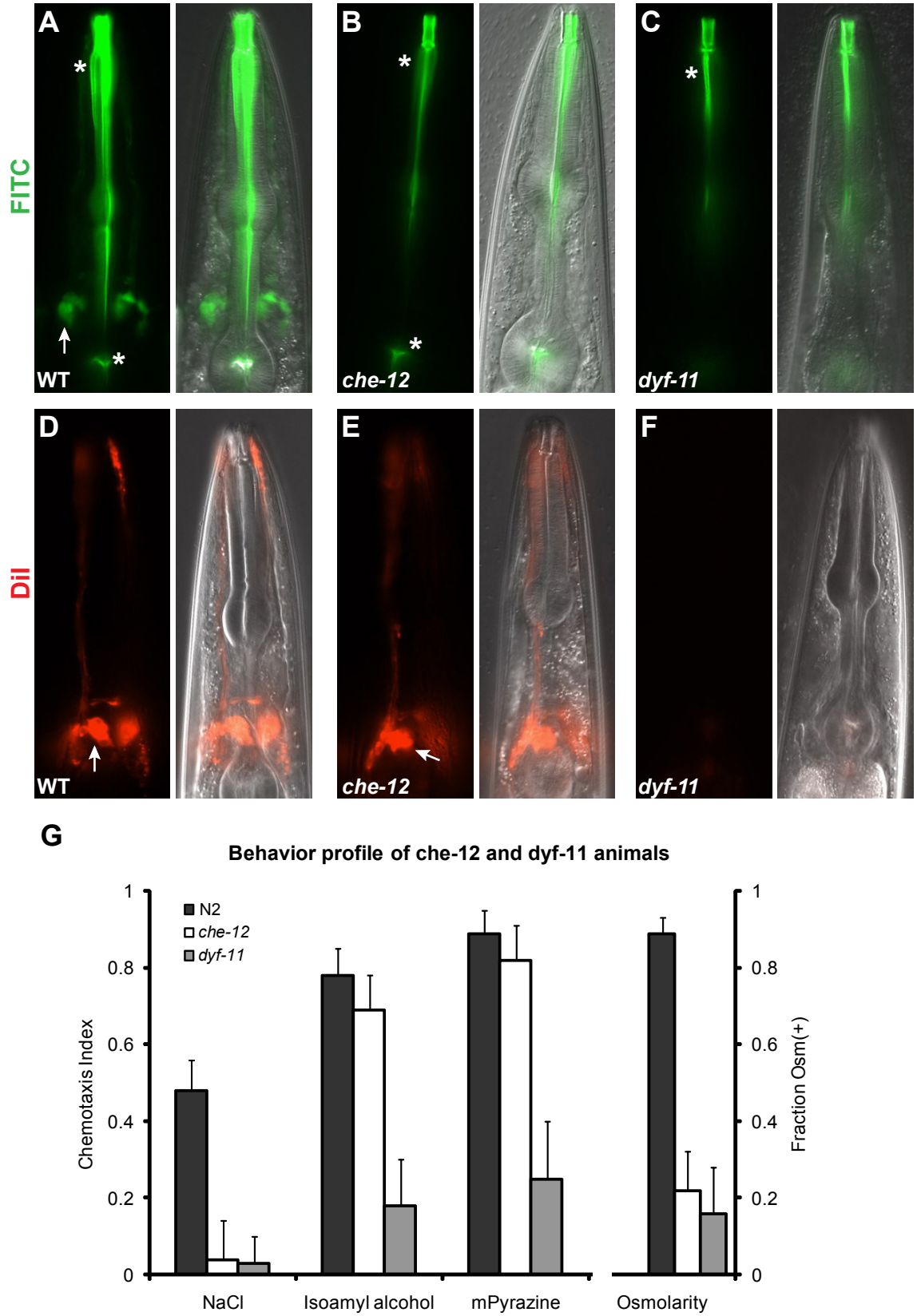

Figure 5.1: Characterization of *che-12* and *dyf-11* mutants

Figure 5.1: Characterization of *che-12* and *dyf-11* mutants

(**A**) Uptake of FITC by amphid sensory neurons in a wild-type animal. Left, fluorescence image; right, fluorescence and DIC overlay of the same image. Arrow, cell bodies; asterisks, non-specific pharyngeal staining. (**B**) A *che-12(mn389)* mutant showing FITC uptake defect. (**C**) *dyf-11(mn392)* animals also fail to take up FITC. (**D**) DiI staining pattern of a wild-type animal. (**E**) *che-12(mn389)* animals can also take up DiI. (**F**) *dyf-11(mn392)* animals fail to take up DiI. (**G**) Behavioral defects of *che-12(mn399)* and *dyf-11(mn392)* mutants. Both mutants fail to chemotax to 0.2M NaCl and are unable to respond to an osmotic barrier. *dyf-11*, but not *che-12*, animals show defects in odortaxis toward 1% isoamyl alcohol and 1% methyl pyrazine. In all figures anterior is up unless otherwise indicated.

dyf-11 is required for sensory neuron dye uptake and chemotaxis

Mutants in the *dyf-11* gene were also previously isolated in screens for animals exhibiting dye uptake defects (Starich et al., 1995), suggesting that this gene may affect cilium structure and/or function. To further characterize the phenotype of *dyf-11* mutants, we tested these animals in dye uptake and behavior assays. A single *dyf-11* allele, *mn392*, is known, and we found that mutants homozygous for this allele displayed a fully penetrant defect in concentrating the two lipophilic dyes FITC and DiI (Figure 5.1, C and F), consistent with previous studies (Starich et al., 1995). *dyf-11*(*mn392*) animals also exhibited strong defects in chemotaxis toward NaCl, isoamyl alcohol, and methyl pyrazine, and in avoidance of a high osmolarity barrier (Figure 5.1G). We further noticed that *dyf-11* mutants could not enter the dauer state, and mutant males showed low mating efficiency, defects that are characteristic of impaired cilia function. Taken together, therefore, these results suggest that *dyf-11* is required for normal sensory neuron function and is likely to play a role within cilia.

Cilia of *che-12* and *dyf-11* mutants are structurally abnormal

To determine the cause of the Dyf and Che defects of *che-12* and *dyf-11* mutants, we examined the structures of amphid cilia in these mutants using fluorescence and electron microscopy. We first focused on the ASE neuron, which mediates attraction to NaCl, a behavior defective in both *che-12* and *dyf-11* mutants. As observed by fluorescence microscopy (Figure 5.2, A-B), the ASER cilium was shortened in *che-12(mn399)* animals expressing the *gcy-5* pro::GFP ASER-specific reporter transgene (Yu

et al., 1997), with an average cilium length of 4.3 ± 0.5 μm (n=10) compared to the wild-type average ASER cilium length of 6.1 ± 0.6 μm (n=10). Cilia were even more severely shortened in *dyf-11(mn392)* animals expressing the same reporter transgene (average length of 1.4 ± 0.3 μm, n=10; Figure 5.2C). These morphological defects could account for the ASE-mediated NaCl chemotaxis defects of *che-12* and *dyf-11* mutants.

Examination of *che-12*(*mn389*) and *dyf-11*(*mn392*) mutants by electron microscopy (EM) revealed defects consistent with the fluorescence imaging studies. Specifically, the channel cilia of *che-12*(*mn389*) animals lacked distal ciliary structures normally pervaded by singlet microtubules (Figure 5.2, J-K; 3/3 animals examined); however, the middle ciliary segment and the transition zone were intact in these animals, as indicated by the presence of doublet microtubules (Figure 5.2L). 3/3 *dyf-11*(*mn392*) animals examined by EM lacked all recognizable ciliary structures (Figure 5.2, H-I), except for the proximal transition zone. We did not observe any sheath glial defects at the EM level in any of the che-12 alleles, contrary to previous reports (Perkins et al., 1986) showing glial secretion defects in the *e1812* allele.

Because *dyf-11*, but not *che-12*, is also required for AWC-mediated odortaxis, we hypothesized that the elaborate wing-like ciliary extensions of the AWC neuron might display structural abnormalities in *dyf-11* animals, but remain normal in *che-12* mutants. Indeed, fluorescence imaging revealed that *dyf-11*(*mn392*), but not *che-12*(*mn399*) animals, lack the wing-like ciliary extensions of AWC neurons (Figure 5.2, D-F). These morphological studies suggest that *che-12* is important for the assembly of distal ciliary structures, and that *dyf-11* is absolutely required for cilium biogenesis.

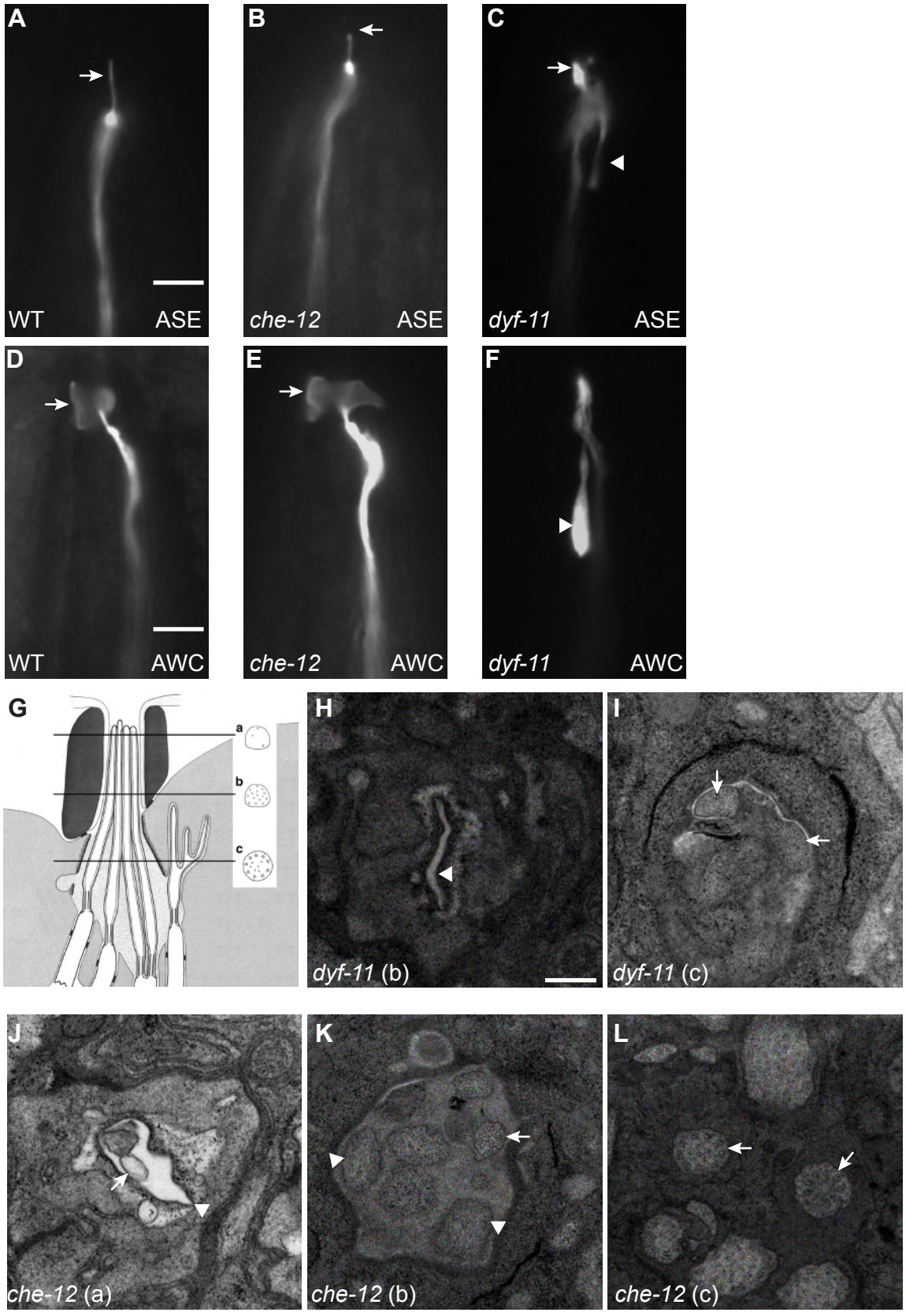

Figure 5.2: *che-12* and *dyf-11* mutants have defects in cilium structure

Figure 5.2: *che-12* and *dyf-11* mutants have defects in cilium structure

(**A**) The ASER cilium, arrow, of a wild-type animal expressing *gcy-5* pro::GFP. (**B**) *che-12(mn399)* animals have a short ASER cilium. (**C**) The stunted ASER cilium, arrow, of a *dyf-11* animal. A backward process is visible, arrowhead. (D) The AWC cilium, arrow, of a wild-type animal expressing *str-2* pro::GFP. (**E**) In *che-12(mn399),* the AWC cilium retains its winged morphology, arrow. (**F**) The AWC cilium fails to spread in *dyf-11* animals. A backward process is present, arrowhead. Scale bar A-F, 5 μm. (**G**) A cartoon of the amphid channel, adapted from Perkins *et al*. (1986). Three of the eight channel neurons are depicted. The locations of EM cross sections are shown. The normal cross-sectional profile of a cilium at each level is diagramed. (**H**) EM cross section at level "b" of a *dyf-11*(*mn392*) animal. Note the empty cavity (arrowhead) where amphid cilia should be located. (**I**) EM cross section of a *dyf-11*(*mn392*) animal at level "c" showing the absence of doublet or any other microtubules in neuronal profiles, arrows. (**J**) EM cross section of a *che-12(mn389)* mutant at level "a". The amphid cilia are short, and so only two of the ten neuronal profiles are evident. Arrowhead, amphid opening. Arrow, the beginning of a cilium. (**K**) EM cross section of the distal segment of a *che-12(mn389)* animal at level "b". No singlet microtubules are seen in most cilia, arrowheads. A cilium containing doublet microtubules is shown, arrow. (**L**) Proximal EM cross section of a *che-12(mn389)* animal at level "c". The cilia appear normal and contain doublet microtubules, arrows. Scale bar H-L, 300 nm. In H-L, dorsal is up.

CHE-12 is a conserved HEAT repeat protein

Previous genetic mapping experiments placed the *che-12* gene in the interval between the *unc-42* and *daf-11* genes on chromosome V (Starich et al., 1995). To narrow this interval further, *unc-42(e270) che-12(mn399) egl-9(n586)* hermaphrodites were crossed to CB4856 (Hodgkin and Doniach, 1997) males, which contain many single nucleotide polymorphisms (SNPs) with respect to N2 (Wicks et al., 2001). From the F2 progeny, Egl non-Unc and Unc non-Egl animals were selected. These recombinants were soaked in FITC to determine their *che-12* genotype. SNP analysis limited the genomic location of *che-12* between the SNPs C12D8:34312 and AC3:3025. Cosmid clones containing DNA spanning this region were injected singly into *che-12* animals and transgenic animals were tested for rescue of the FITC uptake defect. Interestingly, we found that *che-12* animals would not yield transgenic progeny when injected, which necessitated injection of heterozygous animals. It is not clear how this phenotype arises. Cosmid B0024 was the only one to give rescue (3/3 transgenic lines examined; Figure 5.3A), suggesting that this cosmid contained the *che-12* gene. Indeed, a 9.2 kb subclone of cosmid B0024, containing only the B0024.8 gene, was sufficient for rescue (3/3 lines examined). To confirm that B0024.8 was *che-12*, we sequenced the exons and exon/intron junctions of the gene, and identified lesions in all three *che-12* mutants described above (Figure 5.3B). The *che-12*(*e1812*) allele contained a G-to-A transition that disrupts the predicted splice-donor site of intron 16. The *che-12*(*mn389*) allele contained an 88 bp deletion, removing the last 47 bp of exon 13; and the *che-12*(*mn399*) allele harbored an 849 bp deletion, removing most of intron 12, exon 13, and the first 15 bp of exon 14, and is, therefore, likely to be the most defective *che-12* allele of the three.

Sequencing of another reported *che-12* allele, *e1813*, showed that it contained the same lesion present in *che-12*(*e1812*) animals, and was, thus, unlikely to be an independent isolate.

To confirm the predicted *che-12* gene structure (www.wormbase.org, release WS170), we isolated the *che-12* cDNA. Sequence analysis of this cDNA revealed that exon 10 is 291 bp longer than in the predicted transcript. By sequencing genomic DNA from the *che-12* region of wild-type animals, we found that this misprediction arose because a C nucleotide at the beginning of intron 10 was not present in the annotated genomic sequence.

Analysis of the *che-12* cDNA revealed that it encodes a protein of 1282 amino acids. A search of available protein databases using the BLAST program (Altschul et al., 1990) showed that the putative CHE-12 protein shares 34% similarity and 20% identity with a protein predicted to be encoded by human cDNA clone KIAA0423 (Ishikawa et al., 1997), and that has been detected by mass spectroscopy in human fetal brain (Hepner et al., 2005). Sequence analysis of the predicted CHE-12 protein suggests that it probably contains at least seven HEAT repeats, 39 amino-acid long elements that fold to form two anti-parallel α-helices (Andrade and Bork, 1995).

DYF-11 is similar to the mammalian microtubule-associated protein MIP-T3

Previous work had established that *dyf-11(mn392)* was located on the left arm of chromosome X (Starich et al., 1995). To refine this position, *dyf-11*(*mn392*)

hermaphrodites were crossed to CB4856 males. From this cross, 238 dye-filling defective F2 animals were isolated, and DNA prepared from their progeny was characterized for the presence of N2 and CB4856 SNPs. This analysis revealed that *dyf-11* resides between the SNPs F39H12:15494 and F02G3:5645 (Figure 5.3C). This region contains 20 predicted genes, and sequencing of the predicted gene C02H7.1 from *dyf-11(mn392)* animals revealed that it contains a C-to-G mutation, altering codon 140, encoding serine, to an opal nonsense mutation (Figure 5.3D). To confirm that C02H7.1 was indeed *dyf-11*, we introduced the C02H7 cosmid, as well as a 4.1 kb DNA fragment containing only the C02H7.1 coding and regulatory sequences, into *dyf-11*(*mn392*) animals. Both transgenes rescued the dye uptake defect (3 transgenic lines examined for each transgene; Figure 5.3C). Together, these observations strongly suggest that C02H7.1 is *dyf-11*.

To decipher the *dyf-11* gene structure, we isolated and sequenced a full-length cDNA for the gene, confirming the predicted gene structure (www.wormbase.org, release WS170). Comparison of the predicted 535 amino-acid-long DYF-11 protein to proteins in available databases showed that DYF-11 shares 43% similarity and 24% identity with the human protein MIP-T3. MIP-T3 has been shown to interact with taxol-stabilized microtubules and with tubulin *in vitro* (Ling and Goeddel, 2000), suggesting that DYF-11 may directly contact ciliary microtubules. Analysis of the DYF-11 protein sequence revealed two domains of note: a lysine-rich region between amino acids 122 and 214, and a predicted C-terminal coiled-coil region, a domain found in a number of IFT complex B proteins (Cole, 2003), between amino acids 420 and 529.

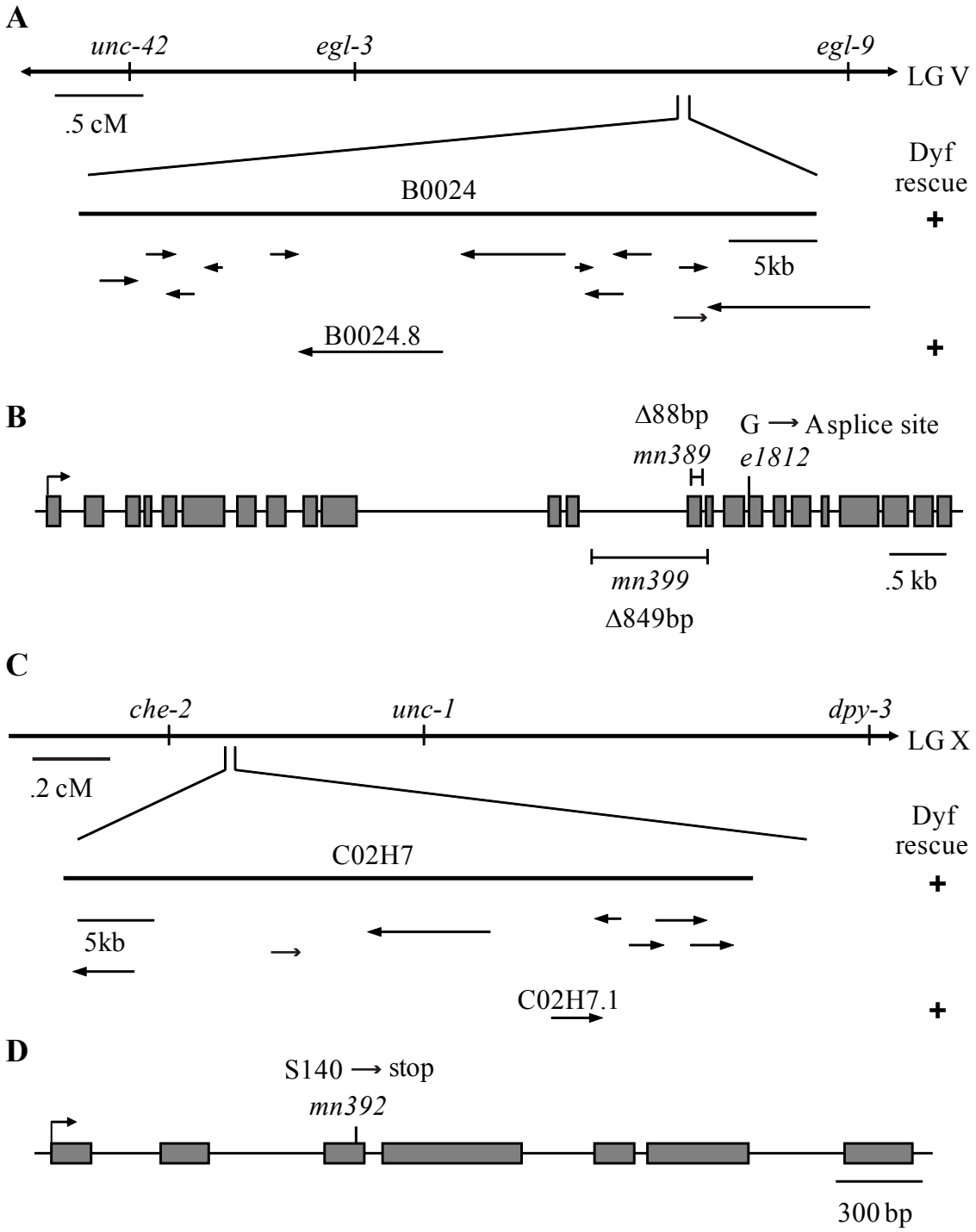

Figure 5.3: The genomic structures of *che-12* and *dyf-11*

(**A**) *che-12* was mapped to the indicated region of chromosome V. The Dyf defect could be rescued by injection of the B0024 cosmid or the B0024.8 gene. (**B**) Genomic structure of B0024.8. The positions of the three alleles are shown. (**C**) *dyf-11* was mapped to the indicated region of chromosome X. A single gene, C02H7.1, within cosmid C02H7, could rescue the Dyf defect. (**D**) Genomic structure of C02H7.1 and position of the *mn392* allele.

che-12 is expressed in a subset of sensory neurons

The phenotypic characterization of *che-12* and *dyf-11* suggested that both genes are likely to be expressed in sensory neurons. To test this idea, we determined the expression pattern of each gene. To examine *che-12* expression, we generated a transgene bearing the 936 bp sequence present immediately upstream of the *che-12* translation start site, fused to the gene encoding GFP, and introduced it into wild-type animals. This same 936 bp promoter fragment, which spans nearly the entire non-coding interval between the stop codon of the upstream gene, *gcy-6*, and the start codon of *che-12*, when driving expression of a *che-12* cDNA::GFP fusion (see below) was sufficient to rescue the dye uptake defects of *che-12*(*mn389*) animals. Inspection of three independent *che-12* pro::GFP transgenic lines showed that *che-12* is expressed in only the subset of amphid neurons that lack wing- or finger-like ciliary extensions (Figure 5.4A), and in the two phasmid neurons (Figure 5.4B). To confirm this expression pattern, we generated animals bearing two transgenes, a *che-12* pro::mCherry reporter and an *osm-6* pro::GFP reporter, which is expressed in most or all ciliated neurons (Collet et al., 1998). Overlap of expression was only seen in amphid and phasmid neurons. These results are consistent with the structural and behavioral defects exhibited by *che-12* mutants and suggest that *che-12* may only function in amphid neurons possessing simple cilia.

dyf-11 is expressed in all ciliated sensory neurons

To visualize the expression pattern of *dyf-11*, we used the 1868 bp immediately upstream of the *dyf-11* translation start site to drive GFP expression in wild-type animals

Figure 5.4: CHE-12 and DYF-11 are expressed in ciliated neurons in a DAF-19 dependent manner

(**A**) CHE-12 is expressed in a subset of amphid neurons. Arrow, neuronal cell bodies; arrowhead, dendritic processes. (**B**) CHE-12 is also present in phasmid neurons. (**C**) Expression of DYF-11 is seen in most ciliated neurons including those of the amphid and labial sensilla, arrows. (**D**) Expression of *che-12* pro::GFP is greatly reduced in *daf-16; daf-19* animals. Compare with panel A. In D and E, image exposure was at least twice as long as in A and C. (**E**) The expression of *dyf-11* pro::GFP also depends on the transcription factor DAF-19. Compare with panel C.

GFP fluorescence was observed in most ciliated neurons, including neurons of the amphid, phasmid, and labial sensilla, as well as the neurons AQR, PQR, ADE, and PDE (Figure 5.4C). This result is consistent with a genome-wide survey of ciliated neuron-expressed genes which demonstrated that C02H7.1 is expressed in the head and tail of *C. elegans* (Kunitomo et al., 2005). Our expression studies are also consistent with the dye-uptake and behavioral defects of *dyf-11* mutants, and suggest that *dyf-11* plays an important role in the function of all cilia in *C. elegans*.

che-12 and *dyf-11* expression is dependent on the transcription factor DAF-19

In *C. elegans*, the expression of most genes encoding cilia-localized proteins requires DAF-19, an RFX transcription factor that recognizes a specific motif, the X-box, in the promoter region of its target genes (Swoboda et al., 2000). To determine whether the transcription of *che-12* and *dyf-11* requires DAF-19, the *che-12* pro::GFP and *dyf-11* pro::GFP transgenes were introduced into *daf-16*(*mu86*); *daf-19(m86)* animals. *daf-19*(*m86*) mutants constitutively arrest in the dauer stage of development, a dormant, protective developmental stage normally entered under harsh environmental conditions (Riddle, 1988). The *daf-16*(*mu86*) mutation suppresses the dauer arrest of *daf-19*(*m86*) mutants, allowing for the propagation of *daf-19* mutant lines (Vowels and Thomas, 1992). Expression of both *che-12* pro::GFP and *dyf-11* pro::GFP reporter transgenes was eliminated, or greatly reduced in *daf-16*(*mu86*)*; daf-19*(*m86*) animals, Figure 5.4, D-E.

It has been previously noted that the C02H7.1 (*dyf-11*) promoter contains a consensus X-box sequence at position -194 with respect to the translation start site

(Blacque et al., 2005). The region upstream of the *che-12* gene contains an X-box motif at position -1013 (Blacque et al., 2005), however, this sequence is located within the upstream gene, *gcy-6*, and was not included in the promoter we used to drive GFP expression. While no consensus X-box sites were found in the 936 bp promoter fragment we used, we did find a sequence, ATCAGCTTGAAAAC, at position -767, that differs from the X-box consensus sequence, RTHNYYWTRRNRAC (Efimenko et al., 2005), at only one position, and that might be used to drive *che-12* expression in the amphid and phasmid neurons. These results strongly suggest that DAF-19, directly or indirectly, controls the expression of both *che-12* and *dyf-11*.

CHE-12 and DYF-11 localize to cilia

The mutant phenotypes and expression patterns of the *che-12* and *dyf-11* genes suggest that they may encode components of cilia. To test this hypothesis directly, we determined the localization of CHE-12::GFP and DYF-11::GFP fusion proteins. Specifically, we examined GFP localization in the ASER amphid neuron of animals expressing either *che-12* cDNA::GFP or *dyf-11* cDNA::GFP transgenes driven by the ASER-specific promoter of the *gcy-5* gene (Yu et al., 1997). To visualize the ASER dendrite, mCherry was co-expressed from the same promoter, using an SL2 trans-splicing acceptor sequence. CHE-12::GFP and DYF-11::GFP localized throughout the ASER cilium (Figure 5.5), and were only faintly detectable in the ASER dendrite. Since both cDNA::GFP fusion transgenes were able to rescue the Dyf phenotype of their respective mutants when expressed using their own promoters, these results suggest that CHE-12

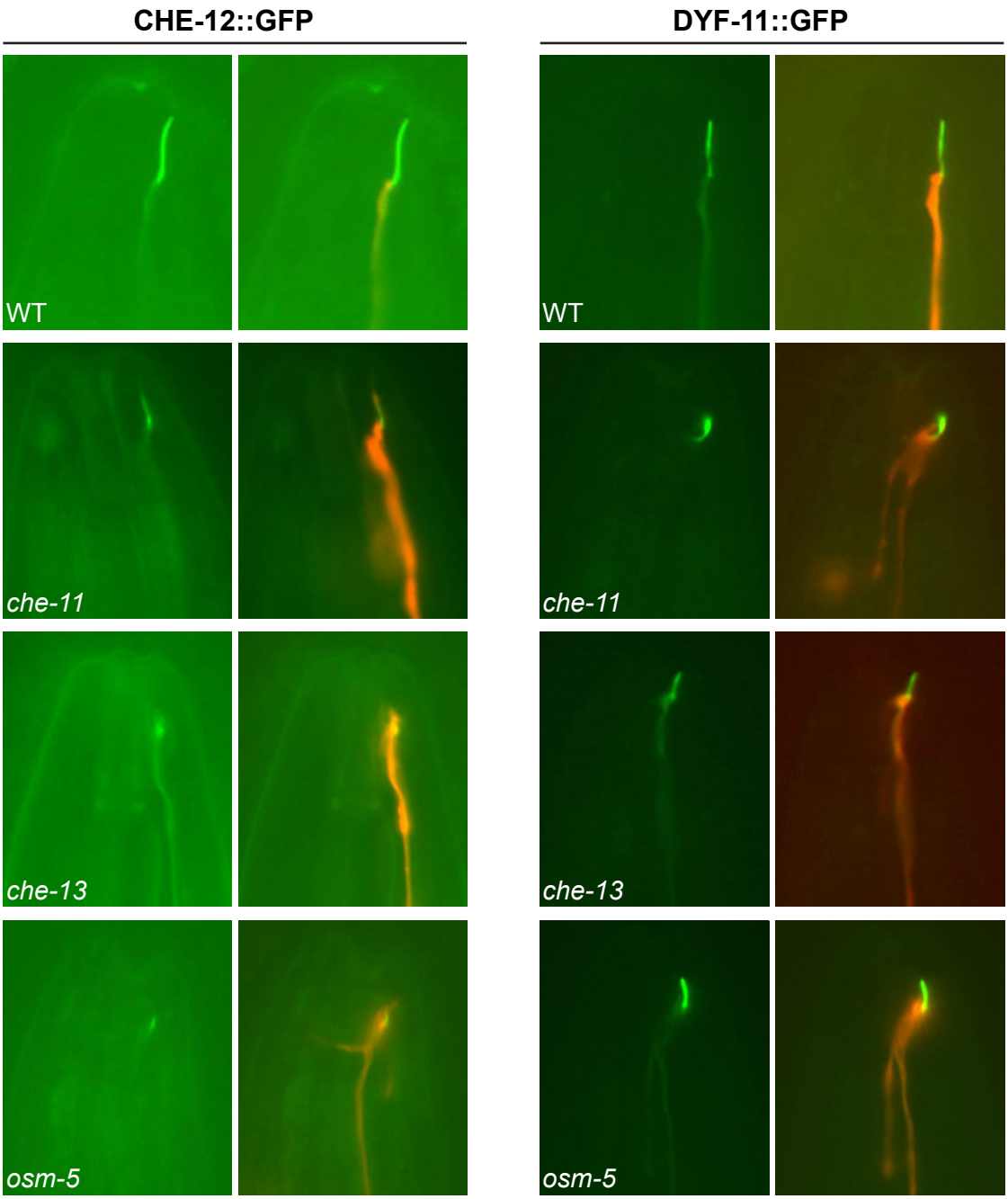

Figure 5.5: CHE-12 and DYF-11 localize to cilia

Left image of a pair, GFP alone. Right image, GFP and mCherry (ASER neuron dendrite) overlay. CHE-12 localizes to the cilium of ASER, arrows. The localization of CHE-12 is disrupted in *che-13(e1805)* and *osm-5(m184)* IFT-B mutants (note low intensity of GFP within cilium), and to a lesser extent in *che-11(e1810)* IFT-A mutants. DYF-11 is normally localized within cilia of wild-type animals. This localization is not affected by the *che-11, che-13*, and *osm-5* mutations. All transgenes are driven by the *gcy-5* promoter, which is expressed specifically in ASER. Scale bar, 5 μm.

and DYF-11 proteins are normally targeted to neuronal sensory cilia, consistent with the ciliary defects observed in *che-12* and *dyf-11* mutants.

che-12 and *dyf-11* act cell-autonomously within ciliated neurons

che-12 and *dyf-11* activities could be required either within a given ciliated neuron for its function, or may influence the activities of nearby neurons non-autonomously. To distinguish between these two possibilities, we used the *sra-6* promoter to express the *che-12* and *dyf-11* cDNAs in only two amphid neurons, ASH and ASI (Troemel et al., 1995), in *che-12*(*mn389*) and *dyf-11*(*mn392*) mutants, respectively. Only two neurons in each amphid were able to take up dye in these transgenic animals (Figure 5.6, B and F), suggesting that both *che-12* and *dyf-11* act cell autonomously.

che-12 and *dyf-11* activities are required continuously for cilium function

To determine the time of action of *che-12* and *dyf-11*, we generated plasmids in which the cDNA of each gene was placed under the control of the *hsp-16.2* heat-inducible promoter (Jones et al., 1986; Fire et al., 1990). Amphid neurons of *che-12*(*mn389*) or *dyf-11*(*mn392*) larvae or adults harboring these plasmids were unable to take up dye at 20ºC (Figure 5.6, A and E). However, dye uptake was restored to both mutant strains after a 30 min heat shock at 34ºC (Figure 5.6, C and G), suggesting that *dyf-11* and *che-12* can function at any time during the life of *C. elegans* to allow proper cilium function. Heat shock expression was also sufficient to rescue the morphological

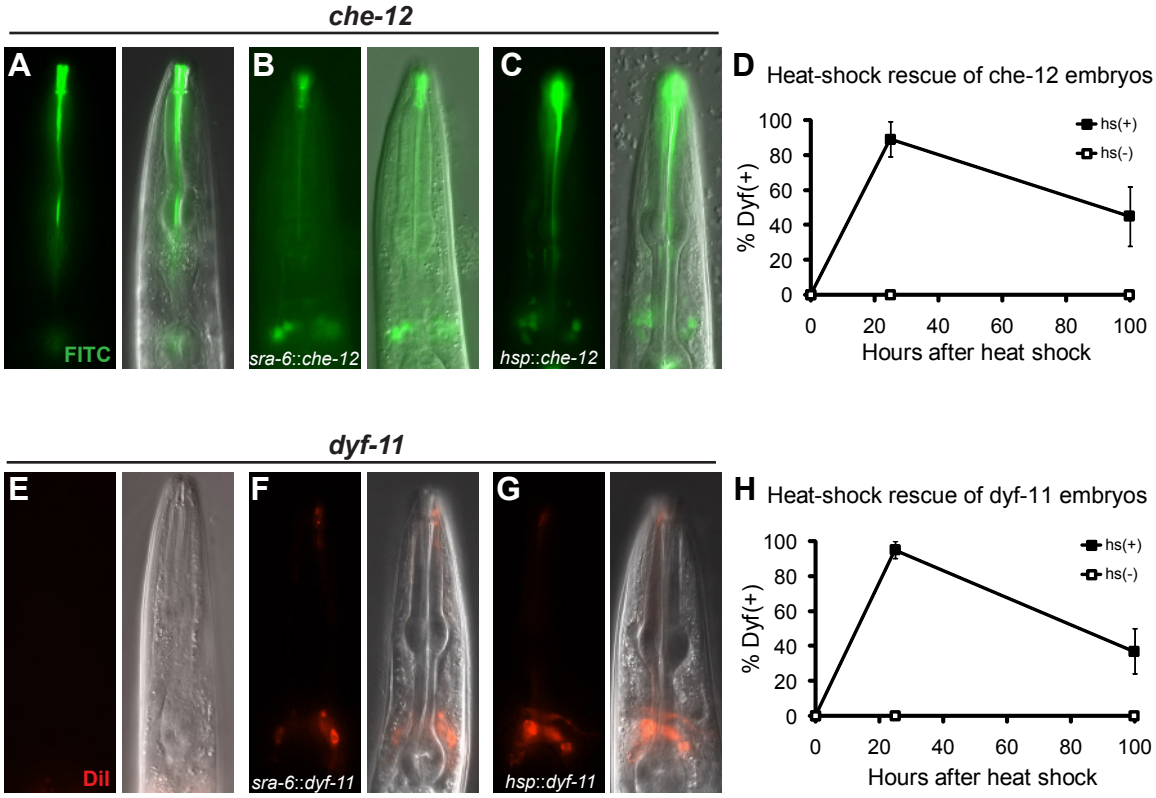

Figure 5.6: CHE-12 and DYF-11 act cell-autonomously and are required continuously for cilium morphology and function

(**A**) che-12(mn389) animals fail to take up FITC, asterisk indicates nonspecific staining. Fourth larval stage (L4) animals are depicted in all images. (**B**) Expression of CHE-12 in a *che-12(mn389)* mutant animal within only two amphid neurons, ASH and ASI, using the *sra-6* promoter, rescues the Dyf defect only within these neurons, arrow. (**C**) A *che-12(mn389)* animal that is provided CHE-12 via heat shock as an adult, is able to take up FITC in several amphid neurons, arrows. (**D**) *che-12(mn389)* embryos carrying extrachromosomal arrays containing the *hsp-16.2* pro::*che-12* cDNA transgene were heat shocked for 30 min at 34C. Dye filling was performed after 24 h to determine initial rescue or after 100 h. (**E**) *dyf-11* animals cannot take up DiI. (**F**) Expression of *dyf-11* in ASH and ASI using the *sra-6* promoter enables only these two neurons to fill with dye, arrow. (**G**) Providing DYF-11 to adult animals via heat shock rescues their Dyf defect. Animals contain an *hsp-16.2* pro::*dyf-11* cDNA transgene. (**H**) Same as D, except that *dyf-11(mn392)* mutants carrying an *hsp-16.2* pro::*dyf-11* transgene were used.

cilia defects, consistent with previous finding (Fujiwara et al., 1999). Thus, 12 h after heat shock ASER cilium length was 6.2 ± 0.5 μm (n=10) in *che-12(mn399)* animals and 6.4 ± 0.6 μm (n=10) in *dyf-11* animals. The ability to rescue ciliary defects in adult animals suggests that it should be possible to devise therapeutic interventions for human ciliopathies.

To determine whether expression of *che-12* and *dyf-11* is required continuously, we administered a heat shock during embryogenesis and examined dye uptake 24 h and 100 h later. The percentage of animals rescued for the dye uptake defect declined with time (Figure 5.6, D and H), indicating that *che-12* and *dyf-11* are required both for development and maintenance of a functional cilium.

CHE-12 may not be an IFT component, but requires IFT for its localization

Some ciliary proteins undergo regular movements within cilia, a phenomenon termed intraflagellar transport (IFT) (Rosenbaum and Witman, 2002; Scholey, 2003). To determine whether this is the case for CHE-12 and DYF-11, we generated wild-type animals carrying extrachromosomal transgenic arrays containing low copy numbers of *che-12* pro::*che-12*::GFP or *dyf-11* pro::*dyf-11*::GFP reporters transgenes, and examined GFP fluorescence dynamics in cilia using a spinning disk confocal microscope. We were unable to see any movement of a rescuing CHE-12::GFP fusion protein in amphid and phasmid neurons in 83 kymographs we generated. By comparison, movement of the IFT component CHE-13 was easily observed in 3/4 kymographs we examined. These

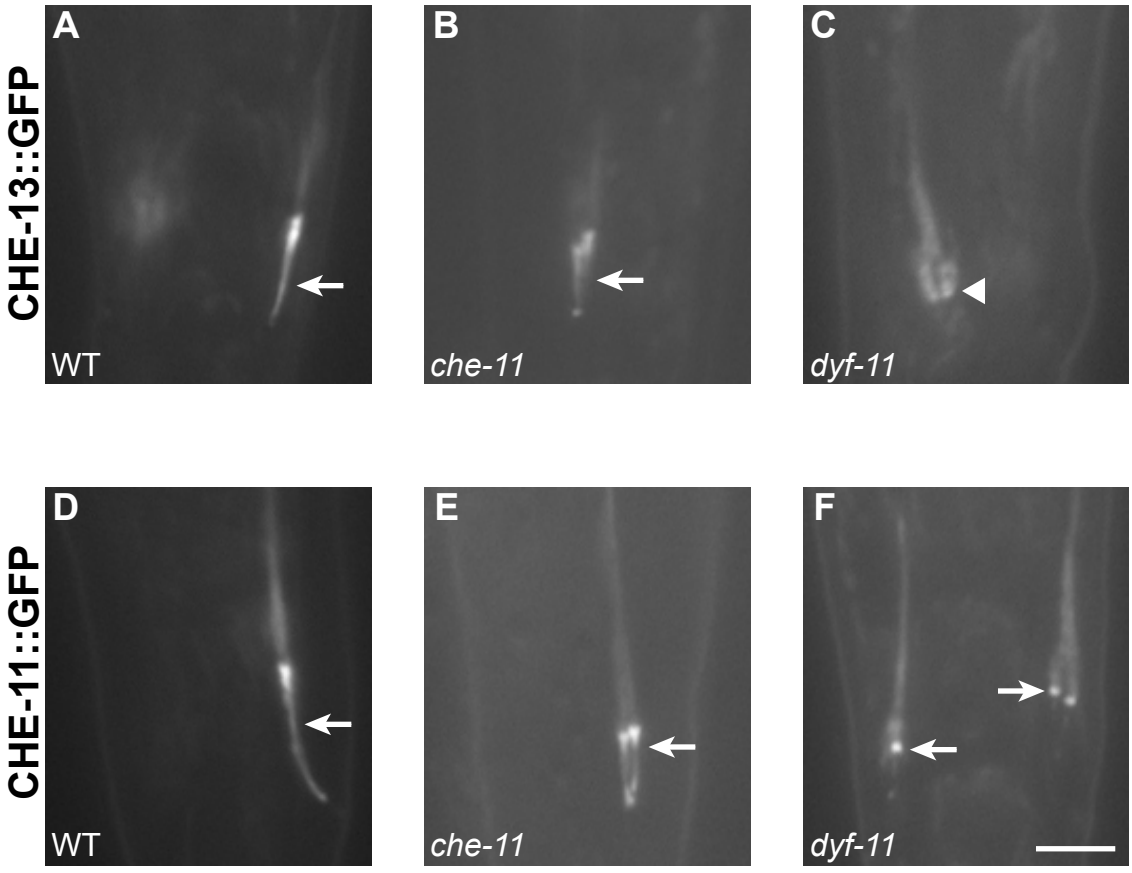

Figure 5.7: Localization of IFT-A and IFT-B proteins in che-12 and dyf-11 mutants
(**A**) Localization of CHE-13::GFP in a phasmid cilium (arrow) of a wild-type animal. (**B**) In *che-12(mn399)* animals, CHE-13::GFP localizes properly. (**C**) CHE-13::GFP fails to localize to the cilia of *dyf-11(mn392)* animals, the base of the cilium is indicated by an arrowhead. (**D**) CHE-11::GFP localization in a wild-type phasmid cilium. (**E**) In *che-12(mn399)* animals, CHE-11::GFP localizes appropriately. (**F**) CHE-11::GFP can occasionally localize to the base of the stunted cilia of *dyf-11* animals. Scale bar, 4 μm.

observations suggest that CHE-12 may not be a component of the IFT machinery and that it may not play a role in ciliary protein transport.

To further test the notion that CHE-12 is not a component of the IFT machinery, we examined the localization of IFT particle-associated proteins in *che-12* mutants. The IFT particle is thought to consist of at least two subunits, A and B. We found that localization of both CHE-11::GFP (associated with the IFT-A subunit) and CHE-13::GFP (associated with the IFT-B subunit) was unaffected in *che-12* mutants (Figure 5.7, B and E), consistent with the hypothesis that *che-12* does not play a role in IFT.

Although CHE-12 is unlikely to be principally associated with IFT particles, its localization within the cilium may still depend on transport by IFT. To establish whether CHE-12 localization is IFT-dependent, we examined the localization of ASER-expressed CHE-12::GFP in IFT-defective mutants. The intensity of CHE-12::GFP signal in the cilium was greatly reduced or absent in *che-13* and *osm-5* mutants (Figure 5.5), two components of the IFT-B complex (Haycraft et al., 2001; Qin et al., 2001; Haycraft et al., 2003). CHE-12::GFP ciliary localization also appeared disrupted, but to a lesser extent, in the IFT-A complex mutant *che-11* (Qin et al., 2001; Christensen et al., 2002). These results suggest that CHE-12 at least partially requires IFT for its localization.

DYF-11 is associated with IFT particles

Unlike CHE-12::GFP, a rescuing DYF-11::GFP protein fusion displayed bidirectional movement within amphid cilia (Figure 5.8, A-B). 23/62 kymographs we

generated showed that DYF-11-containing particles moved anterogradely along the middle segment of amphid cilia with a rate of 0.79 ± 0.08 μm/s and along the distal segment with a rate of 1.19 ± 0.9 μm/s. These velocities agree with those observed in the middle (0.7 μm/s) and the distal segment (1.3 μm/s) for other IFT proteins such as DYF-1, DYF-2, OSM-5, and OSM-6 (Christensen et al., 2002; Snow et al., 2004; Chen et al., 2006), suggesting that DYF-11 associates with IFT particles.

In *bbs-8(nx77)* mutants, the A and B IFT particle subunits dissociate and move independently, with only subunit B entering the distal segment of sensory cilia (Christensen et al., 2002; Blacque et al., 2004). We found that DYF-11::GFP localizes throughout the cilia, including the distal segments, of *bbs-8* mutants (Figure 5.8C). This observation suggests that DYF-11 may be a component of the IFT-B subunit, a hypothesis supported by the severely stunted cilia of *dyf-11* mutants (Figure 5.2C), a feature of other IFT-B complex mutants (Perkins et al., 1986).

To place DYF-11 in the hierarchy of known IFT proteins, we studied its localization in three IFT-defective mutants. DYF-11 localized to cilia in *che-11* (IFT-A), as well as in *che-13* and *osm-5* (IFT-B) animals (Figure 5.5). These observations indicate that the function of these proteins is dispensable for DYF-11 localization, and that DYF-11 probably associates with the IFT particle early in its assembly.

To test this idea further, we examined the localization of CHE-13::GFP (Haycraft et al., 2003) and CHE-11::GFP proteins (Qin et al., 2001) in *dyf-11*(*mn392*) animals. We found that CHE-13::GFP (IFT-B) is not localized to phasmid cilia of *dyf-11* animals (Figure 5.7C), supporting the idea that DYF-11 is part of the IFT-B subunit and that

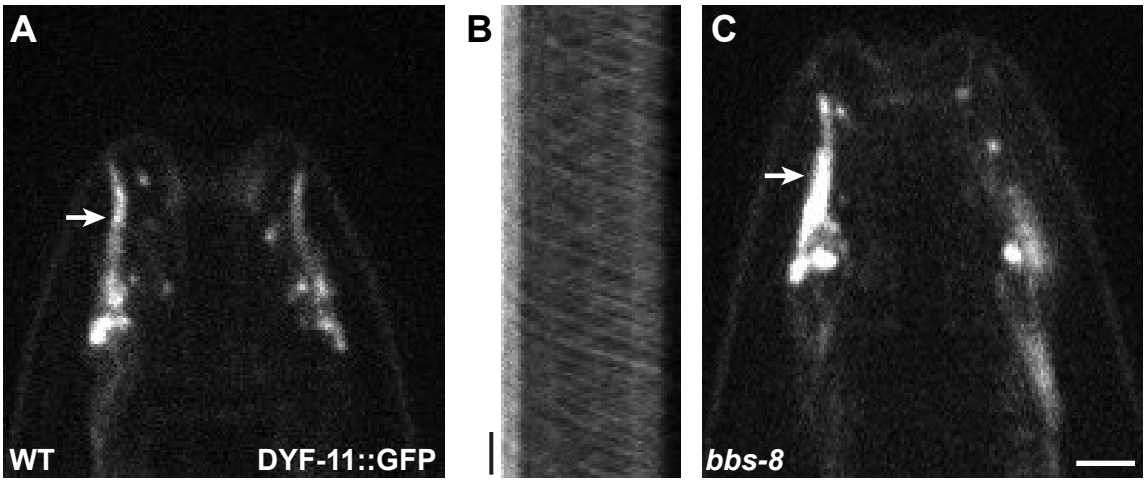

Figure 5.8: DYF-11 may associate with IFT particle B

(**A**) Localization of DYF-11::GFP in the cilia (arrow) of a wild-type animal. (**B**) Kymograph depicting anterograde and retrograde movement of DYF-11::GFP particles in the cilia seen in A. Position is displayed on the horizontal axis, and time on the vertical axis. The transition zone of the cilium is on the left. Vertical scale bar, 5 seconds. (**C**) DYF-11::GFP can enter the distal segment of cilia in a *bbs-8(nx77)* mutant animal, arrow. Scale bar A-C, 2.5 μm.

DYF-11 is likely recruited to the IFT particle before CHE-13. CHE-11::GFP (IFT-A) fluorescence in the cilia of *dyf-11* animals was also greatly reduced (Figure 5.7F), also consistent with an early role for DYF-11 in IFT particle assembly.

Discussion

Cilia, present at the tips of sensory neuron dendrites and on the surfaces of most vertebrate cells (Wheatley et al., 1996), have been the subject of intense study in recent years. Genomic and proteomic efforts to uncover a core group of cilia proteins has revealed the existence of several hundred proteins likely to comprise the cilium proteome, and at least some of these have been directly shown to reside within cilia (Avidor-Reiss et al., 2004; Emoto et al., 2004; Blacque et al., 2005; Efimenko et al., 2005). Many of the ciliary proteins identified to date are components of the intraflagellar transport (IFT) machinery, composed of a multi-protein particle shuttled within the cilium by molecular motors of the kinesin and dynein families (Rosenbaum and Witman, 2002; Scholey, 2003). However, although the IFT mechanism may be complex, it is unlikely that all cilia proteins are components of this machinery. In addition to IFT components, structural proteins must exist that give cilia their shape, and signaling modules must be present that control information flow through the cilium. Here we have explored the roles of two genes, *che-12* and *dyf-11*. Our results suggest that whereas *dyf-11* encodes a newly-described IFT component, *che-12* is likely to encode a protein that acts independently of the IFT machinery to control cilium function and morphology.

che-12 may be a non-IFT component of cilia

In *C. elegans*, mutations affecting cilium morphology generally block the ability of some neurons of the amphid sensory organ to concentrate lipophilic dyes, such as DiI and FITC (Perkins et al., 1986). We show here that among Dyf mutants, *che-12* mutants are unique in their ability to discriminate between the dyes FITC and DiI. Specifically, we show that all known *che-12* mutants are defective in FITC uptake, but only partially blocked for the uptake of DiI. Although the mechanism of dye uptake in *C. elegans* is not known, it is thought to reflect a functional state of particular neurons, since not all neurons exposed to dye are able to concentrate it (Hedgecock et al., 1985). Thus, the defects of *che-12* mutants suggest that mutations in the gene may affect only a subset of neuronal functions, suggesting that CHE-12 may not be a core component of the IFT machinery.

Several of our observations are consistent with this idea. First, CHE-12 protein localizes to cilia, but does so in a diffuse, non-particulate fashion, unlike many IFT components (Collet et al., 1998; Christensen et al., 2002; Haycraft et al., 2003). Further, although we analyzed many cilia expressing a rescuing CHE-12::GFP fusion protein, we were unable to detect any motion of this protein. We could, however, easily detect movements of CHE-13::GFP and DYF-11::GFP (Figure 5.8B).

Second, mutations in *che-12* had no effect on the movement or localization of IFT components we examined, suggesting either that *che-12* is not a component of the IFT complex, or that it is peripherally associated with it and not required for its integrity.

Third, EM studies of all three *che-12* alleles revealed that these animals lack part of the distal segment of at least some amphid sensory cilia (Figure 5.2, J-L). This defect is somewhat reminiscent of defects in the cilia of animals carrying mutations in the IFT-A complex components *che-11* and *daf-10* (Perkins et al., 1986). However, CHE-12 is unlikely to be a component of the IFT-A particle as in *che-11* and *daf-10* mutants, large accumulations of IFT particles along the axoneme are visible (Qin et al., 2001), suggesting that the IFT-A complex plays a crucial role in retrograde transport within the cilium. This defect is not seen in *che-12* mutants.

Although our evidence suggests that CHE-12 protein may be a non-IFT component of cilia, we show that its ciliary localization is dependent on a functioning IFT mechanism. Therefore, we suggest a model in which CHE-12 entry into cilia depends on IFT, but once inside cilia, the protein is released and free to provide IFT-independent functionality to these cellular compartments (Figure 5.9).

che-12 may control the development and function of specific cilia

Our studies of *che-12* mutants reveal that these animals exhibit defects in only a subset of behaviors associated with amphid neurons. Specifically, behaviors associated with the olfactory neurons AWA and AWC seem generally unaffected in *che-12* animals, consistent with the lack of *che-12* expression in these neurons, whereas behaviors associated with neurons penetrating the amphid channel and responsive to soluble stimuli were defective. These observations suggest that *che-12* may provide specialized functions to only a subset of amphid and phasmid neurons bearing simple cilia. It has

already been noted that some cilia genes (*osm-5*, *osm-6*, *che-2*, *che-13*) are expressed in most or all ciliated neurons and are, therefore, required for the general formation of cilia (Efimenko et al., 2005), while others, such as *osm-3* (Tabish et al., 1995), *dyf-3* (Murayama et al., 2005), and *dyf-2* (Chen et al., 2006) are expressed in a subset of ciliated neurons and are hypothesized to lead to specialized ciliary structures (Mukhopadhyay et al., 2007). Genes restricted to only subsets of ciliated neurons seem to possess an asymmetric X-box sequence, the binding site of the ciliogenic transcription factor DAF-19, in their promoters (Swoboda et al., 2000). The *che-12* promoter contains such an asymmetric X-box (ATCAGC TT GAAAAC), further suggesting that CHE-12 might act to promote chemosensory cilia specialization.

We note that a previous EM study of *che-12*(*e1812*) animals reported that these animals have decreased levels of an undefined matrix in the amphid sheath cell, a glial cell that ensheathes the ciliated dendritic endings of the amphid neurons (Perkins et al., 1986), leading to the hypothesis that *che-12* was likely to function in glia. However, both our studies of *che-12* localization and our EM studies are inconsistent with these previous results.

How might CHE-12 function? Analysis of the CHE-12 protein sequence reveals that it contains seven or more HEAT repeats. These motifs, first described in the proteins huntigtin, elongation factor 3, PR65/A subunit of protein phosphatase 2A, and TOR1, are 39 residues long and are often repeated in tandem three or more times within a protein (Andrade and Bork, 1995). Each HEAT motif folds as two antiparallel α-helices, and, as observed in the crystal structure of PR65/A (Groves et al., 1999), the helix pairs are arranged to form a solenoid with a hydrophobic inner core. In CHE-12, the first HEAT

motif occurs at positions 99-135 while the last spans amino acids 1141-1177. Since most of the CHE-12 sequence is comprised of HEAT repeats, it is likely that the tertiary structure of CHE-12 resembles the solenoid formed by PR65/A. Such a structure could act as a scaffold and may be used to anchor ciliary proteins important for both FITC uptake, and for building and stabilizing the distal segment of the cilium. The predicted human protein KIAA0423 shares the same HEAT repeat topology as CHE-12, suggesting that it may also function within cilia in a manner similar to CHE-12.

DYF-11 protein is required early in IFT-B particle assembly

While CHE-12 appears to be required for specialized cilia functions, our studies suggest that DYF-11 probably serves as a core IFT particle protein. Consistent with this idea, DYF-11 is expressed in most, if not all, ciliated neurons, and *dyf-11* animals possess stunted cilia that resemble those of IFT-B class mutants. In addition, we could demonstrate that a DYF-11::GFP rescuing fusion protein is able to undergo both anterograde and retrograde movements within cilia, at speeds consistent with those previously described for IFT. These observations agree with recent published reports (Kunitomo and Iino, 2008; Li et al., 2008; Omori et al., 2008).

The IFT complex can be dissociated into at least two subcomponents termed A and B. Previous studies have shown that in *bbs-8* mutants, the IFT-A and IFT-B particles are separated, and IFT-A is transported along the medial segment by kinesin-2, while IFT-B is driven along the medial as well as the distal segment by OSM-3 (Christensen et al., 2002). We found that DYF-11 localization to distal regions of cilia was unaffected in

bbs-8 mutants, suggesting that DYF-11 is likely to be associated with the IFT-B subparticle.

Previous studies have suggested that the IFT particle is assembled in a series of steps. Analysis of IFT protein localization in different IFT mutant backgrounds has revealed some of this hierarchy of assembly. For example, OSM-5 is mislocalized in *che-13* animals (Haycraft et al., 2003), indicating that CHE-13 acts prior to or together with OSM-5 in IFT complex B assembly. Furthermore, complex A proteins, such CHE-11, are largely unaffected by removal of later acting IFT-B proteins. Interestingly, we showed that while DYF-11 localization was not disrupted in *osm-5* (IFT-B), *che-13* (IFT-B), or *che-11* (IFT-A) mutants (Figure 5.5), localization of OSM-5, CHE-13, and CHE-11 was disrupted in *dyf-11* animals (Figure 5.7, C and F). These results suggest that DYF-11 is likely to function early in IFT particle assembly, and are consistent with a model in which DYF-11 is required for recruitment of OSM-5, CHE-13, and CHE-11 proteins to this particle (Figure 5.9).

DYF-11 might mediate interactions of the IFT particle with microtubules and Rab8

Comparison of the DYF-11 protein sequence to existing protein databases revealed that this protein is conserved in evolution. Its human orthologue, MIP-T3 (microtubule-interacting protein that interacts with TRAF3), was identified in a yeast two-hybrid screen for factors that interact with tumor necrosis factor receptor associated factor 3 (TRAF3) (Ling and Goeddel, 2000). MIP-T3 binds to taxol-stabilized microtubules and to tubulin *in vitro*, and is able to recruit TRAF3 to microtubules in

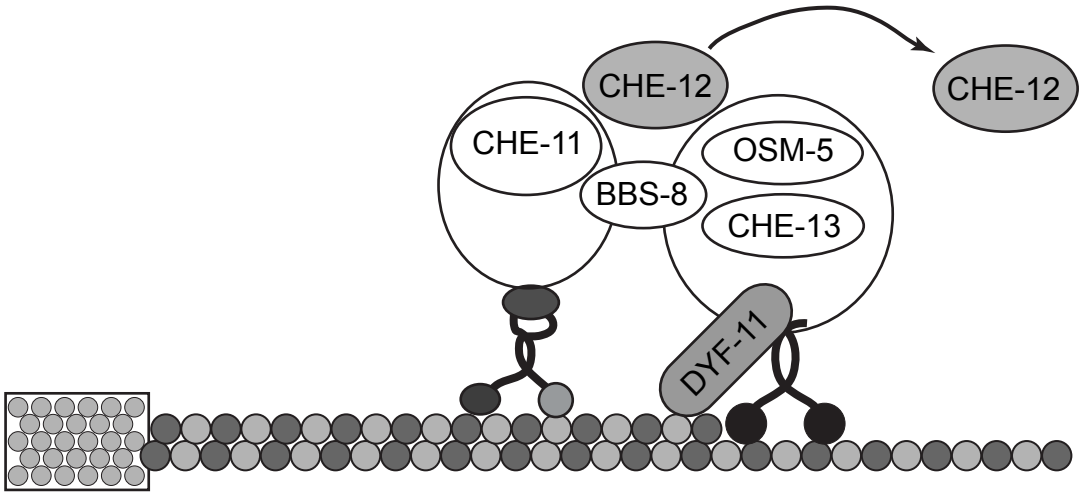

Figure 5.9: A hypothetical model of CHE-12 and DYF-11 roles in sensory cilia
The IFT subcomplexes A and B, linked by the BBS-8 protein, are moved along the ciliary microtubules by the kinesin-2 and OSM-3 motors. DYF-11 might interact with microtubules as well as with the IFT-B protein complex, acting to promote association of CHE-13 and OSM-5 proteins with the complex. CHE-12 is transiently associated with the IFT particle in order to be transported into the cilium, where it is released and accumulates. Note that not all known IFT particle components are shown in this diagram.

HeLa cell lines that overexpress both proteins (Ling and Goeddel, 2000), raising the intriguing possibility that DYF-11 might be associated with ciliary microtubules (Figure 5.9). Although current models suggest that contact of the IFT complex with microtubules is mediated by the motors that move the complex, it is possible that a specific association of complex components with microtubules is required either for their initial assembly, or to facilitate initiation or termination of IFT complex motion by its associated motors.

In support of this mechanism, yeast two-hybrid interactions were identified between Elipsa, the zebrafish DYF-11 homologue, and Rabaptin-5 (Omori et al., 2008). Rabaptin-5 is a cytosolic effector of RAB GTPases that is involved in endocytosis and interacts primarily with Rab5 (Stenmark et al., 1995). Omori and colleagues further showed that Rabaptin-5 could bind to a constitutively active form of Rab8 (Omori et al., 2008). This is particularly interesting as Rab8 is required for proper ciliogenesis, for transport of transmembrane proteins into the cilium (Nachury et al., 2007), and expression of dominant negative form of Rab8 results in accumulation of vesicles at the connecting cilium of photoreceptors (Moritz et al., 2001). Thus, the interactions of DYF-11 with Rabaptin-5 and with microtubules could be one of the mechanisms by which dendritic vesicles are coupled to the IFT particle and loaded onto the axoneme for ciliary transport of transmembrane proteins.

Studies of MIP-T3 also suggest that this protein interacts with the interleukin-13 receptor (IL-13Rα1) (Niu et al., 2003). Interestingly, the association of MIP-T3 with this receptor and with TRAF3 changes after signal transduction has occurred (Ling and Goeddel, 2000; Niu et al., 2003). These observations suggest that DYF-11 may be in a position to control aspects of IFT, perhaps loading of IFT particles onto the axoneme, in

response to environmental cues received by cilia. Consistent with a potential regulatory role in microtubule association, MIP-T3 also interacts with Disrupted-in-Schizophrenia 1 (DISC1), and appears to be required for the recruitment of DISC1, a centrosome associated protein, to microtubules (Morris et al., 2003).

Primary cilia are found on most human cells, and their roles in many aspects of signal transduction are revealed by the pleiotropic defects observed in Bardet-Biedl syndrome (BBS) patients (Ansley et al., 2003). Here we have described two conserved cilia proteins: CHE-12, which might act as a structural scaffold promoting specialized structure and/or function of some cilia; and DYF-11, which acts as an IFT-B particle component. Further studies of these and other cilia components should help to reveal the mechanics of signal transduction and processing performed by this organelle.

Chapter 6

A method for temporal control of cell-specific transgene expression in *C. elegans*

Summary

Cell-specific promoters allow only spatial control of transgene expression in *C. elegans*. The ability to control both the location as well as timing of transgene expression can be beneficial in addressing basic questions regarding gene function, such as when in development does a gene act, or in expressing transgenes, such as ones encoding toxins, when desired. We describe a method, using cell-specific rescue of *heat-shock factor-1* (*hsf-1*) mutants, allowing spatial and temporal regulation of transgene expression. We demonstrate the utility of this method for timed reporter gene expression and for temporal studies of gene function.

Spatial and temporal control of gene expression

The ability to manipulate transgene expression in animals has facilitated the study of many biological processes. While systemic expression of transgenes can be used as an effective tool for studying the consequences of gene activation or inactivation, in many instances it is desirable to control both spatial and temporal aspects of transgene expression. For example, restriction of transgene expression to a specific cell type can allow determination of whether gene function is cell-autonomous or non-autonomous. Likewise, temporal control of transgene expression is critical for determining whether the function of a gene of interest is required continuously or only during specific times.

Several strategies have been developed that allow control of both where and when transgenes are expressed. Spatial resolution is often achieved by the use of tissue- or cell-specific promoters, and timing of transgene expression can be controlled by introduction or withdrawal of small-molecule gene-expression inducers or inhibitors. For example, a fusion protein consisting of the tetracycline repressor fused to the transcription activation domain of VP16 (TetR-VP16), and expressed using a tissue-specific promoter, can promote tissue-specific expression of genes bearing *tetO* cis-acting DNA sequences. Addition of the cell-permeable ligand tetracycline, which binds to and prevents TetR-VP16 from binding *tetO* (Gossen and Bujard, 1992; Gossen et al., 1995), can be used to extinguish expression at specific times. Similarly, Cre recombinase fused to the estrogen receptor, and expressed in specific tissues, can be temporally activated by the addition of tamoxifen (Feil et al., 1996).

An alternative to using small molecules for temporal control is afforded by proteins whose functions are regulated by temperature. For example, by modifying the GAL4/UAS system for controlling cell-type-specific gene expression in *Drosophila* (Brand and Perrimon, 1993), McGuire *et al*. achieved temporal control of GAL4-driven transgenes by introducing a temperature-sensitive form of GAL80, a GAL4 inhibitor, into transgenic flies (McGuire et al., 2003). At permissive temperatures, animals fail to express the transgene because GAL80 inhibits GAL4. Shifting to non-permissive temperatures relieves GAL80 inhibition and allows transgene expression to proceed.

Another strategy for temporal control of transgene expression exploits the heat-shock response, a temperature-dependent stress defense mechanism. The heat-shock response is mediated by heat-shock factor (HSF), a transcription factor that is synthesized constitutively but remains latent during unstressed conditions (Bargmann, 1993). In response to heat stress, HSF trimerizes and binds with high affinity to promoters containing specific binding elements, leading to the transcription of heat-shock proteins (Pelham, 1982; Westwood et al., 1991). Thus, transgenes containing HSF binding elements can be induced, albeit with little cellular specificity, following a temperature shift. Attempts to lend spatial resolution to the heat-shock response by using heated needles (Monsma et al., 1988; Vekris et al., 2000) or focused laser microbeams (Stringham and Candido, 1993; Halfon et al., 1997) to trigger the response in specific cells have been described. However, these physical methods for spatially-restricted heat-shock delivery are labor intensive and potentially damaging to cells, explaining, in part, why they are not in common use.

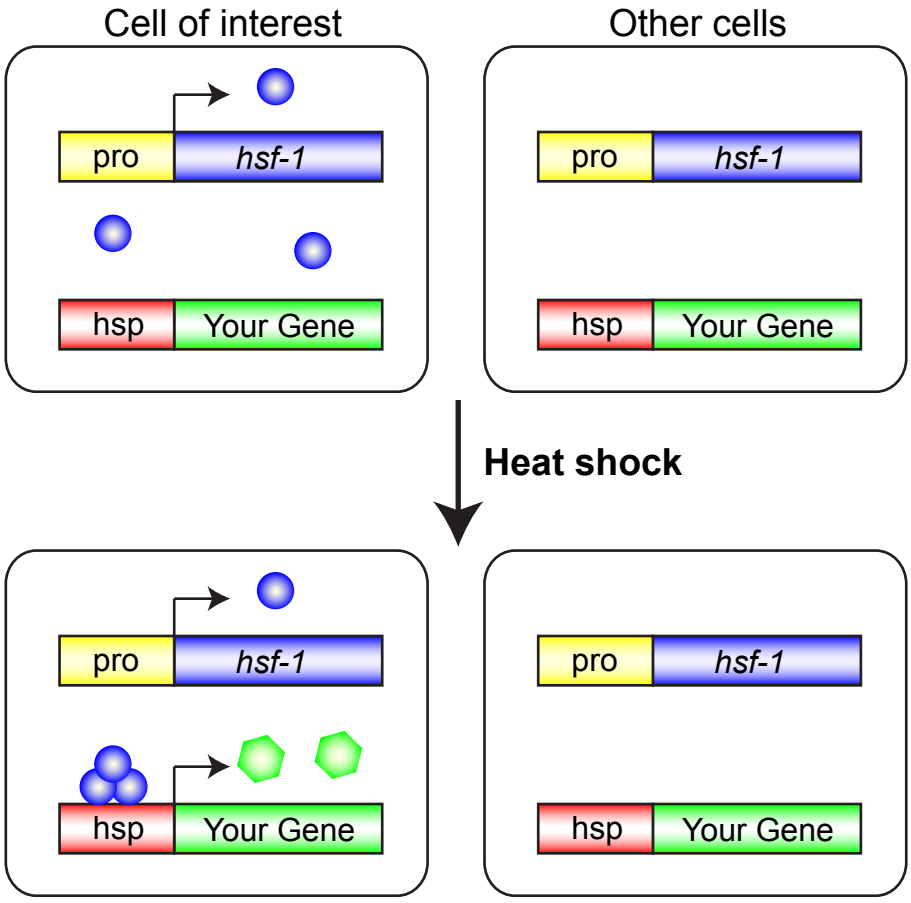

Figure 6.1: Temporal control of cell-specific transgene expression
In an animal lacking the normal heat-shock response due to loss of HSF-1 activity, *hsf-1* is introduced in a desired subset of cells using a cell-specific promoter (pro). Since HSF-1 is present only in targeted cells, heat-shock results in cell-specific transcription from heat-shock responsive promoters (hsp). Therefore, any transgene under the control of a heat-shock promoter will be selectively expressed in the desired cells following a heat shock. Blue circles, HSF-1 protein. Green hexagons, protein of interest.

Results

Restricting the heat shock response to desired cells

Currently, no facile approach is available for combined spatial and temporal regulation of transgene expression in *C. elegans*. Our interest in spatiotemporal control of transgene expression arose from the need to perform genetic ablations of the amphid sheath glia in adult animals. We were unsuccessful in some limited attempts in adopting the GAL4 system to *C. elegans*, therefore, we sought to devise alternative strategies. To develop such a method, we reasoned that cell-specific rescue of mutants defective in the heat-shock response should allow expression of transgenes, following a heat shock, only in rescued cells. The *C. elegans* genome contains a single gene encoding heat-shock factor, *hsf-1*. An allele of *hsf-1*, *sy441*, was previously isolated in a screen for suppressors of an activated Gα protein expressed under the control of a heat-shock responsive promoter (Hajdu-Cronin et al., 2004). Although *hsf-1(sy441)* animals have decreased lifespan, egg-laying defects, and larval arrest at 25ºC, they are otherwise healthy at 20ºC (Hajdu-Cronin et al., 2004). Importantly, however, following a brief heat-shock at 34ºC, *hsf-1(sy441)* animals show a 100-fold reduction in expression of endogenous heat-shock protein mRNAs compared to wild-type animals (Hajdu-Cronin et al., 2004). Thus, cell-specific expression of *hsf-1*, in *hsf-1*(*sy441*) mutants, should restore the normal heat-shock response only in targeted cells and should allow expression of any transgene within rescued cells (Figure 6.1).

Spatial restriction of gene expression after heat shock to glia and sensory neurons

To test this idea, we sought to develop transgenic strains in which we could induce green fluorescent protein (GFP) expression in specific cells following a heat-shock. To this end, we transformed *hsf-1*(*sy441*) mutants with two transgenes simultaneously. The first transgene, referred to as the driver, consisted of the *hsf-1* cDNA under the control of the 5 kb promoter region of the gene *vap-1*, which is expressed specifically within the amphid sheath cell, an easily identifiable glial cell in the head of the animal (Blacque et al., 2005). The second transgene, termed the responder, consisted of the gene encoding GFP under the control of the 400 bp promoter region of the *hsp-16.2* gene (Jones et al., 1986; Fire et al., 1990). In *C. elegans*, the *hsp-16.2* and *hsp-16.41* heat-shock responsive genes are divergently transcribed from a shared 346 bp region that contains three heat-shock factor binding elements (Jones et al., 1986). The *hsp-16.2* promoter expresses most strongly in hypodermal cells and neurons, while the *hsp-16.41* promoter is more efficient in directing expression in the intestine and pharyngeal tissue (Fire et al., 1990; Stringham et al., 1992).

hsf-1(sy441) animals carrying both transgenes as an extrachromosomal array, and raised at 20ºC, did not display detectable GFP expression (Figure 6.2A). However, following administration of a heat-shock at 34ºC for 30 min, GFP expression was observed specifically within the amphid sheath cells (Figure 6.2B). GFP fluorescence was visible within 1 h following the temperature shift and was still present after 24 hours.

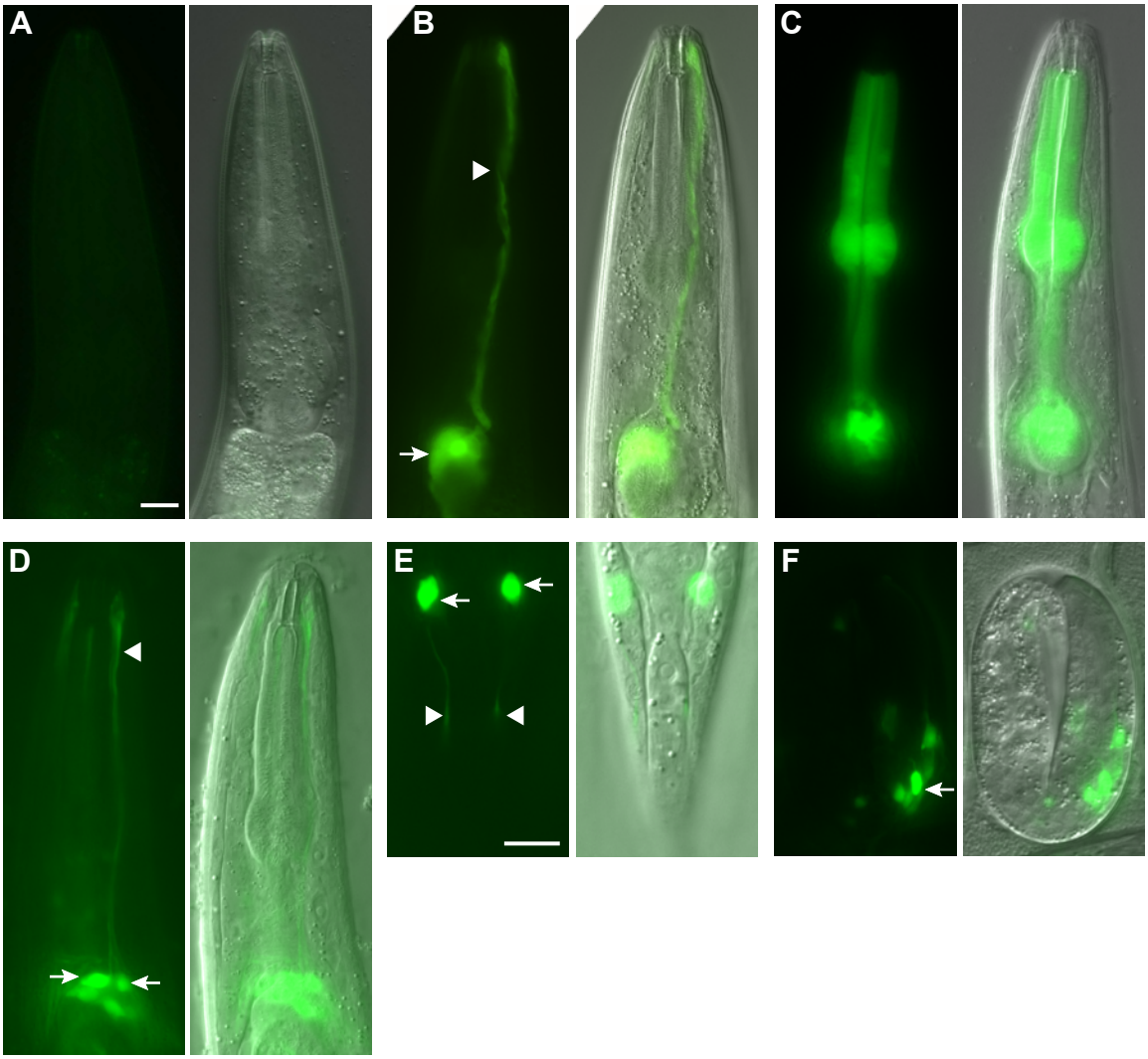

Figure 6.2: Spatiotemporal control of GFP expression using a heat-shock promoter
(**A-B**) Amphid sheath cell-specific labeling. Sheath cell-specific *hsf-1* rescue was achieved by driving *hsf-1* cDNA expression via the *vap-1* promoter; GFP was under the control of the *hsp-16.2* promoter. (**A**) No GFP expression was observed prior to heat-shock. Right panel, DIC image of the same animal. (**B**) Heat-shock resulted in GFP expression within the amphid sheath cell specifically. (**C**) Pharynx GFP expression. An adult animal expressing GFP in pharyngeal muscles after a 30 min heat-shock. The genotype of the animal shown is *hsf-1(sy441); nsEx1730* [*myo-2* pro::*hsf-1*; *hsp-16.2* pro::GFP; *hsp-16.41* pro::GFP; pRF4]. (**D**) Ciliated neuron-specific labeling. Animals in D-F have the genotype *hsf-1*(*sy441*); *nsEx1129* [*osm-6* pro::*hsf-1*; *hsp-16.2* pro::GFP; pRF4]. (**E**) Heat-shock induced GFP expression in ciliated neurons of the phasmid. (**F**) Neuronal GFP labeling in a two-fold embryo. Arrows, cell body; arrowheads, cell process; scale bar (A-D and E-F), 10 μm.

To determine whether this method is applicable to other *C. elegans* cells, we established new *hsf-1*(*sy441*) transgenic lines in which the HSF driver transgene was under the control of the 1.1 kb promoter region of *myo-2*, a gene expressed in pharyngeal muscle (Okkema et al., 1993). These lines also contained both the *hsp-16.2* promoter::GFP and *hsp-16.41* promoter::GFP responder transgenes. Following heat-shock, GFP expression was observed only in the pharynx (Figure 6.2C). We found that GFP expression was fainter in lines containing only the *hsp-16.2* promoter::GFP responder transgene (data not shown), consistent with the reported poorer expression of *hsp-16.2* in pharyngeal muscles.

To extend this method to neurons, *hsf-1*(*sy441*) transgenic lines in which the HSF driver transgene was under the control of the 2.4 kb promoter region of *osm-6*, a gene expressed in all ciliated neurons (Collet et al., 1998). Whereas no GFP was detectable at 20ºC, heat-shock resulted in specific GFP expression within most ciliated neuron classes (Figure 6.2, D-F). Importantly, neuronal staining was observed in larvae and embryos alike (Figure 6.2F), suggesting that this method of cell-specific timed expression can be used in most developmental stages. Similar results were obtained when both the *hsp-16.2* promoter::GFP and *hsp-16.41* promoter::GFP responder transgenes were simultaneously transformed. However, in some of the animals in which both heat-shock promoters were used, GFP was also variably expressed in the intestine. Intestinal expression was also occasionally observed with the *hsp-16.2* promoter alone. We suspect that this expression might reflect cryptic regulatory elements driving intestinal expression within the vectors we used. Indeed, such intestinal misexpression is common to many transcriptional reporter transgenes.

To determine whether this method could be used to study gene function, we sought to rescue a mutant phenotype in a temporally and spatially restricted manner. CHE-2, a conserved WD40 repeat protein, is required for sensory neuron cilium formation and function in *C. elegans* (Fujiwara et al., 1999). In *che-2(e1033)* mutants, neurons of the amphid sensory organ fail to take up lipophilic dyes, such as DiI, presumably because they lack functional cilia. We examined whether *che-2(e1033)* mutants could be rescued by expression of the *che-2* cDNA exclusively within ciliated neurons in L4 larvae. Amphid neurons of *hsf-1(sy441); che-2(e1033)* double mutants, carrying both *osm-6* promoter::*hsf-1* driver and *hsp-16.2* promoter::*che-2* responder transgenes, were unable to take up DiI at 20ºC (Table 6.1; Figure 6.3A). However, transgenic animals exposed to a 30 min heat-shock at 34ºC, and examined 8 h later, displayed robust neuronal dye filling (Table 6.1; Figure 6.3). These results suggest that *che-2* may be continuously required for sensory cilia function, consistent with previous studies (Fujiwara et al., 1999). Less efficient, but reproducible rescue was observed when animals were examined 1 h after heat-shock. These results suggest that the time required to assemble a functional cilium from its components may be as little as 1 h (see also (Fujiwara et al., 1999). No dye-filling after heat-shock was observed in animals carrying only the *hsp-16.2* promoter::*che-2* responder transgene, consistent with a lack of the heat-shock response in *hsf-1(sy441)* mutants.

To test whether *hsf-1* rescue was cell-autonomous, and to test whether dye uptake is a cell-autonomous process or a group property of exposed amphid cilia, we examined *hsf-1*(*sy441*); *che-2*(*e1033*) mutants carrying both *sra-6* promoter::*hsf-1* driver and *hsp-16.2* promoter::CHE-2 responder transgenes. The 2.4 kb *sra-6* promoter is primarily

expressed in the two dye-filling amphid neurons ASI and ASH (Troemel et al., 1995). While transgenic animals grown at 20ºC failed to take up DiI, dye-filling was observed exclusively in the two *sra-6*-expressing neurons 8 h after heat-shock (Figure 6.3) suggesting that *hsf-1* and *che-2* indeed function cell-autonomously. In both the *osm-6* and *sra-6* transgenic lines, rescue was very efficient, reaching nearly 90% in some lines (Table 6.1). Importantly, we never observed rescue in non-heat-shock treated animals, indicating that any leaky expression from the *hsp* promoter is not only below detectable levels of GFP expression but also below detectable levels in this functional assay.

Table 6.1: Neuron-specific rescue of *che-2(e1033)* by heat shock

Promoter driving *hsf-1*	Strain[a]	% Dye-filling[b]	
		- HS	+ HS
	No transgene	0	0
osm-6	line 1	0	73
	line 2	0	53
	line 3	0	90
sra-6	line 1	0	83
	line 2	0	37
	line 3	0	53

[a] All animals have the genotype *hsf-1(sy441); che-2(e1033).* The extrachromosomal arrays used were *Ex*[*osm-6* pro::*hsf-1*, *hsp-16.2* pro::*che-2*, pRF4] and *Ex*[*sra-6* pro::*hsf-1*, *hsp-16.2* pro::*che-2*, pRF4]

[b] Animals were dye-filled 8 h after heat-shock. Animals exhibiting dye filling in any amphid neuron were scored as positive. n=30 in all cases. HS, heat-shock.

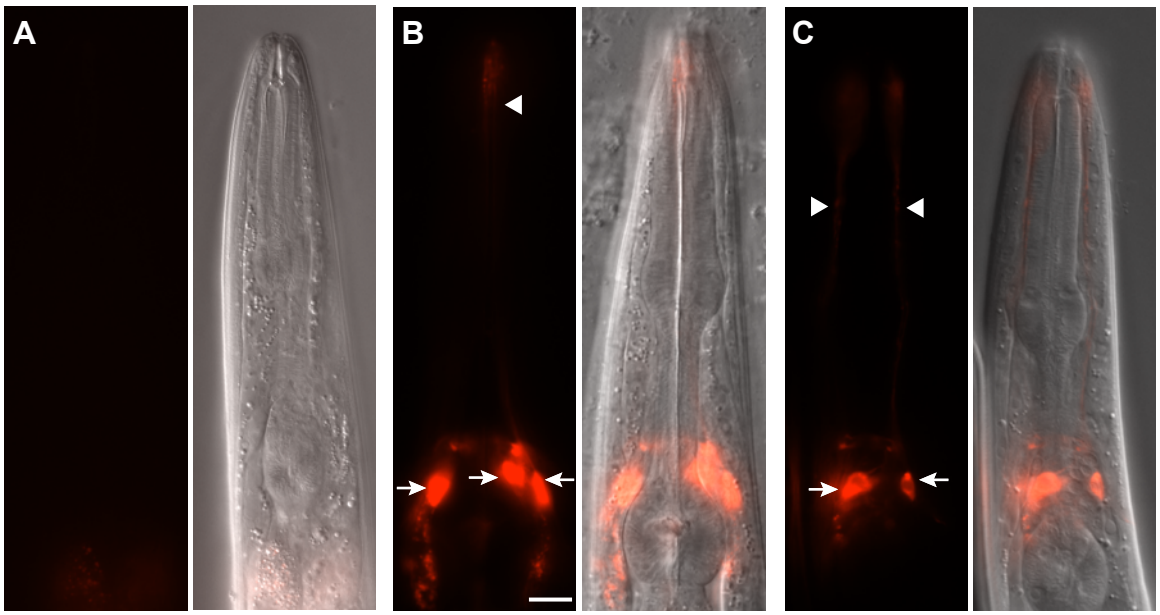

Figure 6.3: Cell-specific rescue of *che-2(e1033)* neuronal dye-filling defects

Dye filling in L4 animals of the genotype *hsf-1(sy441)*; *che-2(e1033)*; *nsEx1555* [*osm-6* pro::*hsf-1*, *hsp-16.2* pro::*che-2*, pRF4] before (**A**) or after a 30 min heat-shock (**B**). Rescue was seen in all dye-filling amphid neurons. Right, panel, DIC image of the same animal. (**C**) Rescue of dye-filling by heat-shock in only two amphid neurons that express *sra-6*. The genotype of the animal shown is *hsf-1(sy441)*; *che-2(e1033)*; *nsEx1552* [*sra-6* pro::*hsf-1*, *hsp-16.2* pro::*che-2,* pRF4]. Anterior, top. Arrows, neuronal cell bodies. Arrowheads, dendritic processes. Scale bar, 10 μm.

Discussion

Temporal control of transgene expression in *C. elegans* has been limited to the use of heat-shock promoters without spatial restriction. Here we have described a method using the heat-shock response to allow both temporal and spatial control of transgene expression. We have shown that this technique can be used to target transgene expression in different cell types, including neurons and glia (Figure 6.2). Importantly, this method allows expression in all larval stages including embryos (Figure 6.2E).

We envision that this technique will be broadly applicable in *C. elegans* and can be used for a variety of applications. In particular, our main interest in developing this technique was to perform genetic cell ablations in adult animals, a stage in which laser-ablations are inefficient, by expression of proapoptotic factors or toxic proteins. From our limited experience, we find that toxin selection is particularly important. For example, expression of the proapoptotic genes CED-3 or EGL-1 (Yuan et al., 1993; Conradt and Horvitz, 1998) was not sufficient to induce apoptosis in adult animals. To overcome this limitation, one might use the split version of CED-3 in which an active caspase is formed by expression of two different CED-3 fragments (Chelur and Chalfie, 2007). Only one CED-3 fragment needs to be under expression of the heat-shock promoter in this case. Use of stronger toxic genes has to be balanced by the fact that leaky expression might cause non-specific cell death in untargeted tissues.

Another exiting possible use of this system is to induce temporal and spatial specific knock-down of gene function. Specifically, it should be possible to drive expression of an RNAi construct to knock-down gene levels in particular cells at specific

times. To prevent intercellular spread of the RNAi effects, these experiments could be performed in the *sid-1* background, a mutant that prevents the systemic effects of small interfering RNAs (Winston et al., 2002). This could be useful to determine the site of action of a gene or to characterize essential genes that are required for viability.

A limitation of this technique is the requirement for a promoter that targets expression of the HSF-1 protein to the desired cells. It is important that this promoter not express in intestinal cells, a common non-specific pattern of expression observed for many *C. elegans* promoters, as even low HSF-1 levels might result in misexpression of the desired gene in intestinal cells. Another drawback of the technique is the variable expression of the gene of interest in different animals. Although heat-shock induction varied among different transgenic lines and was also dependent on the promoter used to drive *hsf-1* expression, we did not observe expression in 100% of the animals in any of the extrachromosomal transgenic lines we generated. This might be ameliorated or even overcome by using integrated transgenes. Lastly, the technique requires that experiments be performed in *hsf-1(sy441)* mutants, restricting its use to temperatures below 25ºC as these mutants are not viable at 25ºC (Hajdu-Cronin et al., 2004).

These limitations notwithstanding, this heat-shock based method of transgene expression is robust and useful for most experimental purposes. Interestingly, a *Drosophila melanogaster* heat-shock factor mutant, hsf^4, is also viable (Jedlicka et al., 1997). Therefore, this method could be extended to this organism as well.

Chapter 7

Conclusions and future directions

Sensory organs as models of glia-neuron interactions

My interests lie in uncovering the mechanisms that enable the development and function of the nervous system. To understand these processes, we have focused on sensory organs as these provide a simple model of the nervous system in general. In particular, we have sought to characterize the roles that glia play within these organs. Perhaps not surprisingly, we find that the development of glia and neurons is coordinated in the amphid sensory organs of *C. elegans* as removal of glia results in shorter dendrites.

Coordinated morphogenesis of glia and neurons is a basic requirement in all nervous systems and characterization of the molecular mechanisms that mediate glia-neuron interactions in amphid development might prove to be more general. Initially, the development of the organ must be visualized to determine how the two glial cells and the twelve neurons come in contact with each other and how they reach their final positions. This is helpful as different hypotheses about molecular players can be put forth based on different types of growth, i.e. which cell type migrates first, do all the neurons contact the glia early on, etc. Further, the role of the socket glial cell has not been investigated and imaging along with embryonic ablations of this cell could reveal any potential roles it plays in development. Perhaps most importantly, the glial ablation results provide a phenotype that could be used to conduct genetic screens for molecules involved in this process. Such screens are being currently pursued by Maxwell Heiman in our laboratory and should identify any glial-neuron interaction modules that might also play a role in other nervous system settings outside sensory organs.

Identifying glial factors that support neuronal function and morphology

A major goal of this work was to catalogue neuronal dysfunction phenotypes that might result after removal of the glial cell that ensheathes the amphid sensory neurons. While not all amphid-mediated behaviors are affected, we find clear roles for glia in supporting the function of some neurons. Moreover, glial absence results in sensory cilia morphology defects in three sheath-embedded neurons.

To better understand how glia function within sensory organs, the molecular pathways that mediate these glial roles must identified. We have made some progress towards this by characterizing FIG-1, a glial gene with neuronal phenotypes. Although further characterization of *fig-1* mutants is needed, in particular with respect to Ca^{2+} dynamics, it would be interesting to find neuronal molecules that interact with FIG-1. Working with *C. elegans*, the best approach might be to suppress the dye filling defects of *fig-1* animals. Even rare mutations can be identified in this screen as it is easy to pick out a dye-filling phasmid even in the presence of many Dyf animals.

The behavioral defects of *fig-1* animals are not as severe as those of glia-ablated animals, suggesting that many glial molecular pathways are required to support neuronal function. As discussed in Chapter 3, screens for abnormal AWC morphology or behavioral defects are likely to yield genes that act within neurons, especially IFT components. To circumvent these genes, we screened by RNAi a set sheath glia-enriched genes but did not discover any genes – apart from *fig-1* – that affected dye filling. Nonetheless, this should not be viewed as conclusive evidence that none of these genes impact neuronal function as RNAi knockdown efficiency can vary for different targets.

As a case in point, we have identified another gene, *kcc-3*, from the set of glia-enriched genes that is required for dye filling but does not give a phenotype by RNAi. *kcc-3* (also known as *K02A2.3*) encodes a potassium/chloride cotransporter that is expressed in all (or almost all) sheath glia (Jessica Tanis and Michael Koelle, personal communication). We found that 100% of *kcc-3(ok228)* mutants, which harbor a 2.6 kb deletion in the *kcc-3* locus, fail to take up dye in the phasmid.

Although further characterization of *kcc-3* is needed, its molecular identity suggests that the glia might control the concentration of chloride or potassium in the amphid channel matrix in which the sensory cilia reside. Regulation of these ions is known to be important in other sensory organs. For example, chloride homeostasis is critical for the function of vertebrate olfactory neuron whose cilia contain large concentrations of intracellular Cl^- (Kaneko et al., 2004). Odor detection ultimately results in opening of Ca^{2+}-activated Cl^- channels (Kurahashi and Yau, 1993; Lowe and Gold, 1993) and Cl^- outflow from the cell accounts for up to 90% of the transduction current (Boccaccio and Menini, 2007). All cells control their potassium levels and the cochlea displays perhaps one of the most sophisticated mechanism of K^+ regulation particularly in generating the potassium-rich endolymph that is required for hearing (Wangemann, 2006). KCC-3 might affect amphid neuron function in an analogous manner by regulating the extracellular concentration of these ions. Indeed, we have found that the amphid channel matrix is abnormally electron-dense in *kcc-3(ok228)* mutants (Appendix Figure 2), suggesting some role for this protein in the homeostasis of this environment. A direct approach to determining if KCC-3 affects neuronal chloride levels would be to measure this concentration using clomeleon, a Cl^--sensitive GFP

derivative (Kuner and Augustine, 2000). Preliminary behavioral analysis of *ok228* mutants did not reveal any defects but these experiments must be repeated and a second recently identified *kcc-3* allele, *tm3649*, must also be tested for behavioral defects. If these animals behave normally, it might be informative to test double mutants that lack *kcc-3* as well as a second channel, such as CLC-type Cl^- channels, as this might stress the system to the point of neuronal dysfunction.

Apart from supporting neuronal function, the sheath glia are also required to maintain the proper sensory cilia morphology of three sheath-embedded neurons. We have been unable to follow this process in real time so we do not know if the structures are lost because the animal grows while the cilia do not or if the cilia would lose their shape in absence of neuronal growth. To separate these processes, the sheath glia should be ablated in animals that do not grow. Ablating the sheath glia in adult animals is difficult since laser ablations are impeded by the thickness of the cuticle and toxins are not very efficient due to the large size of the cell. However, it might be possible to ablate the sheath glia in dauer animals, a stage in which the animal does not grow and follow the dynamics of cilia morphology. The *ver-1* promoter, which is expressed in sheath glia of dauer animals, or the *hsf-1* method could be used to express diphtheria toxin specifically within sheath glia in dauer larvae. If the cilia fail to maintain their morphology, it would suggest that glia actively control cilia shape. Although challenging in dauer larvae, laser ablations could be performed to determine the time course of loss of cilia shape. As discussed in Chapter 3, the most efficient strategy to isolate glial genes that affect cilia morphology is to screen for loss of AFD villi.

How might glia affect neuronal function?

The ablation results show that the presence of the sheath glia is required for most amphid sensory functions. Glial roles in the amphid can be grouped in two broad categories: permissive functions, such as homeostatic maintenance of the amphid channel milieu; or instructive roles, such as actively modulating neuronal excitability by controlled secretion of factors that impact neuronal activation. Although present in a continuum, the key difference is that instructive roles are non-constitutive processes that glia modulate. As an analogy, plant stomata, even though simple pores, play an instructive role in photosynthesis because they can regulate CO_2 availability. For example, stomata close in dry conditions or during the night.

Permissive glial roles in nervous system function have long been hypothesized and several have been verified experimentally more recently. These are undoubtedly important roles as neuronal activity might not be possible without them. It is likely that sheath glia partake in such support roles within the amphid and their molecular elucidation can lead to a better understanding of neuronal-glial physiology.

More excitingly, could sheath glia play instructive roles in the amphid? The ablation experiments presented here do not address this question; we could not observe modulatory glial roles in neuronal activity as we started by removing these cells. Conceptually, however, active glial roles can be divided based in the timescale in which they exert their effect: minutes or hours. This distinction is important experimentally as different techniques are needed to probe these timescales. Fast-acting glial modulation might be mediated by exocytosis of factors that can affect specific sensory neurons

differently or by activation of glial channels that might change the ionic environment of the amphid channel, thereby affecting most neurons. To block glial release, one could take advantage of dominant-negative proteins, such as dynamin or SNARE members, that can block exocytosis in a temperature-sensitive fashion. Behavioral analysis or Ca^{2+} imaging of these animals after a temperature shift might reveal the presence of instructive sheath roles. The difficulty of electrophysiological recordings in the amphid renders testing of ionic modulation difficult, but compounds that block only glial channels might be added in the hope that they gain access to the glia through the amphid pore. These experiments are complicated by the lack of knowledge about the channels expressed in both cell types.

A hint that the sheath might play such active roles is provided by the recent findings that the glial acid-sensitive channel ACD-1 is required for acid avoidance and chemotaxis to lysine (Wang et al., 2008). The ACD-1 channel is constitutively open and is inhibited by acidification, the presumed mechanism by which it enables neuronal avoidance of acids. Wang and colleagues speculate that acidification inhibits ACD-1, thus lowering glial Na^+ levels (Wang et al., 2008). The reduced Na^+ concentration in turn lowers the activity of the Na^+/K^+ pump causing increased levels of extracellular K^+ that affect cilia function. Interestingly, *acd-1* mutants behave normally and a defect is only visible in double mutants that also lack *deg-1*, a neuronal degenerin/epithelial Na^+ channel (DEG/ENaC) (Wang et al., 2008). This suggests that ACD-1 might not always play a role in sensation but might be required only under some conditions. For example, two parallel mechanisms of H^+ detection might exists only one of which is modulated by the glia. Furthermore, one may speculate that an animal should ignore all other stimuli

until it has left an area of high acidity, and the glia are perfectly situated to perform a whole organ temporary inactivation by changing the ionic environment. This might be likened to heterosynaptic depression – depression of nonstimulated synapses after tetanic stimulation of nearby Schaffer collaterals – which some evidence suggests is mediated by astrocytic ATP release (Pascual et al., 2005).

Sheath glia might also modulate neuronal activity over larger time scales. For example, the behavioral repertoire of adult animals might be different from that of larvae as they must balance feeding with mate searching or sensory perception might be altered by long-term environmental cues, including starvation. Carl Procko in our laboratory has shown that the expression of at least one sheath gene, *ver-1*, correlates with environmental temperature, raising the possibility that this is a general mechanism. Transcriptional profiling of sheath glia from animals reared in different conditions could be a fruitful approach to identify other glial molecules whose expression is regulated in a similar manner, providing a handle on these molecular pathways. For example, regulated production of proteins that can regulate neuronal function – perhaps thrombospondin type 1 domain proteins – might alter amphid sensation over time. Interestingly, the *C. elegans* genome encodes at least 43 proteins with TSP1 domains and several of them are very short, consisting only of the TSP1 domain, and might act as competitive inhibitors. Thus, glia might be able to alter neuronal responses in the long-term based on the animal's prior experience. Such long-term glial modulation of neuronal activity might also occur in the mammalian brain where glial tumor necrosis factor-α (TNF-α) is thought to mediate homeostatic synaptic scaling (Stellwagen and Malenka, 2006), a uniform adjustment in the strength of all synapses of a neuron in response to prolonged changes in electrical

activity that keeps firing rates roughly constant. Interestingly, thrombospondin 2 and 4 are among the few genes whose expression is upregulated in the human cortex as compared to that of chimpanzees and macaques (Caceres et al., 2003; Caceres et al., 2007), suggesting that glia, and particularly TSP proteins, might have played some part in the evolution of human of cognition.

In conclusion, this work shows that glia are required for sensory neuron function and we anticipate it will provide an opening towards characterizing the undoubtedly many roles glia play in sensory organ function. These findings will hopefully provide a small step towards a fuller understanding of the 1.4 kg mass that enabled the writing, reading (or skimming), and hopefully appreciation of this thesis.

Experimental procedures

General methods and strains

C. elegans strains were cultured at 20°C as described (Brenner, 1974), unless otherwise indicated. Wild-type animals were Bristol strain N2 and the strain CB4856 (Hodgkin and Doniach, 1997) was used for polymorphism mapping.

Alleles used in this work were:

LGI: *hsf-1(sy441), unc-101(m1), che-3(e1124), che-13(e1805), daf-16(mu86, che-10(e1809))*;
LGII: *daf-19(m86), tph-1(mg280), kcc-3(ok228), lin-26(n156,mc1,mc15)*;
LGIV: *daf-10(e1387), osm-3(p802)*;
LGV: *fig-1(tm2079), egl-9(n586), che-12(e1812*, *mn389, mn399), unc-42(e270), che-11(e1810), bbs-8(nx77), ttx-1(p767), egl-4(ky95), osm-6(p811)*;
LGX: *dyf-11(mn392), daf-13(m66), che-2(e1033), osm-1(p808*, *osm-5(m184,p813).*

The following integrated transgenes and transgenic arrays were used:

cbIs1 [*vap-1* pro(5kb)::nlsGFP, *lin-15*(+)] I,
kyIs90 [*odr-3* pro::*odr-3*(1st 35 aa's)::GFP, *lin-15*(+)] III,
kyIs104 [*str-1* pro::GFP, *lin-15*(+)],
kyIs136 [*str-2* pro::GFP, *lin-15*(+)] X (Sagasti et al., 1999),
kyIs156 [*str-1* pro::*odr-10*::GFP] X,
mnIs17 [*osm-6* pro::GFP, *unc-36*(+)],
ntIs1 [*gcy-5* pro::GFP, *lin-15*(+)] V (Sarafi-Reinach et al., 2001),
oyIs17 [*gcy-8* pro::GFP, *lin-15*(+)] V,
oyIs45 [*odr-1* pro::RFP] V,
oyIs51 [T08G3.3 pro::RFP],

bgEx21 [*unc-53* pro::GFP, pRF4],
kyEx728 [*sra-6* pro::G-CaMP],
kyEx291 [*str-2* pro::*odr-10*::GFP, *lin-15*(+)],
kyEx1440 [*sra-6* pro::*chop2*::Cherry, *elt-2* pro::GFP],
kyEx1449 [*sra-6* pro::*chop2*::Cherry, *elt-2* pro::GFP],
myEx10 [*che-11* pro::*che-11*::GFP, pRF4] (Qin et al., 2001),
yhEx19 [*osm-5* pro::*osm-5*::GFP, pRF4],
yhEx69 [*osm-5* pro::*che-13*::YFP, pRF4],
yhEx90 [*che-13* pro::*che-13*::GFP, pRF4] (Haycraft et al., 2003).

The following integrated transgenes and transgenic arrays were generated in the course of this work:

nsIs53 [*vap-1* pro(2.8kb):RFP, *unc-119*(+)] IV,
"no glia 1" *nsIs109* [*F16F9.3* pro::DT-A(G53E), *unc-122* pro::GFP],
"no glia 2" *nsIs113* [*F16F9.3* pro::DT-A(G53E), *unc-122* pro::GFP] X,
nsIs184 [*fig-1* pro::*fig-1* (short), *exp-1* pro::GFP],

nsEx856 [*F16F9.3* pro::GFP, pRF4],
nsEx992 [*vap-1* pro::*hsf-1*, *hsp-16.2* pro::GFP, pRF4],
nsEx1096 [*F16F9.3* pro::DTA(G53E), *unc-122* pro::GFP],
nsEx1126 [pTB35 (TOPO-B0024.8), *unc-122* pro::GFP + pRF4],
nsEx1129 [*osm-6* pro::*hsf-1*, *hsp-16.2* pro::GFP, pRF4],
nsEx1249 [B0024, pRF4],
nsEx1311 [*che-12* pro::*che-12*p::GFP, pRF4],
nsEx1424 [*lin-26* (E1x)::*egl-1*, pRF4],
nsEx1441 [*che-12* pro::*che-12*::GFP, pRF4],
nsEx1448 [*che-12* pro::GFP, pRF4],
nsEx1552 [*sra-6* pro::*hsf-1*, *hsp-16.2* pro::*che-2*, pRF4],
nsEx1555 [*osm-6* pro::*hsf-1*, *hsp-16.2* pro::*che-2*, pRF4],
nsEx1558 [*hsp-16.2* pro::*che-12*, pRF4],
nsEx1561 [*sra-6* pro::*che-12*, pRF4],
nsEx1702 [*dyf-11* pro::GFP, pRF4],
nsEx1705 [*dyf-11* pro::*dyf-11*::GFP, pRF4],
nsEx1746 [*myo-2* pro::*hsf-1*, *hsp-16.41* pro::GFP, pRF4],
nsEx1758 [*fig-1* pro::GFP, pRF4],
nsEx1761 [*gcy-5* pro::mCherry::SL2::*che-12*::GFP, pRF4],
nsEx1764 [*gcy-5* pro::mCherry::SL2::*dyf-11*::GFP, pRF4],
nsEx1859 [*sra-6* pro::dyf-11, pRF4],
nsEx1862 [*hsp-16.2* pro::*dyf-11*, pRF4],
nsEx1956 [*hsp16.2* pro::*che-12* + pRF4]
nsEx2192 [C38G2, pRF4],
nsEx2150 [*sra-6* pro::*fig-1* (short), *exp-1* pro::GFP],
nsEx2155 [T02B11.3 pro::*fig-1* (short), *exp-1* pro::GFP],
nsEx2209 [*fig-1* pro::*fig-1* (long), *exp-1* pro::GFP],
nsEx2212 [*sra-6* pro::*odr-10*::GFP, pRF4, pSL1180],
nsEx2215 [*odr-1* pro::*odr-10*::GFP, pRF4, pSL1180],
nsEx2218 [*odr-10* pro::*odr-10*::GFP, pRF4, pSL1180],
nsEx2221 [*odr-1* pro::*tax-4*::GFP, pRF4, pSL1180],
nsEx2224 [*odr-1* pro::*tax-4*::GFP, pRF4, pSL1180].

Germline transformations

To generate transgenic animals, adult hermaphrodites were transformed using standard protocols (Mello et al., 1991). Construct and coninjection markers were usually injected at 30 ng/µl each and often an empty vector pSL1180 was added to a total concentration of 100 ng/µl. Often, the coinjection plasmid used was pRF4, which contains the dominant marker pRF4 (Mello et al., 1991); *exp-1* pro::GFP was kindly provided by Eric Jorgensen (Beg and Jorgensen, 2003) and used as a coinjection marker. Stable transgenes were obtained by psoralen integration (Yandell et al., 1994).

Heterozygous *che-12*/+ animals were used for injections as it was difficult to obtain transgenic lines by injecting *che-12* animals directly.

Ablations

Laser ablations were performed as described (Bargmann and Avery, 1995) in L1 larvae of a strain expressing GFP in amphid sheath glia (*cbIs1*). Ablation success was determined by lack of GFP expression and also confirmed in eight animals by EM reconstruction. All cilia morphologies were determined in laser-ablated animals as well as transgenic lines lacking glia. An attenuated form of diphtheria toxin A was expressed specifically within amphid and phasmid sheath cells using the *F16F9.3* promoter region to kill these cells genetically. Transgenic animals carrying pTB29 [*F16F9.3* pro::DT-A(G53E)], injected at 2 ng/µL, and pEP51 [*unc-122* pro::GFP], a gift of Elliot Perens, were obtained by germline injection followed by psoralen integration. In the two lines

characterized, “no glia 1” (*nsIs109*) and “no glia 2” (*nsIs113*), the amphid sheath glia appears to die in late embryos or in early L1 larvae. Laser-ablated animals were tested in NaCl chemotaxis and osmosensation assays and they performed similarly to genetically-ablated animals, indicating that the two ablations are essentially equivalent.

Behavioral analysis

NaCl chemotaxis and odortaxis assays were performed as previously described (Ward, 1973; Bargmann et al., 1993). Attractants were assayed on circular plates; repellents and diacetyl in the experiment shown in Figure 1G were assayed on square plates. All data shown is from 12 assays. The ring assay was used to test osmosensation (Culotti and Russell, 1978). Briefly, a 1 cm ring of 4 M fructose containing the dye Congo Red was made on an NGM plate. Animals were placed inside the ring and followed over the next 10 min to determine the response to the osmotic barrier. Animals avoiding the ring more than six times were classified as normal; those exiting the ring in less than six attempts were deemed defective in osmosensation.

Thermotaxis assays were performed on a 18°-26°C linear temperature gradient (Ryu and Samuel, 2002). Animals were allowed to lay for 8-24 hours and removed from plates. The staged progeny were tested on the first day of adulthood. Briefly, animals were washed twice with S-Basal and spotted onto a 10 cm plate containing 12 mL of NGM agar. The plate was placed onto the temperature gradient with the addition of 1 mL glycerol to its bottom to improve thermal conductivity. The plate was covered with a flat piece of glass. The assay was stopped after 45 min by inverting the plate over

chloroform thus killing the animals. The plates have an imprinted 6x6 square pattern that formed the basis of the 6 temperature bins. The data shown is the average of four assays.

Dye filling

Stock solutions (20 mg/mL) of fluorescein-5-isothiocyanate (FITC "isomer I"; Molecular Probes, Eugene, OR) and 5 mg/mL 1,1'-dioctadecyl-3,3,3',3'-tetramethylindocarbocyanine perchlorate (DiI) (Molecular Probes, Eugene, OR) in *N*,*N*-dimethylformamide were stored at -20°. To assay dye uptake, animals were soaked in 0.4 mg/mL FITC or 5 μg/mL DiI diluted in M9 for up to 4 h.

Heat shock

Animals were placed at 34°C for 30 min, allowed to recover at 20° for 6 h, and scored for dye uptake or imaged.

Mutagenesis

Animals were mutagenized with 30 mM ethyl methanesulfonate (EMS) for 4 hours. Healthy L4 hermaphrodites were selected and propagated on 10 cm NGM agar plates for 6 days. To obtain F2 animals, these plates were bleached and the embryos

were allowed to hatch overnight in M9 buffer. These synchronized F2 larvae were plated as desired and scored after 3 days.

Mapping and cloning of *che-12* and *dyf-11*

unc-42(e270) che-12(mn399) egl-9(n586) hermaphrodites were crossed to CB4856 (Hodgkin and Doniach, 1997) males, which contain many single nucleotide polymorphisms (SNPs) with respect to N2 (Wicks et al., 2001). From the F2 progeny, Egl non-Unc and Unc non-Egl animals were selected. These recombinants were soaked in FITC to determine their *che-12* genotype. DNA was prepared from the progeny of recombinant animals as previously described (Wicks et al., 2001). SNP analysis limited the genomic location of *che-12* between the SNPs C12D8:34312 and AC3:3025. Cosmid clones containing DNA spanning this region were injected singly into *che-12* animals and transgenic animals were tested for rescue of the FITC uptake defect. Cosmid B0024 was the only one to give rescue. Shorter regions of B0024 were amplified by PCR and introduced into *che-12* mutants. A fragment containing the gene B0024.8 yielded animals rescued for dye filling.

Previous work had established that *dyf-11(mn392)* was located on the left arm of chromosome X (Starich et al., 1995). To refine this position, *dyf-11*(*mn392*) hermaphrodites were crossed to CB4856 males. From this cross, 238 dye-filling defective F2 animals were isolated, and DNA prepared from their progeny was characterized for the presence of N2 and CB4856 SNPs. This analysis revealed that *dyf-11* resides between the SNPs F39H12:15494 and F02G3:5645. Sequencing candidate

genes from this region revealed that the gene C02H7.1 contained a nonsense mutation in *dyf-11* animals. Injection of both the C02H7 cosmid and the C02H7.1 genomic region restored dye filling.

Microscopy and imaging

GFP expression patterns were analyzed in stable transgenic lines by conventional fluorescence microscopy using an Axioplan II microscope equipped with an AxioCam camera. Alternatively, imaging was performed on a Zeiss Axiovert 200M microscope equipped with an UltraView spinning disk confocal head using a 100x/1.45 NA objective. Expression patterns for each construct were examined in three independent transgenic lines.

Calcium imaging was performed using a microfluidic device as described (Chalasani et al., 2007). Images were captured at 10 frames/s and were analyzed using MetaMorph and Matlab (Chalasani et al., 2007).

IFT was assayed as previously described (Orozco et al., 1999; Christensen et al., 2002). Transgenic animals anesthetized with 5 mM levamisole were mounted on agar pads and imaged at 21°C. Imaging was performed on a Zeiss Axiovert 200M microscope equipped with an UltraView spinning disk confocal head using a 100x/1.45 NA objective. Images were collected with a Hamamatsu EM-CCD (C9100-12) camera at 0.333s/frame for 5 min. Kymographs were created using MetaMorph.

Electron microscopy

Animals were fixed, stained, embedded in resin, and serially sectioned using standard methods (Lundquist et al., 2001). Imaging was performed with an FEI Tecnai G2 Spirit BioTwin transmission electron microscope equipped with a Gatan 4K x 4K digital camera.

Channelrhodopsin2

An overnight culture (5mL) of *E. coli* (strain OP50) was pelleted and concentrated to 50 μL. To this, 1 μL of 50 mM retinal (a gift of Navin Pokala and Cori Bargmann) was added. After vortexing, the mixture was spotted in NGM plates. Animals expressing ChR2-mCherry were transferred and cultivated on these plates for at least 2 hours. Animals were assayed on a dissecting microscope by exposing them for about 1 s to excitation light using a GFP Plant fluorescence filter 470/40 nm. Animals initiating backward movement within 2 s were scored responsive. The animals were not responding to UV light per se as omission of retinal, a channelrhodopsin2 obligate cofactor, resulted in unresponsive animals.

RNAi

RNAi was performed as described using published clones (Kamath et al., 2003). To screen the candidate genes, 4 L4 larvae were placed on seeded RNAi plates and their progeny screened after 4 days by dye filling.

Plasmid constructions

Most of the vectors used in this work have the pPD vector backbone (Fire et al., 1990; Miller et al., 1999). Most cDNAs isolated were amplified by PCR from a mixed-stage cDNA library (Schumacher et al., 2005). In some cases, dual transcripts from the same promoter were generated by using the SL2 acceptor sequence (HUANG *et al*., 2001). The diphtheria toxin used was from the pJF142 [*unc-122* pro::DT-A(K52E)] plasmid, a gift of Hanna Fares (Fares and Greenwald, 2001), which also contains a D79G mutation that should not affect toxin activity.

Table 8.1: List of plasmids used in this work

Name	Pro	cDNA	Notes
pTB2	*vap-1*		5kb promoter vap-1 into PstI/BamHI of pPD49.78.
pTB3	*vap-1*	CED-3	5kb promoter vap-1 into PstI/BamHI of pPD49.78. CED-3 cDNA into BamHI/NcoI.
pTB4	*vap-1*	HSF-1	5kb promoter vap-1 into PstI/BamHI of pPD49.78. HSF-1 cDNA into XmaI/NheI.
pTB8	*vap-1*	DT-A	vap-1 promoter as PstI/BamHI from pEP2 into PstI/BamHI of pJF142. Backbone pPD95.77. DT-A K52E is 10% as active (also has D79G mutation).
pTB8B	*vap-1*	DT-A(G53E)	pTB8 derivative. Has G53E mutation. (also has D79G mutation).
pTB8C	*vap-1*	DT-A(K52E G53E)	pTB8 derivative. Has K52E and G53E mutation. (also has D79G mutation).
pTB11	*hsp16.2*	nlsGFP	SphI/BamHI hsp16.2 promoter from pPD49.78 into SphI/BamHI of pPD95.69.
pTB12	*hsp16.41*	nlsGFP	SphI/BamHI hsp16.41 promoter from pPD49.83 into SphI/BamHI of pPD95.69.
pTB13	*vap-1*	EGL-1	5kb promoter vap-1 into PstI/BamHI of pPD49.78. EGL-1 cDNA into BamHI/NcoI. The EGL-1 cDNA not as in wormbase, it starts at position 46.
pTB28	*F16F9.3*	EGL-1	2kb *F16F9.3* promoter into PstI/BamHI of pPD49.78 (made by Carl Procko). EGL-1 cDNA into BamHI/NcoI. The EGL-1 cDNA not as in Wormbase,

Name	Pro	cDNA	Notes
			it starts at position 46.
pTB29	*F16F9.3*	DT-A(G53E)	F16F19.3 promoter as Pst/BamHI from Carl Procko into Pst/Bam of pTB8B. DT-A G53E (also has D79G mutation).
pTB30	*gcy-7*	HSF-1	Xma/Spe fragment of pTB4 into Xma/Spe of gcy-7::mCherry. This replaces mCherry+3UTR with HSF1+3UTR.
pTB31	*F16F9.3*	HSF-1	2kb *F16F9.3* promoter into PstI/BamHI of pPD49.78. HSF-1 from pTB4 into Xma/NheI.
pTB32	*hsp-16.2*	DT-A(G53E)	hs16.2 Sal-Bam promoter (note there are two Sal sites) into Sal/Bam of pTB8B. DT-A has G53E mutation. (also has D79G mutation).
pTB34	*osm-6*	HSF-1	XmaI/SpeI HSF-1+3UTR from pTB4 into Xma/Spe of 95.75-osm-6. Maya seems to have droped osm-6 as XbaI fragment.
pTB35		B0024.8	pCR2.1-TOPO-B0024.4.8. The region includes B0024.4 and .8 in the forward orientation as in genome. That is, .4 is forward while .8 reverse.
pTB39	*che-12*	GFP	1kb che-12 promoter including ATc (g was changed) in 95.75 as Sal/Bam.
pTB41	*che-12*	NLSmCherry	1kb che-12 promoter including ATc (g was changed) from pTB39 into 69-NLSmCHERRY as a Sal/Bam fragment.
pTB45	*che-12*	CHE-12::GFP	che-12 promoter from pTB39 as Pst/Xma into Pst/Xma. Note this cDNA has two silent mutations at about 3kb. CHE-12 is KpnI/AgeI.
pTB46	*lin-26 E1*	EGL-1	E1 region of lin-26 promoter as a Sal/Xba fragment from Max Heiman's vector into Sal/Xba of osm-6::EGL-1. Also has minimal myo-2 promoter
pTB47	*lin-26 E1s*	EGL-1	The Xho/BamHI fragment of the lin-26 E1 promoter, taken as a Xho/Xba fragment from Max Heiman's vector into Sal/Xba of osm-6::EGL-1. Also has minimmal myo-2 promoter.
pTB48	*hsp16.2*	CHE-12	CHE-12 cDNA as KpnI/SacI into 49.78. It has two silent mutations at about 3kb in cDNA as do all my CHE-12 cDNAs.
pTB49	*sra-6*		2.4kb sr-a6 promoter starting from endogenous Sph put into pSM (Bargmann lab pPD48.26 modified vector) as Sph/Bam fragment.
pTB50	*sra-6*	CHE-12	2.4kb sra-6 promoter from endogenous SphI to ATG, put into pSM as a Sph/Bam fragment. CHE-12 added as a Xma/Sac piece.
pTB51	*hsp16.2*	CHE-2	CHE-2 cDNA as a Bam/Nco fragment into Bam/Nco of pPD49.78.

Name	Pro	cDNA	Notes
pTB52	*sra-6*	HSF-1	2.4kb sra-6 promoter from pTB49 as Sph/Xma into Sph/Xma of pTB4. Essentially replace vap-1 with sra-6.
pTB53	*che-12*	CHE-13:: mCherry	1kb che-12 promoter as Sal/Bam. CHE-13 cDNA as Xma/Kpn.
pTB56	*dyf-11*	nlsGFP	dyf-11 promoter Sph/Sal into pPD95.69.
pTB57		DYF-11::GFP	DYF-11 cDNA missing A of TGA as Sal/Bam. Sequenced and clean.
pTB58	*dyf-11*	DYF-11::GFP	dyf-11 promoter as Sph/Sal in pTB59
pTB59	*dyf-11*	DYF-11	Replace the DYF-11 cDNA of pTB58 with a cDNA that has the stop codon.
pTB60		DYF-11::GFP	SphI/Xba DYF-11 PCR fragment replaced in pTB57 to introduce NgoM IV site, this removes dyf-11 promoter. Sequenced and clean.
pTB61		DYF-11	SphI/Xba DYF-11 cDNA PCR fragment replaced in pTB59 to introduce NgoM IV site, this removes dyf-11 promoter. Sequenced and clean.
pTB62	*gcy-5*	mCherry::SL2:: DYF-11::GFP	NgoMIV/XhoI DYF-11::GFP fragment of pTB60 into NgoMIV/XhoI of gcy-5::mCherry::SL2::DYF-7::GFP from Max Heiman. So, replace DYF-7 with DYF-11.
pTB64	*gcy-5*	mCherry::SL2:: CHE-12::GFP	XmaI/XhoI CHE-12::GFP fragment of pTB45 into NgoMIV/XhoI of gcy-5::mCherry::SL2::DYF-7::GFP from Max Heiman. So, replace DYF-7 with CHE-12.
pTB65	*hsp16.2*	DYF-11	NgoM/Xma DYF-11 from pTB61 into Xma of pPD49.78.
pTB66	*sra-6*	DYF-11	NgoMIV/XmaI DYF11 from pTB61 into XmaI of pTB49, downstream of sra-6 promoter.
pTB68	*myo-2*	HSF-1	HSF1+3'UTR from pTB4 as Xma/Spe into Xma/Spe of Max's myo-2::GFP. Note this myo-2 promoter is the long version and expresses in pharynx.
pTB72	*odr-1*	CHE-12	CHE-12 cDNA + unc-54 3'UTR as Xma/Spe from pTB48 into Xma/Spe of and odr-1::mCherry vector (pSM background). CHE-12 is KpnI/SacI.
pTB73	*srh-142*	EGL-1	1451bp srh-142 promoter (expresses in ADF) into PstI/BamHI pTB13.
pTB74		ODR-10::GFP	ODR-10 cDNA PCRed without stop codon into BamHI/AgeI of pPD95.75.
pTB75		OSM-9::GFP	OSM-9 cDNA PCRed without stop codon into XmaI of pPD95.75. Confirmed orientation but OSM-9 was not sequenced so could be dirty.
pTB76	*sra-6*	ODR-10::GFP	sra-6 promoter as Sph/Bam from pTB49 into Sph/Bam of pTB74.
pTB77	*sra-6*	OSM-9::GFP	OSM-9::GFP + 3'UTR as Xba/Apa into Nhe/Apa of pTB49.

Name	Pro	cDNA	Notes
pTB78	*odr-1*	ODR-10::GFP	ODR-10::GFP Xba/Apa fragment from pTB74 into Xba/Apa of odr-1::mCherry.
pTB79	*odr-1*	OSM-9::GFP	OSM-9::GFP Xba/Apa fragment from pTB75 into Xba/Apa of odr-1::mCherry.
pTB82	*odr-1*	TAX-2::GFP	TAX-2 cDNA without stop PCRed as Xma/Age into Xma/Age of pTB79. TAX-2 has the mutation C1595T (T533L).
pTB83	*odr-1*	TAX-4::GFP	TAX-4 cDNA without stop PCRed as Xba/Xma into Xba/Xma of pTB79. TAX-4 cDNA is clean.
pTB85	*srh-142*	TPH-1	3182bp srh-142 promoter as Sph/Bam and TPH-1 cDNA from clone yk1176f10 (has second intron unspliced) as Bam/Nco. Backbone 49.26.

Appendix

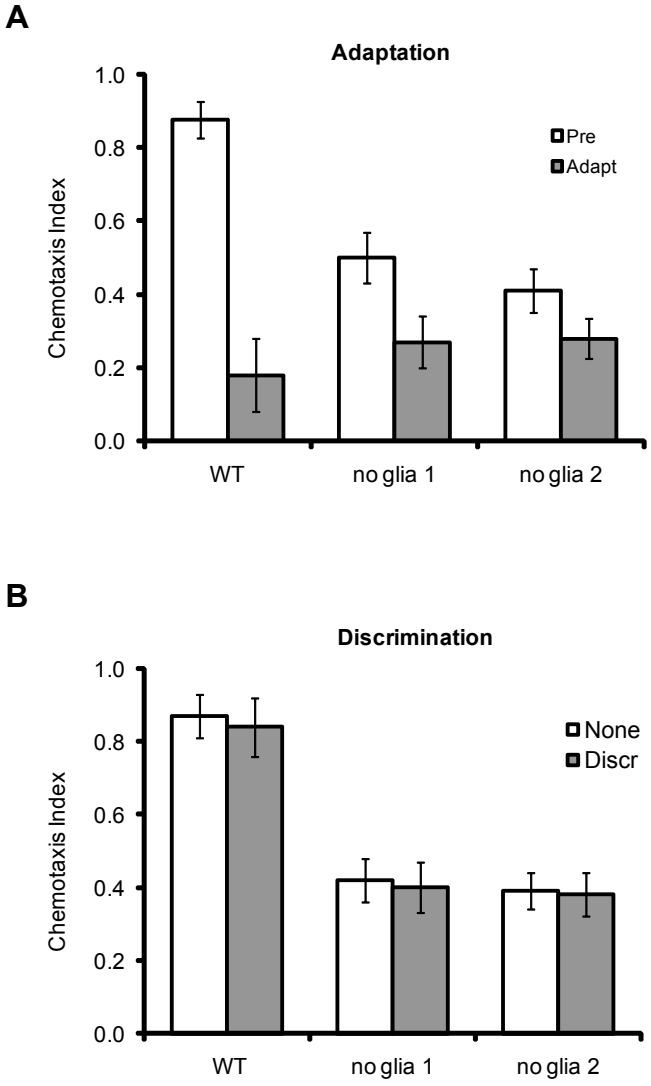

Appendix Figure 1: Glia are not required for adaptation or discrimination

(**A**) Animals were starved for one hour on agar plates, to the adaptation group 1 µl of diacetyl was added on an agar plug on the cover of the plate. Standard chemotaxis assays towards 0.1% diacetly were performed. (**B**) Discrimination assays were performed by adding 1µL diacetyl to the agar of the chemotaxis plate. Assays towards 1% methyl pyrazine were performed in standard plates (None) or discrimination plates (Discr).

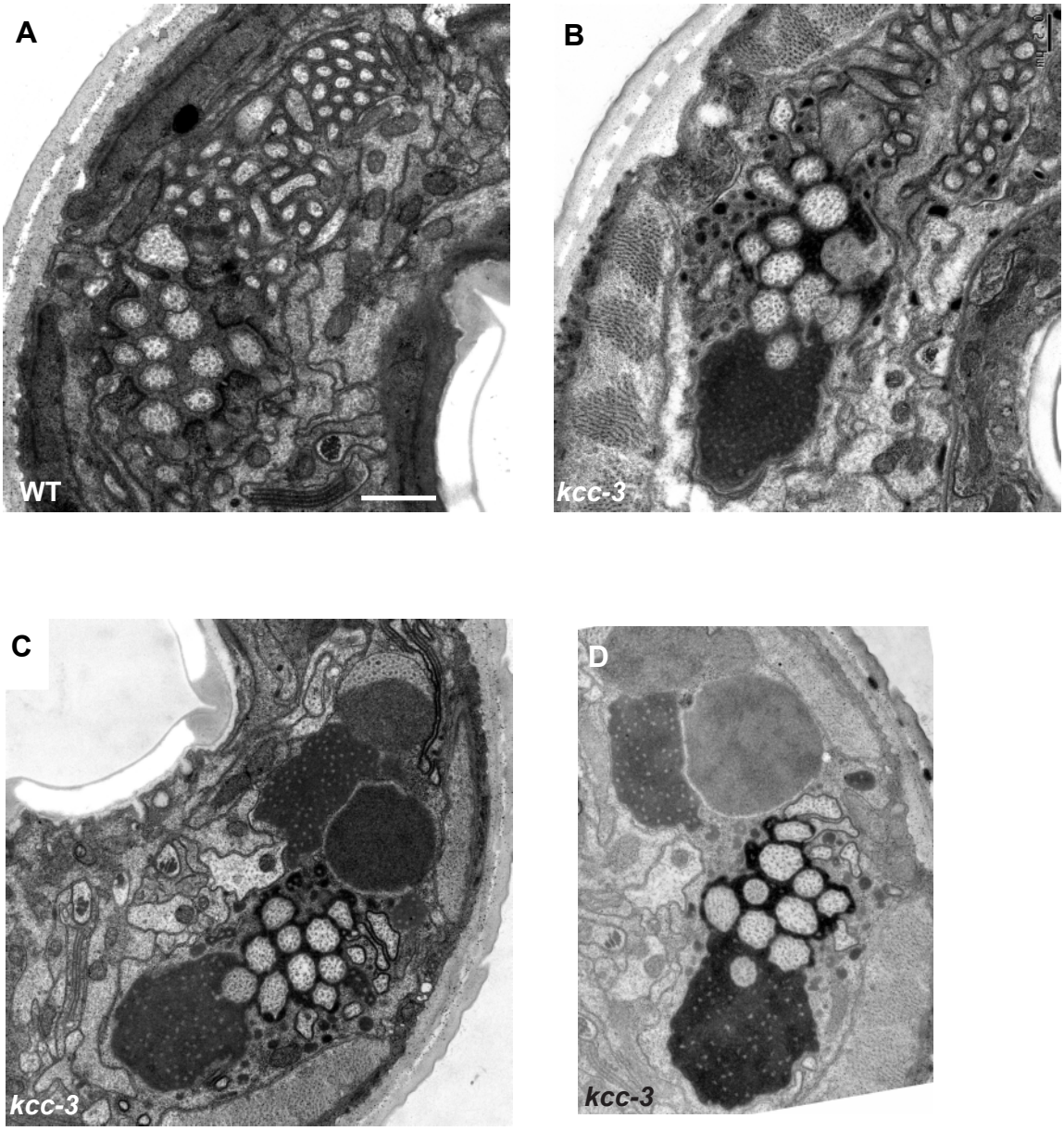

Appendix Figure 2: Abnormal glia secretion in *kcc-3(ok228)* mutants

(**A**) An EM image of a wild-type animal; the sheath glia-secreted matrix can seen surrounding the sensory cilia and AFD villi. (**B-D**) In *kcc-3(ok228)* mutants the glial secretion is abnormally electron-dense. Strcutures resmbling crystals are observed in the extracellular matrix, see panel D. Scale bar, 1 μm.

References

Adams, J.C. (2001). Thrombospondins: multifunctional regulators of cell interactions. Annu Rev Cell Dev Biol *17*, 25-51.

Adams, J.C., and Tucker, R.P. (2000). The thrombospondin type 1 repeat (TSR) superfamily: diverse proteins with related roles in neuronal development. Dev Dyn *218*, 280-299.

Agulhon, C., Petravicz, J., McMullen, A.B., Sweger, E.J., Minton, S.K., Taves, S.R., Casper, K.B., Fiacco, T.A., and McCarthy, K.D. (2008). What is the role of astrocyte calcium in neurophysiology? Neuron *59*, 932-946.

Albert, P.S., Brown, S.J., and Riddle, D.L. (1981). Sensory control of dauer larva formation in *Caenorhabditis elegans*. J Comp Neurol *198*, 435-451.

Albert, P.S., and Riddle, D.L. (1983). Developmental alterations in sensory neuroanatomy of the *Caenorhabditis elegans* dauer larva. J Comp Neurol *219*, 461-481.

Altschul, S.F., Gish, W., Miller, W., Myers, E.W., and Lipman, D.J. (1990). Basic local alignment search tool. J Mol Biol *215*, 403-410.

Andrade, M.A., and Bork, P. (1995). HEAT repeats in the Huntington's disease protein. Nat Genet *11*, 115-116.

Ansley, S.J., Badano, J.L., Blacque, O.E., Hill, J., Hoskins, B.E., Leitch, C.C., Kim, J.C., Ross, A.J., Eichers, E.R., Teslovich, T.M., *et al.* (2003). Basal body dysfunction is a likely cause of pleiotropic Bardet-Biedl syndrome. Nature *425*, 628-633.

Araque, A., Martin, E.D., Perea, G., Arellano, J.I., and Buno, W. (2002). Synaptically released acetylcholine evokes Ca^{2+} elevations in astrocytes in hippocampal slices. J Neurosci *22*, 2443-2450.

Arber, S., and Caroni, P. (1995). Thrombospondin-4, an extracellular matrix protein expressed in the developing and adult nervous system promotes neurite outgrowth. J Cell Biol *131*, 1083-1094.

Avidor-Reiss, T., Maer, A.M., Koundakjian, E., Polyanovsky, A., Keil, T., Subramaniam, S., and Zuker, C.S. (2004). Decoding cilia function: defining specialized genes required for compartmentalized cilia biogenesis. Cell *117*, 527-539.

Awasaki, T., and Ito, K. (2004). Engulfing action of glial cells is required for programmed axon pruning during *Drosophila* metamorphosis. Curr Biol *14*, 668-677.

Awasaki, T., Lai, S.L., Ito, K., and Lee, T. (2008). Organization and postembryonic development of glial cells in the adult central brain of *Drosophila*. J Neurosci *28*, 13742-13753.

Awasaki, T., Tatsumi, R., Takahashi, K., Arai, K., Nakanishi, Y., Ueda, R., and Ito, K. (2006). Essential role of the apoptotic cell engulfment genes draper and *ced-6* in programmed axon pruning during *Drosophila* metamorphosis. Neuron *50*, 855-867.

Bacaj, T., Tevlin, M., Lu, Y., and Shaham, S. (2008). Glia are essential for sensory organ function in *C. elegans*. Science *322*, 744-747.

Baehr, W., Wu, S.M., Bird, A.C., and Palczewski, K. (2003). The retinoid cycle and retina disease. Vision Res *43*, 2957-2958.

Banerjee, S., and Bhat, M.A. (2007). Neuron-glial interactions in blood-brain barrier formation. Annu Rev Neurosci *30*, 235-258.

Banker, G.A. (1980). Trophic interactions between astroglial cells and hippocampal neurons in culture. Science *209*, 809-810.

Bargmann, C.I. (1993). Genetic and cellular analysis of behavior in *C. elegans*. Annu Rev Neurosci *16*, 47-71.

Bargmann, C.I. (1998). Neurobiology of the *Caenorhabditis elegans* genome. Science *282*, 2028-2033.

Bargmann, C.I., and Avery, L. (1995). Laser killing of cells in *Caenorhabditis elegans*. Methods Cell Biol *48*, 225-250.

Bargmann, C.I., Hartwieg, E., and Horvitz, H.R. (1993). Odorant-selective genes and neurons mediate olfaction in *C. elegans*. Cell *74*, 515-527.

Bargmann, C.I., and Horvitz, H.R. (1991a). Chemosensory neurons with overlapping functions direct chemotaxis to multiple chemicals in *C. elegans*. Neuron *7*, 729-742.

Bargmann, C.I., and Horvitz, H.R. (1991b). Control of larval development by chemosensory neurons in *Caenorhabditis elegans*. Science *251*, 1243-1246.

Bargmann, C.I., Thomas, J.H., and Horvitz, H.R. (1990). Chemosensory cell function in the behavior and development of *Caenorhabditis elegans*. Cold Spring Harb Symp Quant Biol *55*, 529-538.

Barres, B.A. (2008). The mystery and magic of glia: a perspective on their roles in health and disease. Neuron *60*, 430-440.

Bartel, D.L., Sullivan, S.L., Lavoie, E.G., Sevigny, J., and Finger, T.E. (2006). Nucleoside triphosphate diphosphohydrolase-2 is the ecto-ATPase of type I cells in taste buds. J Comp Neurol *497*, 1-12.

Battye, R., Stevens, A., and Jacobs, J.R. (1999). Axon repulsion from the midline of the *Drosophila* CNS requires slit function. Development *126*, 2475-2481.

Beg, A.A., and Jorgensen, E.M. (2003). EXP-1 is an excitatory GABA-gated cation channel. Nat Neurosci *6*, 1145-1152.

Beierlein, M., and Regehr, W.G. (2006). Brief bursts of parallel fiber activity trigger calcium signals in Bergmann glia. J Neurosci *26*, 6958-6967.

Bell, L.R., Stone, S., Yochem, J., Shaw, J.E., and Herman, R.K. (2006). The molecular identities of the *Caenorhabditis elegans* intraflagellar transport genes *dyf-6, daf-10* and *osm-1*. Genetics *173*, 1275-1286.

Bergmann, A., Tugentman, M., Shilo, B.Z., and Steller, H. (2002). Regulation of cell number by MAPK-dependent control of apoptosis: a mechanism for trophic survival signaling. Dev Cell *2*, 159-170.

Bezzi, P., Carmignoto, G., Pasti, L., Vesce, S., Rossi, D., Rizzini, B.L., Pozzan, T., and Volterra, A. (1998). Prostaglandins stimulate calcium-dependent glutamate release in astrocytes. Nature *391*, 281-285.

Bigiani, A. (2001). Mouse taste cells with glialike membrane properties. J Neurophysiol *85*, 1552-1560.

Blacque, O.E., Perens, E.A., Boroevich, K.A., Inglis, P.N., Li, C., Warner, A., Khattra, J., Holt, R.A., Ou, G., Mah, A.K., *et al.* (2005). Functional genomics of the cilium, a sensory organelle. Curr Biol *15*, 935-941.

Blacque, O.E., Reardon, M.J., Li, C., McCarthy, J., Mahjoub, M.R., Ansley, S.J., Badano, J.L., Mah, A.K., Beales, P.L., Davidson, W.S., *et al.* (2004). Loss of *C. elegans* BBS-7 and BBS-8 protein function results in cilia defects and compromised intraflagellar transport. Genes Dev *18*, 1630-1642.

Boccaccio, A., and Menini, A. (2007). Temporal development of cyclic nucleotide-gated and Ca^{2+} -activated Cl^{-} currents in isolated mouse olfactory sensory neurons. J Neurophysiol *98*, 153-160.

Booth, G.E., Kinrade, E.F.V., and Hidalgo, A. (2000). Glia maintain follower neuron survival during *Drosophila* CNS development. Development *127*, 237-244.

Brand, A.H., and Perrimon, N. (1993). Targeted gene expression as a means of altering cell fates and generating dominant phenotypes. Development *118*, 401-415.

Brechbuhl, J., Klaey, M., and Broillet, M.C. (2008). Grueneberg ganglion cells mediate alarm pheromone detection in mice. Science *321*, 1092-1095.

Breipohl, W., Laugwitz, H.J., and Bornfeld, N. (1974). Topological relations between the dendrites of olfactory sensory cells and sustentacular cells in different vertebrates. An ultrastructural study. J Anat *117*, 89-94.

Brenner, M., Kisseberth, W.C., Su, Y., Besnard, F., and Messing, A. (1994). GFAP promoter directs astrocyte-specific expression in transgenic mice. J Neurosci *14*, 1030-1037.

Brenner, S. (1974). Genetics of *Caenorhabditis elegans*. Genetics *77*, 71-94.
Browne, P.C., Miller, J.J., and Detwiler, T.C. (1988). Kinetics of the formation of thrombin-thrombospondin complexes: involvement of a 77-kDa intermediate. Arch Biochem Biophys *265*, 534-538.

Buck, L., and Axel, R. (1991). A novel multigene family may encode odorant receptors: a molecular basis for odor recognition. Cell *65*, 175-187.

Bush, T.G., Savidge, T.C., Freeman, T.C., Cox, H.J., Campbell, E.A., Mucke, L., Johnson, M.H., and Sofroniew, M.V. (1998). Fulminant jejuno-ileitis following ablation of enteric glia in adult transgenic mice. Cell *93*, 189-201.

Bushong, E.A., Martone, M.E., Jones, Y.Z., and Ellisman, M.H. (2002). Protoplasmic astrocytes in CA1 stratum radiatum occupy separate anatomical domains. J Neurosci *22*, 183-192.

Caceres, M., Lachuer, J., Zapala, M.A., Redmond, J.C., Kudo, L., Geschwind, D.H., Lockhart, D.J., Preuss, T.M., and Barlow, C. (2003). Elevated gene expression levels distinguish human from non-human primate brains. Proc Natl Acad Sci USA *100*, 13030-13035.

Caceres, M., Suwyn, C., Maddox, M., Thomas, J.W., and Preuss, T.M. (2007). Increased cortical expression of two synaptogenic thrombospondins in human brain evolution. Cereb Cortex *17*, 2312-2321.

Cahoy, J.D., Emery, B., Kaushal, A., Foo, L.C., Zamanian, J.L., Christopherson, K.S., Xing, Y., Lubischer, J.L., Krieg, P.A., Krupenko, S.A., *et al.* (2008). A transcriptome database for astrocytes, neurons, and oligodendrocytes: a new resource for understanding brain development and function. J Neurosci *28*, 264-278.

Cassada, R.C., and Russell, R.L. (1975). The dauerlarva, a post-embryonic developmental variant of the nematode *Caenorhabditis elegans*. Dev Biol *46*, 326-342.

Chalasani, S.H., Chronis, N., Tsunozaki, M., Gray, J.M., Ramot, D., Goodman, M.B., and Bargmann, C.I. (2007). Dissecting a circuit for olfactory behaviour in Caenorhabditis elegans. Nature *450*, 63-70.

Chao, M.Y., Komatsu, H., Fukuto, H.S., Dionne, H.M., and Hart, A.C. (2004). Feeding status and serotonin rapidly and reversibly modulate a *Caenorhabditis elegans* chemosensory circuit. Proc Natl Acad Sci USA *101*, 15512-15517.

Chelur, D.S., and Chalfie, M. (2007). Targeted cell killing by reconstituted caspases. Proc Natl Acad Sci USA *104*, 2283-2288.

Chen, N., Mah, A., Blacque, O.E., Chu, J., Phgora, K., Bakhoum, M.W., Newbury, C.R., Khattra, J., Chan, S., Go, A., *et al.* (2006). Identification of ciliary and ciliopathy genes in *Caenorhabditis elegans* through comparative genomics. Genome Biol *7*, R126.

Christensen, M., Estevez, A., Yin, X., Fox, R., Morrison, R., McDonnell, M., Gleason, C., Miller, D.M., 3rd, and Strange, K. (2002). A primary culture system for functional analysis of *C. elegans* neurons and muscle cells. Neuron *33*, 503-514.

Christopherson, K.S., Ullian, E.M., Stokes, C.C.A., Mullowney, C.E., Hell, J.W., Agah, A., Lawler, J., Mosher, D.F., Bornstein, P., and Barres, B.A. (2005). Thrombospondins are astrocyte-secreted proteins that promote CNS synaptogenesis. Cell *120*, 421-433.

Chung, Y.D., Zhu, J., Han, Y., and Kernan, M.J. (2001). *nompA* encodes a PNS-specific, ZP domain protein required to connect mechanosensory dendrites to sensory structures. Neuron *29*, 415-428.

Colbert, H.A., Smith, T.L., and Bargmann, C.I. (1997). OSM-9, a novel protein with structural similarity to channels, is required for olfaction, mechanosensation, and olfactory adaptation in *Caenorhabditis elegans*. J Neurosci *17*, 8259-8269.

Cole, D.G. (2003). The intraflagellar transport machinery of *Chlamydomonas reinhardtii*. Traffic *4*, 435-442.

Cole, D.G., Diener, D.R., Himelblau, A.L., Beech, P.L., Fuster, J.C., and Rosenbaum, J.L. (1998). *Chlamydomonas* kinesin-II-dependent intraflagellar transport (IFT): IFT particles contain proteins required for ciliary assembly in *Caenorhabditis elegans* sensory neurons. J Cell Biol *141*, 993-1008.

Collet, J., Spike, C.A., Lundquist, E.A., Shaw, J.E., and Herman, R.K. (1998). Analysis of *osm-6*, a gene that affects sensory cilium structure and sensory neuron function in *Caenorhabditis elegans*. Genetics *148*, 187-200.

Colón-Ramos, D.A., Margeta, M.A., and Shen, K. (2007). Glia promote local synaptogenesis through UNC-6 (netrin) signaling in *C. elegans*. Science *318*, 103-106.

Colosimo, M.E., Brown, A., Mukhopadhyay, S., Gabel, C., Lanjuin, A.E., Samuel, A.D., and Sengupta, P. (2004). Identification of thermosensory and olfactory neuron-specific genes via expression profiling of single neuron types. Curr Biol *14*, 2245-2251.

Conradt, B., and Horvitz, H.R. (1998). The *C. elegans* protein EGL-1 is required for programmed cell death and interacts with the Bcl-2-like protein CED-9. Cell *93*, 519-529.

Cui, W., Allen, N.D., Skynner, M., Gusterson, B., and Clark, A.J. (2001). Inducible ablation of astrocytes shows that these cells are required for neuronal survival in the adult brain. Glia *34*, 272-282.

Culotti, J.G., and Russell, R.L. (1978). Osmotic avoidance defective mutants of the nematode *Caenorhabditis elegans*. Genetics *90*, 243-256.

Danysz, W., and Parsons, C.G. (1998). Glycine and N-methyl-D-aspartate receptors: physiological significance and possible therapeutic applications. Pharmacol Rev *50*, 597-664.

de Bono, M., and Bargmann, C.I. (1998). Natural variation in a neuropeptide Y receptor homolog modifies social behavior and food response in *C. elegans*. Cell *94*, 679-689.

Dearborn, R., Jr., and Kunes, S. (2004). An axon scaffold induced by retinal axons directs glia to destinations in the *Drosophila* optic lobe. Development *131*, 2291-2303.

Delaney, C.L., Brenner, M., and Messing, A. (1996). Conditional ablation of cerebellar astrocytes in postnatal transgenic mice. J Neurosci *16*, 6908-6918.

DeLange, R.J., Williams, L.C., Drazin, R.E., and Collier, R.J. (1979). The amino acid sequence of fragment A, an enzymically active fragment of diphtheria toxin. III. The chymotryptic peptides, the peptides derived by cleavage at tryptophan residues, and the complete sequence of the protein. J Biol Chem *254*, 5838-5842.

Dombeck, D.A., Khabbaz, A.N., Collman, F., Adelman, T.L., and Tank, D.W. (2007). Imaging large-scale neural activity with cellular resolution in awake, mobile mice. Neuron *56*, 43-57.

Dusenbery, D.B., Sheridan, R.E., and Russell, R.L. (1975). Chemotaxis defective mutants of nematode *Caenorhabditis elegans*. Genetics *80*, 297-309.

Dwyer, N.D., Adler, C.E., Crump, J.G., L'Etoile, N.D., and Bargmann, C.I. (2001). Polarized dendritic transport and the AP-1 mu1 clathrin adaptor UNC-101 localize odorant receptors to olfactory cilia. Neuron *31*, 277-287.

Edmondson, J.C., and Hatten, M.E. (1987). Glial-guided granule neuron migration in vitro: a high-resolution time-lapse video microscopic study. J Neurosci *7*, 1928-1934.

Efimenko, E., Blacque, O.E., Ou, G., Haycraft, C.J., Yoder, B.K., Scholey, J.M., Leroux, M.R., and Swoboda, P. (2006). *Caenorhabditis elegans* DYF-2, an orthologue of human

WDR19, is a component of the intraflagellar transport machinery in sensory cilia. Mol Biol Cell *17*, 4801-4811.

Efimenko, E., Bubb, K., Mak, H.Y., Holzman, T., Leroux, M.R., Ruvkun, G., Thomas, J.H., and Swoboda, P. (2005). Analysis of *xbx* genes in *C. elegans*. Development *132*, 1923-1934.

Emoto, K., He, Y., Ye, B., Grueber, W.B., Adler, P.N., Jan, L.Y., and Jan, Y.N. (2004). Control of dendritic branching and tiling by the Tricornered-kinase/Furry signaling pathway in *Drosophila* sensory neurons. Cell *119*, 245-256.

Fares, H., and Greenwald, I. (2001). Genetic analysis of endocytosis in *Caenorhabditis elegans*: coelomocyte uptake defective mutants. Genetics *159*, 133-145.

Feil, R., Brocard, J., Mascrez, B., LeMeur, M., Metzger, D., and Chambon, P. (1996). Ligand-activated site-specific recombination in mice. Proc Natl Acad Sci USA *93*, 10887-10890.

Fellin, T., Pascual, O., Gobbo, S., Pozzan, T., Haydon, P.G., and Carmignoto, G. (2004). Neuronal synchrony mediated by astrocytic glutamate through activation of extrasynaptic NMDA receptors. Neuron *43*, 729-743.

Felt, B.T., and Vande Berg, J.S. (1976). Ultrastructure of the blowfly chemoreceptor sensillum (*Phormia regina*). J Morphol *150*, 763-783.

Feng, Z., and Ko, C.P. (2008). Schwann cells promote synaptogenesis at the neuromuscular junction via transforming growth factor-beta1. J Neurosci *28*, 9599-9609.

Fiacco, T.A., Agulhon, C., Taves, S.R., Petravicz, J., Casper, K.B., Dong, X., Chen, J., and McCarthy, K.D. (2007). Selective stimulation of astrocyte calcium *in situ* does not affect neuronal excitatory synaptic activity. Neuron *54*, 611-626.

Fiacco, T.A., and McCarthy, K.D. (2004). Intracellular astrocyte calcium waves *in situ* increase the frequency of spontaneous AMPA receptor currents in CA1 pyramidal neurons. J Neurosci *24*, 722-732.

Finger, T.E., Danilova, V., Barrows, J., Bartel, D.L., Vigers, A.J., Stone, L., Hellekant, G., and Kinnamon, S.C. (2005). ATP signaling is crucial for communication from taste buds to gustatory nerves. Science *310*, 1495-1499.

Finnemann, S.C. (2003). Focal adhesion kinase signaling promotes phagocytosis of integrin-bound photoreceptors. EMBO J *22*, 4143-4154.

Fire, A., Harrison, S.W., and Dixon, D. (1990). A modular set of lacZ fusion vectors for studying gene expression in *Caenorhabditis elegans*. Gene *93*, 189-198.

Freeman, M.R., Delrow, J., Kim, J., Johnson, E., and Doe, C.Q. (2003). Unwrapping glial biology: Gcm target genes regulating glial development, diversification, and function. Neuron *38*, 567-580.

Frokjaer-Jensen, C., Kindt, K.S., Kerr, R.A., Suzuki, H., Melnik-Martinez, K., Gerstbreih, B., Driscol, M., and Schafer, W.R. (2006). Effects of voltage-gated calcium channel subunit genes on calcium influx in cultured *C. elegans* mechanosensory neurons. J Neurobiol *66*, 1125-1139.

Fujiwara, M., Ishihara, T., and Katsura, I. (1999). A novel WD40 protein, CHE-2, acts cell-autonomously in the formation of *C. elegans* sensory cilia. Development *126*, 4839-4848.

Fuss, S.H., Omura, M., and Mombaerts, P. (2005). The Grueneberg ganglion of the mouse projects axons to glomeruli in the olfactory bulb. Eur J Neurosci *22*, 2649-2654.

Gal, A., Li, Y., Thompson, D.A., Weir, J., Orth, U., Jacobson, S.G., Apfelstedt-Sylla, E., and Vollrath, D. (2000). Mutations in MERTK, the human orthologue of the RCS rat retinal dystrophy gene, cause retinitis pigmentosa. Nat Genet *26*, 270-271.

Gasque, P. (2004). Complement: a unique innate immune sensor for danger signals. Mol Immunol *41*, 1089-1098.

Geren, B.B., and Raskind, J. (1953). Development of the Fine Structure of the Myelin Sheath in Sciatic Nerves of Chick Embryos. Proc Natl Acad Sci USA *39*, 880-884.

Getchell, T.V. (1986). Functional properties of vertebrate olfactory receptor neurons. Physiol Rev *66*, 772-818.

Gilmour, D.T., Maischein, H.M., and Nusslein-Volhard, C. (2002). Migration and function of a glial subtype in the vertebrate peripheral nervous system. Neuron *34*, 577-588.

Gossen, M., and Bujard, H. (1992). Tight control of gene expression in mammalian cells by tetracycline-responsive promoters. Proc Natl Acad Sci USA *89*, 5547-5551.

Gossen, M., Freundlieb, S., Bender, G., Muller, G., Hillen, W., and Bujard, H. (1995). Transcriptional activation by tetracyclines in mammalian cells. Science *268*, 1766-1769.

Gray, J.M., Karow, D.S., Lu, H., Chang, A.J., Chang, J.S., Ellis, R.E., Marletta, M.A., and Bargmann, C.I. (2004). Oxygen sensation and social feeding mediated by a *C. elegans* guanylate cyclase homologue. Nature *430*, 317-322.

Grosche, J., Matyash, V., Moller, T., Verkhratsky, A., Reichenbach, A., and Kettenmann, H. (1999). Microdomains for neuron-glia interaction: parallel fiber signaling to Bergmann glial cells. Nat Neurosci *2*, 139-143.

Groves, M.R., Hanlon, N., Turowski, P., Hemmings, B.A., and Barford, D. (1999). The structure of the protein phosphatase 2A PR65/A subunit reveals the conformation of its 15 tandemly repeated HEAT motifs. Cell *96*, 99-110.

Hajdu-Cronin, Y.M., Chen, W.J., and Sternberg, P.W. (2004). The L-type cyclin CYL-1 and the heat-shock-factor HSF-1 are required for heat-shock-induced protein expression in *Caenorhabditis elegans*. Genetics *168*, 1937-1949.

Halfon, M.S., Kose, H., Chiba, A., and Keshishian, H. (1997). Targeted gene expression without a tissue-specific promoter: creating mosaic embryos using laser-induced single-cell heat shock. Proc Natl Acad Sci USA *94*, 6255-6260.

Hallberg, E., and Hansson, B.S. (1999). Arthropod sensilla: morphology and phylogenetic considerations. Microsc Res Tech *47*, 428-439.

Hansel, D.E., Eipper, B.A., and Ronnett, G.V. (2001). Neuropeptide Y functions as a neuroproliferative factor. Nature *410*, 940-944.

Hartenstein, V. (1997). Introduction to insect sensory organs as a model system in sensory physiology and developmental biology. Microsc Res Tech *39*, 467-469.

Hartenstein, V., and Posakony, J.W. (1989). Development of adult sensilla on the wing and notum of *Drosophila melanogaster*. Development *107*, 389-405.

Haycraft, C.J., Schafer, J.C., Zhang, Q., Taulman, P.D., and Yoder, B.K. (2003). Identification of CHE-13, a novel intraflagellar transport protein required for cilia formation. Exp Cell Res *284*, 251-263.

Haycraft, C.J., Swoboda, P., Taulman, P.D., Thomas, J.H., and Yoder, B.K. (2001). The *C. elegans* homolog of the murine cystic kidney disease gene *Tg737* functions in a ciliogenic pathway and is disrupted in *osm-5* mutant worms. Development *128*, 1493-1505.

Haydon, P.G. (2001). Glia: Listening and talking to the synapse. Nat Rev Neurosci *2*, 185-193.

Hedgecock, E.M., Culotti, J.G., Thomson, J.N., and Perkins, L.A. (1985). Axonal guidance mutants of *Caenorhabditis elegans* identified by filling sensory neurons with fluorescein dyes. Dev Biol *111*, 158-170.

Hedgecock, E.M., and Russell, R.L. (1975). Normal and mutant thermotaxis in nematode Caenorhabditis elegans. Proc Natl Acad Sci USA *72*, 4061-4065.

Hegg, C.C., Irwin, M., and Lucero, M.T. (2009). Calcium store-mediated signaling in sustentacular cells of the mouse olfactory epithelium. Glia *57*, 634-644.

Heiman, M.G., and Shaham, S. (2009). DEX-1 and DYF-7 establish sensory dendrite length by anchoring dendritic tips during cell migration. Cell *137*, 344-55.

Hepner, F., Myung, J.K., Ulfig, N., Pollak, A., and Lubec, G. (2005). Detection of hypothetical proteins in human fetal perireticular nucleus. J Proteome Res *4*, 2379-2385.

Herman, R.K. (1984). Analysis of genetic mosaics of the nematode *Caneorhabditis elegans*. Genetics *108*, 165-180.

Hidalgo, A., and Booth, G.E. (2000). Glia dictate pioneer axon trajectories in the *Drosophila* embryonic CNS. Development *127*, 393-402.

Hidalgo, A., Kinrade, E.F., and Georgiou, M. (2001). The *Drosophila* neuregulin *vein* maintains glial survival during axon guidance in the CNS. Dev Cell *1*, 679-690.

Hidalgo, A., Urban, J., and Brand, A.H. (1995). Targeted ablation of glia disrupts axon tract formation in the *Drosophila* CNS. Development *121*, 3703-3712.

Hilliard, M.A., Apicella, A.J., Kerr, R., Suzuki, H., Bazzicalupo, P., and Schafer, W.R. (2005). *In vivo* imaging of *C. elegans* ASH neurons: cellular response and adaptation to chemical repellents. EMBO J *24*, 63-72.

Hilliard, M.A., Bargmann, C.I., and Bazzicalupo, P. (2002). *C. elegans* responds to chemical repellents by integrating sensory inputs from the head and the tail. Curr Biol *12*, 730-734.

Hodgkin, J., and Doniach, T. (1997). Natural variation and copulatory plug formation in *Caenorhabditis elegans*. Genetics *146*, 149-164.

Holmes, W.E., Sliwkowski, M.X., Akita, R.W., Henzel, W.J., Lee, J., Park, J.W., Yansura, D., Abadi, N., Raab, H., Lewis, G.D., *et al.* (1992). Identification of heregulin, a specific activator of p185erbB2. Science *256*, 1205-1210.

Hosoya, T., Takizawa, K., Nitta, K., and Hotta, Y. (1995). *glial cells missing*: a binary switch between neuronal and glial determination in *Drosophila*. Cell *82*, 1025-1036.

Inglis, P.N., Boroevich, K.A., and Leroux, M.R. (2006). Piecing together a ciliome. Trends Genet *22*, 491-500.

Ishikawa, K., Nagase, T., Nakajima, D., Seki, N., Ohira, M., Miyajima, N., Tanaka, A., Kotani, H., Nomura, N., and Ohara, O. (1997). Prediction of the coding sequences of unidentified human genes. VIII. 78 new cDNA clones from brain which code for large proteins *in vitro*. DNA Res *4*, 307-313.

Jahromi, B.S., Robitaille, R., and Charlton, M.P. (1992). Transmitter release increases intracellular calcium in perisynaptic Schwann cells *in situ*. Neuron *8*, 1069-1077.

Jedlicka, P., Mortin, M.A., and Wu, C. (1997). Multiple functions of *Drosophila* heat shock transcription factor *in vivo*. EMBO J *16*, 2452-2462.

Jessen, K.R., and Mirsky, R. (2005). The origin and development of glial cells in peripheral nerves. Nat Rev Neurosci *6*, 671-682.

Jones, B.W., Fetter, R.D., Tear, G., and Goodman, C.S. (1995). *glial cells missing*: a genetic switch that controls glial versus neuronal fate. Cell *82*, 1013-1023.

Jones, D., Russnak, R.H., Kay, R.J., and Candido, E.P. (1986). Structure, expression, and evolution of a heat shock gene locus in *Caenorhabditis elegans* that is flanked by repetitive elements. J Biol Chem *261*, 12006-12015.

Kalderon, N., Alfieri, A.A., and Fuks, Z. (1990). Beneficial effects of x-irradiation on recovery of lesioned mammalian central nervous tissue. Proc Natl Acad Sci USA *87*, 10058-10062.

Kamath, R.S., Fraser, A.G., Dong, Y., Poulin, G., Durbin, R., Gotta, M., Kanapin, A., Le Bot, N., Moreno, S., Sohrmann, M., *et al.* (2003). Systematic functional analysis of the *Caenorhabditis elegans* genome using RNAi. Nature *421*, 231-237.

Kaneko, H., Putzier, I., Frings, S., Kaupp, U.B., and Gensch, T. (2004). Chloride accumulation in mammalian olfactory sensory neurons. J Neurosci *24*, 7931-7938.

Kang, J., Jiang, L., Goldman, S.A., and Nedergaard, M. (1998). Astrocyte-mediated potentiation of inhibitory synaptic transmission. Nat Neurosci *1*, 683-692.

Kaplan, J.M., and Horvitz, H.R. (1993). A dual mechanosensory and chemosensory neuron in *Caenorhabditis elegans*. Proc Natl Acad Sci USA *90*, 2227-2231.

Khurgel, M., Koo, A.C., and Ivy, G.O. (1996). Selective ablation of astrocytes by intracerebral injections of alpha-aminoadipate. Glia *16*, 351-358.

Kidd, T., Bland, K.S., and Goodman, C.S. (1999). Slit is the midline repellent for the robo receptor in *Drosophila*. Cell *96*, 785-794.

Komatsu, H., Mori, I., Rhee, J.S., Akaike, N., and Ohshima, Y. (1996). Mutations in a cyclic nucleotide-gated channel lead to abnormal thermosensation and chemosensation in *C. elegans*. Neuron *17*, 707-718.

Koos, D.S., and Fraser, S.E. (2005). The Grueneberg ganglion projects to the olfactory bulb. Neuroreport *16*, 1929-1932.

Kozminski, K.G., Beech, P.L., and Rosenbaum, J.L. (1995). The *Chlamydomonas* kinesin-like protein FLA10 is involved in motility associated with the flagellar membrane. J Cell Biol *131*, 1517-1527.

Kozminski, K.G., Johnson, K.A., Forscher, P., and Rosenbaum, J.L. (1993). A motility in the eukaryotic flagellum unrelated to flagellar beating. Proc Natl Acad Sci USA *90*, 5519-5523.

Kuhara, A., Okumura, M., Kimata, T., Tanizawa, Y., Takano, R., Kimura, K.D., Inada, H., Matsumoto, K., and Mori, I. (2008). Temperature sensing by an olfactory neuron in a circuit controlling behavior of *C. elegans*. Science *320*, 803-807.

Kulik, A., Haentzsch, A., Luckermann, M., Reichelt, W., and Ballanyi, K. (1999). Neuron-glia signaling via alpha(1) adrenoceptor-mediated Ca(2+) release in Bergmann glial cells *in situ*. J Neurosci *19*, 8401-8408.

Kuner, T., and Augustine, G.J. (2000). A genetically encoded ratiometric indicator for chloride: capturing chloride transients in cultured hippocampal neurons. Neuron *27*, 447-459.

Kunitomo, H., and Iino, Y. (2008). *Caenorhabditis elegans* DYF-11, an orthologue of mammalian Traf3ip1/MIP-T3, is required for sensory cilia formation. Genes Cells *13*, 13-25.

Kunitomo, H., Uesugi, H., Kohara, Y., and Iino, Y. (2005). Identification of ciliated sensory neuron-expressed genes in *Caenorhabditis elegans* using targeted pull-down of poly(A) tails. Genome Biol *6*, R17.

Kurahashi, T., and Yau, K.W. (1993). Co-existence of cationic and chloride components in odorant-induced current of vertebrate olfactory receptor cells. Nature *363*, 71-74.

Landmann, F., Quintin, S., and Labouesse, M. (2004). Multiple regulatory elements with spatially and temporally distinct activities control the expression of the epithelial differentiation gene *lin-26* in *C. elegans*. Dev Biol *265*, 478-490.

Largo, C., Cuevas, P., Somjen, G.G., Martin del Rio, R., and Herreras, O. (1996). The effect of depressing glial function in rat brain *in situ* on ion homeostasis, synaptic transmission, and neuron survival. J Neurosci *16*, 1219-1229.

Lawton, D.M., Furness, D.N., Lindemann, B., and Hackney, C.M. (2000). Localization of the glutamate-aspartate transporter, GLAST, in rat taste buds. Eur J Neurosci *12*, 3163-3171.

Le Douarin, N., Dulac, C., Dupin, E., and Cameron-Curry, P. (1991). Glial cell lineages in the neural crest. Glia *4*, 175-184.

Lee, C.J., Mannaioni, G., Yuan, H., Woo, D.H., Gingrich, M.B., and Traynelis, S.F. (2007). Astrocytic control of synaptic NMDA receptors. J Physiol *581*, 1057-1081.

Lehner, B., Calixto, A., Crombie, C., Tischler, J., Fortunato, A., Chalfie, M., and Fraser, A.G. (2006). Loss of LIN-35, the *Caenorhabditis elegans* ortholog of the tumor suppressor p105Rb, results in enhanced RNA interference. Genome Biol *7*, R4.

Lewis, J.A., and Hodgkin, J.A. (1977). Specific neuroanatomical changes in chemosensory mutants of nematode *Caenorhabditis elegans*. J Comp Neurol *172*, 489-510.

Li, C., Inglis, P.N., Leitch, C.C., Efimenko, E., Zaghloul, N.A., Mok, C.A., Davis, E.E., Bialas, N.J., Healey, M.P., Heon, E., *et al.* (2008). An essential role for DYF-11/MIP-T3 in assembling functional intraflagellar transport complexes. PLoS Genet *4*, e1000044.

Lin, W.C., Sanchez, H.B., Deerinck, T., Morris, J.K., Ellisman, M., and Lee, K.F. (2000). Aberrant development of motor axons and neuromuscular synapses in erbB2-deficient mice. Proc Natl Acad Sci USA *97*, 1299-1304.

Ling, L., and Goeddel, D.V. (2000). MIP-T3, a novel protein linking tumor necrosis factor receptor-associated factor 3 to the microtubule network. J Biol Chem *275*, 23852-23860.

Lints, R., and Emmons, S.W. (1999). Patterning of dopaminergic neurotransmitter identity among *Caenorhabditis elegans* ray sensory neurons by a TGFbeta family signaling pathway and a Hox gene. Development *126*, 5819-5831.

Lowe, G., and Gold, G.H. (1993). Nonlinear amplification by calcium-dependent chloride channels in olfactory receptor cells. Nature *366*, 283-286.

Lundquist, E.A., Reddien, P.W., Hartwieg, E., Horvitz, H.R., and Bargmann, C.I. (2001). Three *C. elegans* Rac proteins and several alternative Rac regulators control axon guidance, cell migration and apoptotic cell phagocytosis. Development *128*, 4475-4488.

MacDonald, J.M., Beach, M.G., Porpiglia, E., Sheehan, A.E., Watts, R.J., and Freeman, M.R. (2006). The *Drosophila* cell corpse engulfment receptor Draper mediates glial clearance of severed axons. Neuron *50*, 869-881.

Makino, N., Ookawara, S., Katoh, K., Ohta, Y., Ichikawa, M., and Ichimura, K. (2009). The morphological change of supporting cells in the olfactory epithelium after bulbectomy. Chem Senses *34*, 171-179.

Marshall, C.A., Suzuki, S.O., and Goldman, J.E. (2003). Gliogenic and neurogenic progenitors of the subventricular zone: who are they, where did they come from, and where are they going? Glia *43*, 52-61.

Mathis, C., Hindelang, C., LeMeur, M., and Borrelli, E. (2000). A transgenic mouse model for inducible and reversible dysmyelination. J Neurosci *20*, 7698-7705.

Matyash, V., Filippov, V., Mohrhagen, K., and Kettenmann, H. (2001). Nitric oxide signals parallel fiber activity to Bergmann glial cells in the mouse cerebellar slice. Mol Cell Neurosci *18*, 664-670.

Mauch, D.H., Nagler, K., Schumacher, S., Goritz, C., Muller, E.C., Otto, A., and Pfrieger, F.W. (2001). CNS synaptogenesis promoted by glia-derived cholesterol. Science *294*, 1354-1357.

McGuire, S.E., Le, P.T., Osborn, A.J., Matsumoto, K., and Davis, R.L. (2003). Spatiotemporal rescue of memory dysfunction in *Drosophila*. Science *302*, 1765-1768.

McKenna, M.P., Hekmat-Scafe, D.S., Gaines, P., and Carlson, J.R. (1994). Putative *Drosophila* pheromone-binding proteins expressed in a subregion of the olfactory system. J Biol Chem *269*, 16340-16347.

Mello, C.C., Kramer, J.M., Stinchcomb, D., and Ambros, V. (1991). Efficient gene transfer in *C.elegans*: extrachromosomal maintenance and integration of transforming sequences. EMBO J *10*, 3959-3970.

Meyer-Franke, A., Kaplan, M.R., Pfrieger, F.W., and Barres, B.A. (1995). Characterization of the signaling interactions that promote the survival and growth of developing retinal ganglion cells in culture. Neuron *15*, 805-819.

Meyer, D., Yamaai, T., Garratt, A., Riethmacher-Sonnenberg, E., Kane, D., Theill, L.E., and Birchmeier, C. (1997). Isoform-specific expression and function of neuregulin. Development *124*, 3575-3586.

Miller, D.M., 3rd, Desai, N.S., Hardin, D.C., Piston, D.W., Patterson, G.H., Fleenor, J., Xu, S., and Fire, A. (1999). Two-color GFP expression system for *C. elegans*. Biotechniques *26*, 914-918, 920-911.

Mitchell, B.K., Itagaki, H., and Rivet, M.P. (1999). Peripheral and central structures involved in insect gustation. Microsc Res Tech *47*, 401-415.

Monsma, S.A., Ard, R., Lis, J.T., and Wolfner, M.F. (1988). Localized heat-shock induction in *Drosophila melanogaster*. J Exp Zool *247*, 279-284.

Mori, I., and Ohshima, Y. (1995). Neural regulation of thermotaxis in *Caenorhabditis elegans*. Nature *376*, 344-348.

Moritz, O.L., Tam, B.M., Hurd, L.L., Peranen, J., Deretic, D., and Papermaster, D.S. (2001). Mutant rab8 impairs docking and fusion of rhodopsin-bearing post-Golgi membranes and causes cell death of transgenic *Xenopus* rods. Mol Biol Cell *12*, 2341-2351.

Morris, J.A., Kandpal, G., Ma, L., and Austin, C.P. (2003). DISC1 (Disrupted-In-Schizophrenia 1) is a centrosome-associated protein that interacts with MAP1A, MIPT3, ATF4/5 and NUDEL: regulation and loss of interaction with mutation. Hum Mol Genet *12*, 1591-1608.

Morrison, E.E., and Costanzo, R.M. (1990). Morphology of the human olfactory epithelium. J Comp Neurol *297*, 1-13.

Morrison, E.E., and Costanzo, R.M. (1992). Morphology of olfactory epithelium in humans and other vertebrates. Microsc Res Tech *23*, 49-61.

Mukhopadhyay, A., Deplancke, B., Walhout, A.J., and Tissenbaum, H.A. (2005). *C. elegans* tubby regulates life span and fat storage by two independent mechanisms. Cell Metab *2*, 35-42.

Mukhopadhyay, S., Lu, Y., Qin, H., Lanjuin, A., Shaham, S., and Sengupta, P. (2007). Distinct IFT mechanisms contribute to the generation of ciliary structural diversity in *C. elegans*. EMBO J *26*, 2966-2980.

Mukhopadhyay, S., Lu, Y., Shaham, S., and Sengupta, P. (2008). Sensory signaling-dependent remodeling of olfactory cilia architecture in *C. elegans*. Dev Cell *14*, 762-774.

Muller, C.M., and Best, J. (1989). Ocular dominance plasticity in adult cat visual cortex after transplantation of cultured astrocytes. Nature *342*, 427-430.

Murayama, T., Toh, Y., Ohshima, Y., and Koga, M. (2005). The *dyf-3* gene encodes a novel protein required for sensory cilium formation in *Caenorhabditis elegans*. J Mol Biol *346*, 677-687.

Nachury, M.V., Loktev, A.V., Zhang, Q., Westlake, C.J., Peranen, J., Merdes, A., Slusarski, D.C., Scheller, R.H., Bazan, J.F., Sheffield, V.C., *et al.* (2007). A core complex of BBS proteins cooperates with the GTPase Rab8 to promote ciliary membrane biogenesis. Cell *129*, 1201-1213.

Nagel, G., Szellas, T., Huhn, W., Kateriya, S., Adeishvili, N., Berthold, P., Ollig, D., Hegemann, P., and Bamberg, E. (2003). Channelrhodopsin-2, a directly light-gated cation-selective membrane channel. Proc Natl Acad Sci USA *100*, 13940-13945.

Nakai, J., Ohkura, M., and Imoto, K. (2001). A high signal-to-noise Ca(2+) probe composed of a single green fluorescent protein. Nat Biotechnol *19*, 137-141.

Navarrete, M., and Araque, A. (2008). Endocannabinoids mediate neuron-astrocyte communication. Neuron *57*, 883-893.

Nave, K.A., and Trapp, B.D. (2008). Axon-glial signaling and the glial support of axon function. Annu Rev Neurosci *31*, 535-561.

Newman, E.A. (2005). Calcium increases in retinal glial cells evoked by light-induced neuronal activity. J Neurosci *25*, 5502-5510.

Niu, Y., Murata, T., Watanabe, K., Kawakami, K., Yoshimura, A., Inoue, J., Puri, R.K., and Kobayashi, N. (2003). MIP-T3 associates with IL-13Ralpha1 and suppresses STAT6 activation in response to IL-13 stimulation. FEBS Lett *550*, 139-143.

Nomura, T., Takahashi, S., and Ushiki, T. (2004). Cytoarchitecture of the normal rat olfactory epithelium: light and scanning electron microscopic studies. Arch Histol Cytol *67*, 159-170.

Okano, M., and Takagi, S.F. (1974). Secretion and electrogenesis of the supporting cell in the olfactory epithelium. J Physiol *242*, 353-370.

Okkema, P.G., Harrison, S.W., Plunger, V., Aryana, A., and Fire, A. (1993). Sequence requirements for myosin gene expression and regulation in Caenorhabditis elegans. Genetics *135*, 385-404.

Omori, Y., Zhao, C., Saras, A., Mukhopadhyay, S., Kim, W., Furukawa, T., Sengupta, P., Veraksa, A., and Malicki, J. (2008). Elipsa is an early determinant of ciliogenesis that links the IFT particle to membrane-associated small GTPase Rab8. Nat Cell Biol *10*, 437-444.

Orozco, J.T., Wedaman, K.P., Signor, D., Brown, H., Rose, L., and Scholey, J.M. (1999). Movement of motor and cargo along cilia. Nature *398*, 674.

Ou, G., Blacque, O.E., Snow, J.J., Leroux, M.R., and Scholey, J.M. (2005). Functional coordination of intraflagellar transport motors. Nature *436*, 583-587.

Panatier, A., Theodosis, D.T., Mothet, J.P., Touquet, B., Pollegioni, L., Poulain, D.A., and Oliet, S.H. (2006). Glia-derived D-serine controls NMDA receptor activity and synaptic memory. Cell *125*, 775-784.

Parpura, V., Basarsky, T.A., Liu, F., Jeftinija, K., Jeftinija, S., and Haydon, P.G. (1994). Glutamate-mediated astrocyte-neuron signalling. Nature *369*, 744-747.

Pascual, O., Casper, K.B., Kubera, C., Zhang, J., Revilla-Sanchez, R., Sul, J.Y., Takano, H., Moss, S.J., McCarthy, K., and Haydon, P.G. (2005). Astrocytic purinergic signaling coordinates synaptic networks. Science *310*, 113-116.

Pasti, L., Volterra, A., Pozzan, T., and Carmignoto, G. (1997). Intracellular calcium oscillations in astrocytes: a highly plastic, bidirectional form of communication between neurons and astrocytes *in situ*. J Neurosci *17*, 7817-7830.

Pazour, G.J., and Witman, G.B. (2003). The vertebrate primary cilium is a sensory organelle. Curr Opin Cell Biol *15*, 105-110.

Pelham, H.R. (1982). A regulatory upstream promoter element in the *Drosophila* hsp 70 heat-shock gene. Cell *30*, 517-528.

Peng, H.B., Yang, J.F., Dai, Z., Lee, C.W., Hung, H.W., Feng, Z.H., and Ko, C.P. (2003). Differential effects of neurotrophins and schwann cell-derived signals on neuronal survival/growth and synaptogenesis. J Neurosci *23*, 5050-5060.

Perea, G., and Araque, A. (2005). Properties of synaptically evoked astrocyte calcium signal reveal synaptic information processing by astrocytes. J Neurosci *25*, 2192-2203.

Perea, G., and Araque, A. (2007). Astrocytes potentiate transmitter release at single hippocampal synapses. Science *317*, 1083-1086.

Perens, E.A., and Shaham, S. (2005). *C. elegans daf-6* encodes a patched-related protein required for lumen formation. Dev Cell *8*, 893-906.

Perkins, L.A., Hedgecock, E.M., Thomson, J.N., and Culotti, J.G. (1986). Mutant sensory cilia in the nematode *Caenorhabditis elegans*. Dev Biol *117*, 456-487.

Pfrieger, F.W., and Barres, B.A. (1997). Synaptic efficacy enhanced by glial cells in vitro. Science *277*, 1684-1687.

Piet, R., and Jahr, C.E. (2007). Glutamatergic and purinergic receptor-mediated calcium transients in Bergmann glial cells. J Neurosci *27*, 4027-4035.

Pikielny, C.W., Hasan, G., Rouyer, F., and Rosbash, M. (1994). Members of a family of *Drosophila* putative odorant-binding proteins are expressed in different subsets of olfactory hairs. Neuron *12*, 35-49.

Pippenger, M.A., Sims, T.J., and Gilmore, S.A. (1990). Development of the rat corticospinal tract through an altered glial environment. Brain Res Dev Brain Res *55*, 43-50.

Politis, M.J., and Houle, J.D. (1985). Effect of cytosine arabinofuranoside (AraC) on reactive gliosis *in vivo*. An immunohistochemical and morphometric study. Brain Res *328*, 291-300.

Pollack, G.S., and Balakrishnan, R. (1997). Taste sensilla of flies: function, central neuronal projections, and development. Microsc Res Tech *39*, 532-546.

Porter, J.T., and McCarthy, K.D. (1996). Hippocampal astrocytes in situ respond to glutamate released from synaptic terminals. J Neurosci *16*, 5073-5081.

Porter, J.T., and McCarthy, K.D. (1997). Astrocytic neurotransmitter receptors *in situ* and *in vivo*. Prog Neurobiol *51*, 439-455.

Pumplin, D.W., Yu, C., and Smith, D.V. (1997). Light and dark cells of rat vallate taste buds are morphologically distinct cell types. J Comp Neurol *378*, 389-410.

Qin, H., Burnette, D.T., Bae, Y.K., Forscher, P., Barr, M.M., and Rosenbaum, J.L. (2005). Intraflagellar transport is required for the vectorial movement of TRPV channels in the ciliary membrane. Curr Biol *15*, 1695-1699.

Qin, H., Rosenbaum, J.L., and Barr, M.M. (2001). An autosomal recessive polycystic kidney disease gene homolog is involved in intraflagellar transport in *C. elegans* ciliated sensory neurons. Curr Biol *11*, 457-461.

Rakic, P. (1971). Neuron-glia relationship during granule cell migration in developing cerebellar cortex. A Golgi and electronmicroscopic study in Macacus Rhesus. J Comp Neurol *141*, 283-312.

Rakic, P. (1972). Mode of cell migration to the superficial layers of fetal monkey neocortex. J Comp Neurol *145*, 61-83.

Reddy, L.V., Koirala, S., Sugiura, Y., Herrera, A.A., and Ko, C.P. (2003). Glial cells maintain synaptic structure and function and promote development of the neuromuscular junction *in vivo*. Neuron *40*, 563-580.

Reist, N.E., and Smith, S.J. (1992). Neurally evoked calcium transients in terminal Schwann cells at the neuromuscular junction. Proc Natl Acad Sci USA *89*, 7625-7629.

Riddle, D.L. (1988). The dauer larva. In The nematode *Caenorhabditis elegans*, W.B. Wood, ed. (New York, Cold Spring Harbor Laboratory Press), pp. 393-412.

Riddle, D.L., Swanson, M.M., and Albert, P.S. (1981). Interacting genes in nematode dauer larva formation. Nature *290*, 668-671.

Riethmacher, D., Sonnenberg-Riethmacher, E., Brinkmann, V., Yamaai, T., Lewin, G.R., and Birchmeier, C. (1997). Severe neuropathies in mice with targeted mutations in the ErbB3 receptor. Nature *389*, 725-730.

Roayaie, K., Crump, J.G., Sagasti, A., and Bargmann, C.I. (1998). The G alpha protein ODR-3 mediates olfactory and nociceptive function and controls cilium morphogenesis in *C. elegans* olfactory neurons. Neuron *20*, 55-67.

Robitaille, R. (1998). Modulation of synaptic efficacy and synaptic depression by glial cells at the frog neuromuscular junction. Neuron *21*, 847-855.

Roper, S.D. (1989). The cell biology of vertebrate taste receptors. Annu Rev Neurosci *12*, 329-353.

Roper, S.D. (1992). The microphysiology of peripheral taste organs. J Neurosci *12*, 1127-1134.

Roppolo, D., Ribaud, V., Jungo, V.P., Luscher, C., and Rodriguez, I. (2006). Projection of the Gruneberg ganglion to the mouse olfactory bulb. Eur J Neurosci *23*, 2887-2894.

Rosenbaum, J.L., and Witman, G.B. (2002). Intraflagellar transport. Nat Rev Mol Cell Biol *3*, 813-825.

Rothberg, J.M., Jacobs, J.R., Goodman, C.S., and Artavanis-Tsakonas, S. (1990). slit: an extracellular protein necessary for development of midline glia and commissural axon pathways contains both EGF and LRR domains. Genes Dev *4*, 2169-2187.

Royer, S.M., and Kinnamon, J.C. (1991). HVEM serial-section analysis of rabbit foliate taste buds: I. Type III cells and their synapses. J Comp Neurol *306*, 49-72.

Ryu, W.S., and Samuel, A.D. (2002). Thermotaxis in *Caenorhabditis elegans* analyzed by measuring responses to defined thermal stimuli. J Neurosci *22*, 5727-5733.

Sagasti, A., Hobert, O., Troemel, E.R., Ruvkun, G., and Bargmann, C.I. (1999). Alternative olfactory neuron fates are specified by the LIM homeobox gene *lim-4*. Genes Dev *13*, 1794-1806.

Sarafi-Reinach, T.R., Melkman, T., Hobert, O., and Sengupta, P. (2001). The *lin-11* LIM homeobox gene specifies olfactory and chemosensory neuron fates in *C. elegans*. Development *128*, 3269-3281.

Satterlee, J.S., Sasakura, H., Kuhara, A., Berkeley, M., Mori, I., and Sengupta, P. (2001). Specification of thermosensory neuron fate in *C. elegans* requires *ttx-1*, a homolog of otd/Otx. Neuron *31*, 943-956.

Sawin, E.R., Ranganathan, R., and Horvitz, H.R. (2000). *C. elegans* locomotory rate is modulated by the environment through a dopaminergic pathway and by experience through a serotonergic pathway. Neuron *26*, 619-631.

Schafer, J.C., Winkelbauer, M.E., Williams, C.L., Haycraft, C.J., Desmond, R.A., and Yoder, B.K. (2006). IFTA-2 is a conserved cilia protein involved in pathways regulating longevity and dauer formation in *Caenorhabditis elegans*. J Cell Sci *119*, 4088-4100.

Scholey, J.M. (2003). Intraflagellar transport. Annu Rev Cell Dev Biol *19*, 423-443.
Schumacher, B., Schertel, C., Wittenburg, N., Tuck, S., Mitani, S., Gartner, A., Conradt, B., and Shaham, S. (2005). *C. elegans ced-13* can promote apoptosis and is induced in response to DNA damage. Cell Death Differ *12*, 153-161.

Schummers, J., Yu, H., and Sur, M. (2008). Tuned responses of astrocytes and their influence on hemodynamic signals in the visual cortex. Science *320*, 1638-1643.

Sengupta, P., Chou, J.H., and Bargmann, C.I. (1996). *odr-10* encodes a seven transmembrane domain olfactory receptor required for responses to the odorant diacetyl. Cell *84*, 899-909.

Serrano, A., Haddjeri, N., Lacaille, J.C., and Robitaille, R. (2006). GABAergic network activation of glial cells underlies hippocampal heterosynaptic depression. J Neurosci *26*, 5370-5382.

Shanbhag, S.R., Park, S.K., Pikielny, C.W., and Steinbrecht, R.A. (2001). Gustatory organs of *Drosophila melanogaster*: fine structure and expression of the putative odorant-binding protein PBPRP2. Cell Tissue Res *304*, 423-437.

Signor, D., Wedaman, K.P., Orozco, J.T., Dwyer, N.D., Bargmann, C.I., Rose, L.S., and Scholey, J.M. (1999). Role of a class DHC1b dynein in retrograde transport of IFT motors and IFT raft particles along cilia, but not dendrites, in chemosensory neurons of living *Caenorhabditis elegans*. J Cell Biol *147*, 519-530.

Singla, V., and Reiter, J.F. (2006). The primary cilium as the cell's antenna: signaling at a sensory organelle. Science *313*, 629-633.

Smith, P.J., Leech, C.A., and Treherne, J.E. (1984). Glial repair in an insect central nervous system: effects of selective glial disruption. J Neurosci *4*, 2698-2711.

Snow, J.J., Ou, G., Gunnarson, A.L., Walker, M.R., Zhou, H.M., Brust-Mascher, I., and Scholey, J.M. (2004). Two anterograde intraflagellar transport motors cooperate to build sensory cilia on *C. elegans neurons*. Nat Cell Biol *6*, 1109-1113.

Sofroniew, M.V., Bush, T.G., Blumauer, N., Kruger, L., Mucke, L., and Johnson, M.H. (1999). Genetically-targeted and conditionally-regulated ablation of astroglial cells in the central, enteric and peripheral nervous systems in adult transgenic mice. Brain Res *835*, 91-95.

Spacek, J. (1985). Three-dimensional analysis of dendritic spines. III. Glial sheath. Anat Embryol (Berl) *171*, 245-252.

Starich, T.A., Herman, R.K., Kari, C.K., Yeh, W.H., Schackwitz, W.S., Schuyler, M.W., Collet, J., Thomas, J.H., and Riddle, D.L. (1995). Mutations affecting the chemosensory neurons of *Caenorhabditis elegans*. Genetics *139*, 171-188.

Steinberg, R.H., Wood, I., and Hogan, M.J. (1977). Pigment epithelial ensheathment and phagocytosis of extrafoveal cones in human retina. Philos Trans R Soc Lond B Biol Sci *277*, 459-474.

Stellwagen, D., and Malenka, R.C. (2006). Synaptic scaling mediated by glial TNF-alpha. Nature *440*, 1054-1059.

Stenmark, H., Vitale, G., Ullrich, O., and Zerial, M. (1995). Rabaptin-5 is a direct effector of the small GTPase Rab5 in endocytic membrane fusion. Cell *83*, 423-432.

Stevens, B., Allen, N.J., Vazquez, L.E., Howell, G.R., Christopherson, K.S., Nouri, N., Micheva, K.D., Mehalow, A.K., Huberman, A.D., Stafford, B., *et al.* (2007). The classical complement cascade mediates CNS synapse elimination. Cell *131*, 1164-1178.

Storan, M.J., and Key, B. (2006). Septal organ of Gruneberg is part of the olfactory system. J Comp Neurol *494*, 834-844.

Stork, T., Engelen, D., Krudewig, A., Silies, M., Bainton, R.J., and Klambt, C. (2008). Organization and function of the blood-brain barrier in *Drosophila*. J Neurosci *28*, 587-597.

Strauss, O. (2005). The retinal pigment epithelium in visual function. Physiol Rev *85*, 845-881.

Streit, W.J. (2001). Microglia and macrophages in the developing CNS. Neurotoxicology *22*, 619-624.

Stringham, E.G., and Candido, E.P. (1993). Targeted single-cell induction of gene products in *Caenorhabditis elegans*: a new tool for developmental studies. J Exp Zool *266*, 227-233.

Stringham, E.G., Dixon, D.K., Jones, D., and Candido, E.P. (1992). Temporal and spatial expression patterns of the small heat shock (*hsp16*) genes in transgenic *Caenorhabditis elegans*. Mol Biol Cell *3*, 221-233.

Sulston, J.E., and Horvitz, H.R. (1977). Post-embryonic cell lineages of the nematode, *Caenorhabditis elegans*. Dev Biol *56*, 110-156.

Sulston, J.E., Schierenberg, E., White, J.G., and Thomson, J.N. (1983). The embryonic-cell lineage of the nematode *Caenorhabditis elegans*. Dev Biol *100*, 64-119.

Suzuki, Y., Takeda, M., and Farbman, A.I. (1996). Supporting cells as phagocytes in the olfactory epithelium after bulbectomy. J Comp Neurol *376*, 509-517.

Swanson, M.M., and Riddle, D.L. (1981). Critical periods in the development of the *Caenorhabditis elegans* dauer larva. Dev Biol *84*, 27-40.

Swoboda, P., Adler, H.T., and Thomas, J.H. (2000). The RFX-type transcription factor DAF-19 regulates sensory neuron cilium formation in *C. elegans*. Mol Cell *5*, 411-421.

Sze, J.Y., Victor, M., Loer, C., Shi, Y., and Ruvkun, G. (2000). Food and metabolic signalling defects in a *Caenorhabditis elegans* serotonin-synthesis mutant. Nature *403*, 560-564.

Tabish, M., Siddiqui, Z.K., Nishikawa, K., and Siddiqui, S.S. (1995). Exclusive expression of *C. elegans osm-3* kinesin gene in chemosensory neurons open to the external environment. J Mol Biol *247*, 377-389.

Takahashi, N., Roach, A., Teplow, D.B., Prusiner, S.B., and Hood, L. (1985). Cloning and characterization of the myelin basic protein gene from mouse: one gene can encode both 14 kd and 18.5 kd MBPs by alternate use of exons. Cell *42*, 139-148.

Tan, P.L., Barr, T., Inglis, P.N., Mitsuma, N., Huang, S.M., Garcia-Gonzalez, M.A., Bradley, B.A., Coforio, S., Albrecht, P.J., Watnick, T., *et al.* (2007). Loss of Bardet Biedl syndrome proteins causes defects in peripheral sensory innervation and function. Proc Natl Acad Sci USA *104*, 17524-17529.

Theodosis, D.T., and Poulain, D.A. (1993). Activity-dependent neuronal-glial and synaptic plasticity in the adult mammalian hypothalamus. Neuroscience *57*, 501-535.

Tobin, D., Madsen, D., Kahn-Kirby, A., Peckol, E., Moulder, G., Barstead, R., Maricq, A., and Bargmann, C. (2002). Combinatorial expression of TRPV channel proteins defines their sensory functions and subcellular localization in *C. elegans* neurons. Neuron *35*, 307-318.

Tordai, H., Banyai, L., and Patthy, L. (1999). The PAN module: the N-terminal domains of plasminogen and hepatocyte growth factor are homologous with the apple domains of the prekallikrein family and with a novel domain found in numerous nematode proteins. FEBS Lett *461*, 63-67.

Troemel, E.R., Chou, J.H., Dwyer, N.D., Colbert, H.A., and Bargmann, C.I. (1995). Divergent seven transmembrane receptors are candidate chemosensory receptors in *C. elegans*. Cell *83*, 207-218.

Troemel, E.R., Kimmel, B.E., and Bargmann, C.I. (1997). Reprogramming chemotaxis responses: Sensory neurons define olfactory preferences in *C. elegans*. Cell *91*, 161-169.

Troemel, E.R., Sagasti, A., and Bargmann, C.I. (1999). Lateral signaling mediated by axon contact and calcium entry regulates asymmetric odorant receptor expression in *C. elegans*. Cell *99*, 387-398.

Ullian, E.M., Harris, B.T., Wu, A., Chan, J.R., and Barres, B.A. (2004). Schwann cells and astrocytes induce synapse formation by spinal motor neurons in culture. Mol Cell Neurosci *25*, 241-251.

Ullian, E.M., Sapperstein, S.K., Christopherson, K.S., and Barres, B.A. (2001). Control of synapse number by glia. Science *291*, 657-661.

Vekris, A., Maurange, C., Moonen, C., Mazurier, F., De Verneuil, H., Canioni, P., and Voisin, P. (2000). Control of transgene expression using local hyperthermia in combination with a heat-sensitive promoter. J Gene Med *2*, 89-96.

Ventura, R., and Harris, K.M. (1999). Three-dimensional relationships between hippocampal synapses and astrocytes. J Neurosci *19*, 6897-6906.

Vilhardt, F. (2005). Microglia: phagocyte and glia cell. Int J Biochem Cell Biol *37*, 17-21.

Vincent, S., Vonesch, J.L., and Giangrande, A. (1996). *glide* directs glial fate commitment and cell fate switch between neurones and glia. Development *122*, 131-139.

Vogalis, F., Hegg, C.C., and Lucero, M.T. (2005). Electrical coupling in sustentacular cells of the mouse olfactory epithelium. J Neurophysiol *94*, 1001-1012.

Vogt, R.G., Prestwich, G.D., and Lerner, M.R. (1991). Odorant-binding-protein subfamilies associate with distinct classes of olfactory receptor neurons in insects. J Neurobiol *22*, 74-84.

Vogt, R.G., and Riddiford, L.M. (1981). Pheromone binding and inactivation by moth antennae. Nature *293*, 161-163.

Vowels, J.J., and Thomas, J.H. (1992). Genetic analysis of chemosensory control of dauer formation in *Caenorhabditis elegans*. Genetics *130*, 105-123.

Vowels, J.J., and Thomas, J.H. (1994). Multiple chemosensory defects in *daf-11* and *daf-21* mutants of *Caenorhabditis elegans*. Genetics *138*, 303-316.

Wagner, B., Natarajan, A., Grunaug, S., Kroismayr, R., Wagner, E.F., and Sibilia, M. (2006). Neuronal survival depends on EGFR signaling in cortical but not midbrain astrocytes. EMBO J *25*, 752-762.

Wang, X., Lou, N., Xu, Q., Tian, G.F., Peng, W.G., Han, X., Kang, J., Takano, T., and Nedergaard, M. (2006). Astrocytic Ca^{2+} signaling evoked by sensory stimulation *in vivo*. Nat Neurosci *9*, 816-823.

Wang, Y., Apicella, A., Jr., Lee, S.K., Ezcurra, M., Slone, R.D., Goldmit, M., Schafer, W.R., Shaham, S., Driscoll, M., and Bianchi, L. (2008). A glial DEG/ENaC channel functions with neuronal channel DEG-1 to mediate specific sensory functions in *C. elegans*. EMBO J *27*, 2388-2399.

Wangemann, P. (2006). Supporting sensory transduction: cochlear fluid homeostasis and the endocochlear potential. J Physiol *576*, 11-21.

Ward, S. (1973). Chemotaxis by the nematode *Caenorhabditis elegans*: identification of attractants and analysis of the response by use of mutants. Proc Natl Acad Sci USA *70*, 817-821.

Ward, S., Thomson, N., White, J.G., and Brenner, S. (1975). Electron microscopical reconstruction of the anterior sensory anatomy of the nematode *Caenorhabditis elegans*. J Comp Neurol *160*, 313-337.

Ware, R.W., Clark, D., Crossland, K., and Russell, R.L. (1975). The nerve ring of the nematode *Caenorhabditis elegans*: sensory input and motor output. J Comp Neurol *162*, 71-110.

Watts, R.J., Hoopfer, E.D., and Luo, L. (2003). Axon pruning during *Drosophila* metamorphosis: evidence for local degeneration and requirement of the ubiquitin-proteasome system. Neuron *38*, 871-885.

Watts, R.J., Schuldiner, O., Perrino, J., Larsen, C., and Luo, L. (2004). Glia engulf degenerating axons during developmental axon pruning. Curr Biol *14*, 678-684.

Westwood, J.T., Clos, J., and Wu, C. (1991). Stress-induced oligomerization and chromosomal relocalization of heat-shock factor. Nature *353*, 822-827.

Wheatley, D.N., Wang, A.M., and Strugnell, G.E. (1996). Expression of primary cilia in mammalian cells. Cell Biol Int *20*, 73-81.

White, J.G., Southgate, E., Thomson, J.N., and Brenner, S. (1986). The structure of the nervous system of the nematode *Caenorhabditis elegans*. Philos Trans R Soc Lond B Biol Sci *314*, 1-340.

Whitear, M. (1976). Apical secretion from taste bud and other epithelial cells in amphibians. Cell Tissue Res *172*, 389-404.

Wicks, S.R., Yeh, R.T., Gish, W.R., Waterston, R.H., and Plasterk, R.H. (2001). Rapid gene mapping in *Caenorhabditis elegans* using a high density polymorphism map. Nat Genet *28*, 160-164.

Winston, W.M., Molodowitch, C., and Hunter, C.P. (2002). Systemic RNAi in *C. elegans* requires the putative transmembrane protein SID-1. Science *295*, 2456-2459.

Woldeyesus, M.T., Britsch, S., Riethmacher, D., Xu, L., Sonnenberg-Riethmacher, E., Abou-Rebyeh, F., Harvey, R., Caroni, P., and Birchmeier, C. (1999). Peripheral nervous system defects in erbB2 mutants following genetic rescue of heart development. Genes Dev *13*, 2538-2548.

Wright, K.A. (1980). Nematode sense organs. In Nematodes as Biological Models, B.M. Zuckerman, ed. (New York, Academic Press), pp. 237-295.

Xiong, W.C., and Montell, C. (1995). Defective glia induce neuronal apoptosis in the *repo* visual system of *Drosophila*. Neuron *14*, 581-590.

Yandell, M.D., Edgar, L.G., and Wood, W.B. (1994). Trimethylpsoralen induces small deletion mutations in *Caenorhabditis elegans*. Proc Natl Acad Sci USA *91*, 1381-1385.

Yang, Y., Ge, W., Chen, Y., Zhang, Z., Shen, W., Wu, C., Poo, M., and Duan, S. (2003). Contribution of astrocytes to hippocampal long-term potentiation through release of D-serine. Proc Natl Acad Sci USA *100*, 15194-15199.

Yoshimura, S., Murray, J.I., Lu, Y., Waterston, R.H., and Shaham, S. (2008). *mls-2* and *vab-3* control glia development, *hlh-17*/Olig expression and glia-dependent neurite extension in *C. elegans*. Development *135*, 2263-2275.

Yu, S., Avery, L., Baude, E., and Garbers, D.L. (1997). Guanylyl cyclase expression in specific sensory neurons: a new family of chemosensory receptors. Proc Natl Acad Sci USA *94*, 3384-3387.

Yu, T.W., and Bargmann, C.I. (2001). Dynamic regulation of axon guidance. Nat Neurosci *4 Suppl*, 1169-1176.

Yuan, J., Shaham, S., Ledoux, S., Ellis, H.M., and Horvitz, H.R. (1993). The *C. elegans* cell death gene *ced-3* encodes a protein similar to mammalian interleukin-1 beta-converting enzyme. Cell *75*, 641-652.

Zhang, Y., Lu, H., and Bargmann, C.I. (2005). Pathogenic bacteria induce aversive olfactory learning in *Caenorhabditis elegans*. Nature *438*, 179-184.

Zhou, H., Mazzulla, M.J., Kaufman, J.D., Stahl, S.J., Wingfield, P.T., Rubin, J.S., Bottaro, D.P., and Byrd, R.A. (1998). The solution structure of the N-terminal domain of hepatocyte growth factor reveals a potential heparin-binding site. Structure *6*, 109-116.

Ziegenfuss, J.S., Biswas, R., Avery, M.A., Hong, K., Sheehan, A.E., Yeung, Y.G., Stanley, E.R., and Freeman, M.R. (2008). Draper-dependent glial phagocytic activity is mediated by Src and Syk family kinase signalling. Nature *453*, 935-939.